Nanoscale

Accepted Manuscript

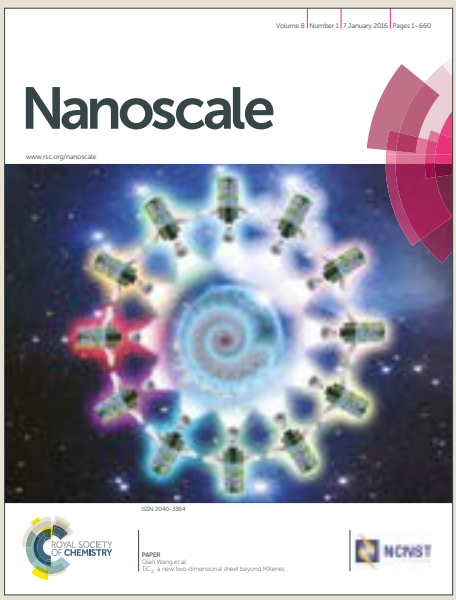

ROYAL SOCIETY OF CHEMISTRY

rsc.li/nanoscale

View Article Online
DOI: 10.1039/C7NR01878A

Physicomechanical properties of spark plasma sintered carbon nanotube-containing ceramic matrix nanocomposites

Abolfazl Azarniya[*a], Saeed Sovizi[a], Amir Azarniya[a], Mohammad Reza Rahmani Taji Boyuk[a], Temel Varol[b], Palaniyandi Nithyadharseni[c], Hamid Reza Madaah Hosseini[*a], Seeram Ramakrishna[d], M.V. Reddy[e,f]

[a] Department of Materials Science and Engineering, Sharif University of Technology, P.O. Box 11155-9466, Azadi Avenue, Tehran, Iran

[b] Department of Metallurgical and Materials Engineering, Engineering Faculty, Karadeniz Technical University, Trabzon, Turkey

[c] Energy Materials, Materials Science and Manufacturing (MSM), Council for Scientific and Industrial Research (CSIR), Pretoria 0001, South Africa

[d] Department of Mechanical Engineering, National University of Singapore, 9 Engineering Drive 1, Singapore 117576, Singapore

[e] Department of Materials Science and Engineering, National University of Singapore, Singapore 117546, Singapore

[f] Department of Physics, National University of Singapore, Singapore 117542, Singapore

Corresponding authors:

1. Abolfazl Azarniya: azarniya_abolfazl@mehr.sharif.edu; and a.azarnia1369@gmail.com

Phone number: +989224514107

2. Prof. Hamid Reza Madaah Hosseini: madaah@sharif.edu

Abstract

Recently, a wide variety of research works have focused on carbon nanotube (CNT) - ceramic matrix nanocomposites. In many cases, these novel materials are produced through conventional powder metallurgy methods including hot pressing, conventional sintering, and hot isostatic pressing. However, spark plasma sintering (SPS) as a novel and efficient consolidation technique is exploited for full densification of high-temperature ceramic systems. In these binary

View Article Online
DOI: 10.1039/C7NR01878A

nanocomposites, CNTs are added to ceramic matrices to noticeably modify their inferior properties and SPS is employed to produce fully dense compacts. In this review, a broad overview of these systems is provided and the potential influences of CNTs on their functional and structural properties are addressed. The technical challenges are then mentioned and the ongoing debates over conquering these drawbacks are fully highlighted. The used structural classification is material-oriented. It contributes the readers to easily find the material systems of interest. The SPSed CNT-containing ceramic matrix nanocomposites are generally categorized into four main classes: CNT-oxide systems; CNT-nitride systems, CNT-carbide systems, and CNT-boride systems. A large number of original curves and bubble maps are provided to fully summarize the experimental results reported in the literature. They pave the way for obviously selecting the ceramic systems required for each industrial application. The properties in consideration include relative density, hardness, yield strength, fracture toughness, electrical and thermal conductivities, modulus, and flexural strength. These unique graphs facilitate the comparison between the reported results and contribute the reader to easily distinguish the best method for producing the ceramic systems of interest and optimal conditions in which the superior properties can be reached. The authors have concentrated on the microstructure evolution-physicomechanical properties relationships and tried to relate each property to pertinent microstructural phenomena and address why the properties are degraded or enhanced with the variation of SPS conditions or material parameters.

Keywords

Carbon nanotube, ceramic composite, spark plasma sintering, mechanical properties

1. Introduction

Carbon nanotubes (CNTs) as nanosized allotropes of carbon, were discovered by Sumio Iijima in 1991[1] and seized many promising opportunities in nanoscience and nanotechnology applications[2]. These fabulous materials bear a seamless cylindrical shape which can be formed by wrapping a single graphene sheet along the axial direction. The mechanical, electronic, functional, and optical properties of CNTs strongly depend on the chirality, geometrical parameters, and atomic arrangement and then synthesis techniques[3, 4]. A great deal of effort is conducted to elucidate the mechanical, thermal and electrical properties of CNT particles, nanofibers and bundles. Theoretical calculations claim that CNTs benefit from an electrical behavior similar to metals or semiconductors and can be tailored for a variety of sophisticated applications[5]. These types of CNTs are referred to as metallic or semiconducting CNTs[3]. In another study, Lourie and coworkers [6] measured the stress required for buckling of a single CNT

View Article Online
DOI: 10.1039/C7NR01878A

as 100-150 GPa, that is, much more than stress required for fracturing high-strength ceramics. The axial stiffness of an individual perfect CNT, matches that of the best carbon fibers (approximately 1 TPa), while the tensile strength is an order of magnitude higher (around 50 GPa)[7]. Such exceptional properties make CNTs popular for producing ultra-strong, ultra-tough, and highly efficient electrical or thermal components. For this reason, many attempts have been made to enhance some properties of brittle or non-efficient ceramics by adding CNTs[8]. However, there exist some significant challenges about applicability of CNTs in ceramic matrices among which the followings are the most important:

(i) **Homogeneous dispersion of CNTs in ceramic matrix.** Often, it is difficult to obtain a uniform distribution of CNTs in ceramic or metallic matrices and a critical challenge is intrinsic tendency of CNTs to agglomerate. The entanglement of these tubes gives rise to nonuniform and anisotropic properties of ceramic based composites[9]. To overcome this challenge, a broad spectrum of novel dispersion methods is developed to provide better CNT dispersion with` enhanced properties. Recently, novel dispersion methods such as in-situ growth of CNTs by chemical vapor deposition (CVD)[10], colloidal processing[11], and electrophoretic deposition (EPD)[12] have been developed and a uniform dispersion of CNTs in ceramic matrices are reported.

(ii) **Suitable interfacial adhesion.** Thermal and electrical conductivities of CNT-reinforced ceramic matrix nanocomposites thoroughly depend on the interfacial adhesion and surface defects. A weak CNT / ceramic matrix interface gives rise to a change in the interfacial thermal or electrical resistance due to enhanced phonon or charge carrier scattering [13, 14]. From a mechanical properties point of view, CNTs should bear a strong interfacial adhesion so that the ceramic matrix is able to transfer applied load to CNT reinforcement. Moreover, other toughening mechanisms such as crack bridging, pullout, and crack deflection can occur depending on interfacial strength. In the case of exceedingly poor interfacial bonding, CNT particles serve as microcracks and deteriorate mechanical properties of ceramic matrices [7]. Therefore, interface engineering is required to obtain superior mechanical or physical properties of CNT-reinforced ceramic matrix nanocomposites.

(iii) **Thermal degradation of CNTs** in the presence of a ceramic matrix at high processing temperatures and pressures. A review on literature confirms that high applied pressures, high sintering temperatures and long processing times can adversely affect the integrity and original nature of CNTs and result in an allotropic phase transformation [15] or physicomechanical damage accumulation [16]. Such phenomena are widely observed in spark plasma sintered CNT-ceramic matrix nanocomposites.

(iv) **Appropriate sinterability and densification.** One of the main challenges over brittle ceramics is poor sinterability and difficulty in obtaining a full densification due to low self-diffusion coefficient and weak covalent bond between the constituents[17-19]. Using

View Article Online
DOI: 10.1039/C7NR01878A

appropriate sintering aids such as, carbon and alumina or employing sophisticated sintering techniques such as hot isostatic pressing (HIP) and spark plasma sintering (SPS) are proposed to solve the pertinent challenges [17, 18].

Theoretically, it is expected that if the aforementioned requirements are met, it is possible to obtain fully dense composites with superior mechanical and physical properties. In practice, a wide variety of dispersion methods are invented to avoid nonuniform distribution of CNTs in ceramic matrix and some surface modifications are conducted to enhance the interfacial bonding. Also, SPS procedure is exploited to densify CNT-ceramic powder blends to full compaction and remove the porosities which enable microcrack initiation and its fast propagation. Recently, this method has been applied for fab/ricating highly dense bulk materials ranging from magnetic materials to ceramics with comparatively lower temperatures and short processing times. Since the dominant mechanisms behind SPS still remain unclear, sintering is contradictorily generated via spark discharge and/or plasma formation between particles [20]. This technique is recently used in a variety of applications in energy storage devices such as solid electrolytes, carbon-based supercapacitor materials and anode materials for lithium ion batteries and solid oxide fuel cells [21-27].

It is a general belief that in the SPS process, the sample experiences the electrical resistance-induced heating as a result of pulsed dc voltage in die assembly as well as uniaxial pressure under inert atmosphere or vacuum (Fig. 1). Electrical discharge between particles under the applied pressure due to sparking results in the pure densification of the powder. Besides fast cooling rates (up to 300 K min^{-1}), rapid heating rates (up to 600 K min^{-1}) are main characteristics of this method thanks to non-insulating property of graphite cylinder, considerable radiative loss, and high incoming power [28].

View Article Online
DOI: 10.1039/C7NR01878A

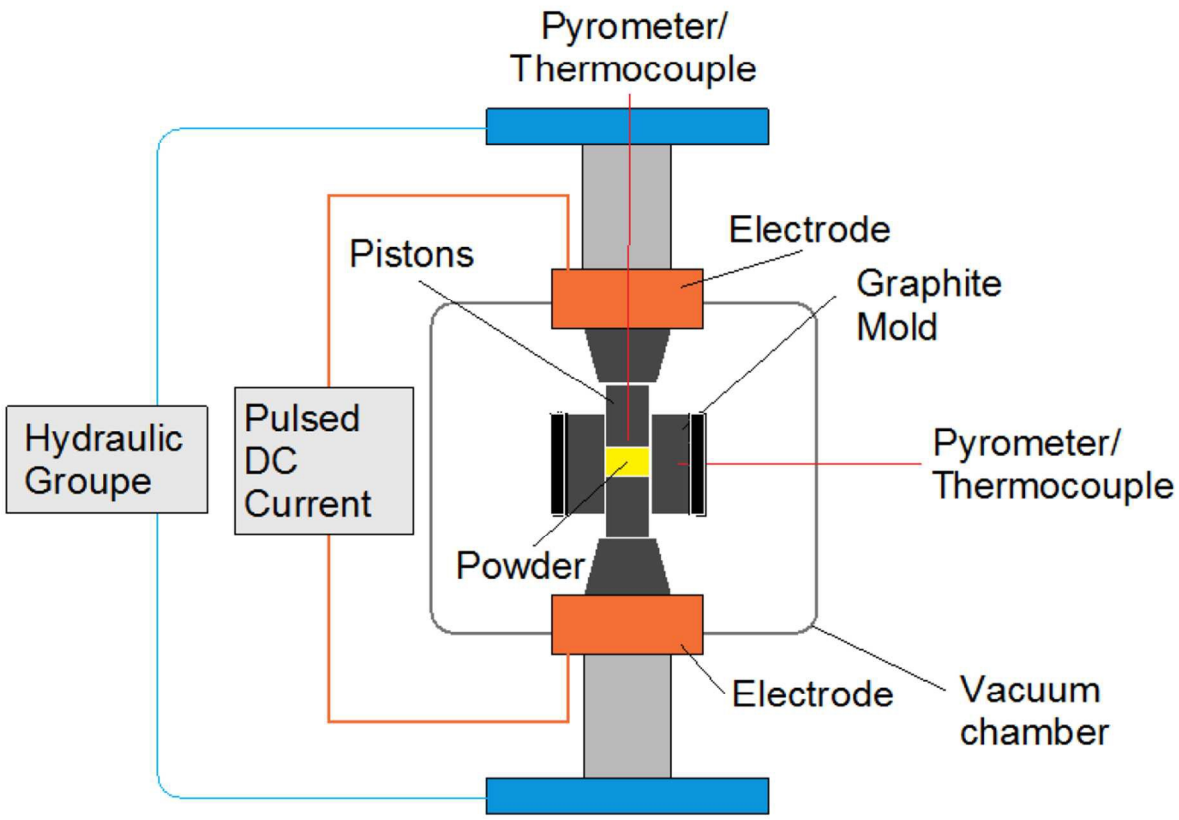

Fig. 1. A schematic illustration of the SPS apparatus and its constituent parts (Reproduced from ref. 28 with permission from Taylor & Francis Group [28]).

The SPS route is well-known as an efficient and practical approach for full sintering of those materials needing higher processing temperatures in conventional methods. An analytical model has demonstrated that the SPS compacts generally experience higher temperatures than ones shown by an optical pyrometer placed at top of graphite die for checking the temperature during the process. If some assumptions are made for simplification, the maximum temperature difference between the SPSed compact and outside of the cylinder can be expressed as:

(Eq. 1) $$\Delta T_{max} = \frac{\varepsilon \sigma T_0^4 r_0}{2k}$$ [28]

where r_0 is radius of cylinder, ε is emissivity, σ is Stefan–Boltzmann constant, k is thermal conductivity, and T_0 is die surface temperature. Therefore, the SPSed samples experience higher sintering temperatures than conventional techniques. Experimental results for TiB_2-Si_3N_4 composites and alumina (of submicrometric grain size) are in good agreement with the modeling outcomes. Meanwhile, monitoring the processing time for attaining the equilibrium temperature

View Article Online
DOI: 10.1039/C7NR01878A

in an SPS process has shown that when the term Kt/a^2 (where t is sintering time and a is particle radius) move near 1, temperature approaches to an equilibrium value. This implies that the time for reaching equilibrium temperature is few minutes. These conditions can create a characteristic temperature gradient in the compact, especially if the sample size increases. All in all, SPS technique becomes profitable because of high loading ability, low processing time, the ability to precisely control the sintering time, and possibility to use a broad spectrum of processing conditions along with high cooling and heating rates; although the high cooling/heating rates can limit reproducibility and create sharp temperature gradients [28].

A comparative study between SPS and conventional techniques obviously proves the practical superiority of the SPS method over others. Bala´zsi et al. [29] prepared multi-walled CNT (MWCNT)-Si_3N_4 nanocomposites by both SPS (1500-1650 °C, 3-5 min, and 50-100 MPa) and HIP (1230-17000 °C, 0-60 min, and 2 MPa) routes. Enhanced mechanical properties as well as fully dense samples were observed in SPS rather than HIP. Moreover, no grain growth was reported in SPSed compacts due to short processing time. At the same time, HIP-processed samples contained porosities [29]. Another study is done by Tapaszto´ et al. [30], who prepared Si_3N_4– based composites reinforced by single-walled CNTs (SWCNTs), MWCNTs, carbon black (CB), and exfoliated graphite (GR) through HIP (1700 °C, 3 h and 20 MPa) and SPS (1000-1650 °C, 3-5 min and 50-100 MPa). The experimental measurements confirmed that elastic modulus and hardness of SPSed samples are higher than those of HIPed ones.

The present review paper strives to scrutinize the potential effects of CNTs on the mechanical and physical properties of SPSed engineering ceramics and provide a broad overview of the unsolved challenges and suggested solutions for them.

2. Spark plasma sintering of CNT-ceramic matrix nanocomposites

2.1. CNT-Oxide ceramic matrix nanocomposites

2.1.1. CNT- ZrO_2 nanocomposites

Zirconium dioxide (ZrO_2) as an n-type semiconductor experiences a structural phase transformation from tetragonal (t) to monolithic structure (m) at 950 °C during cooling, as well as an approximately 4% volume expansion which induces microcracking and catastrophic fracture. The t → m allotropic phase transformation can be suppressed by the incorporation of lower valance oxide dopants such as Y_2O_3, MgO and CaO to selectively stabilize tetragonal or cubic zirconia and improve its fracture toughness [31]. Notably, the applied tensile stresses to zirconia-based ceramics persuade this transformation at the front of advancing cracks and hinder its further propagation due to the volume change-arisen compressive stresses. This phenomenon is called “phase transformation toughening mechanism” in ZrO_2. Another possible toughening mechanism is referred to as “ferroelastic domain switching” in which the c-axis of tetragonal unit cell switches or aligns along the maximum stress axis [32]. Moreover, some zirconia-based

View Article Online
DOI: 10.1039/C7NR01878A

ceramics such as magnesia-partially stabilized zirconia (Mg-PSZ) exhibit R-curve behavior (i.e. an increase in crack growth resistance during crack extension, especially large ones) [33]. Owing to their unique mechanical characteristics coupled with an appropriate combination of fracture toughness and strength (K_{Ic}=4-5 MPa.m$^{1/2}$ and strength >1000 MPa in the case of 3Y-ZrO_2), excellent biocompatibility, and aesthetic appearance, zirconia-based ceramic composites can be utilized in numerous applications from dental bridges to oxygen sensors, from grinding media to fuel cells, and from cutting tools to femoral heads [34, 35]. Contrary to the mentioned advantages, these materials generally suffer from low temperature degradation (LTD) in humid environments, moderate fracture toughness, unsatisfactory thermoelectric properties, and slow subcritical crack growth [32]. Doping with ceria is an effective approach to enhance fracture toughness of zirconia and its resistance to LTD [36]. As another approach, grain size reduction into the nanoscale can increase the resistance to LTD, but diminishes fracture toughness due to a reduction in the transformation toughening capability [37]. One of the promising strategies to enhance the fracture toughness as well as LTD is the inclusion of second phase in zirconia matrix such as CNTs. This section will cover these topics and address their different aspects.

A great deal of efforts has been made to fabricate fully dense zirconia-based components using SPS process. Recently, Melk et al. [38] investigated the effect of transformation toughening on the fracture stress (σ_f) and K_{Ic} of hot pressed and SPSed 3Y-ZrO_2 with grain sizes of 330 nm and 177 nm, respectively, both with similar artificial surface cracks. They reported a higher σ_f and K_{Ic} for hot pressed specimen, but lower hardness values. It is ascribed to the severity of phase transformation-induced toughening in SPSed specimens due to their smaller grain size.

Numerous research works have been done over the past decade investigating the considerable implications of CNT incorporation on the biocompatibility, mechanical and physical properties of SPSed zirconia matrix nanocomposites with the aim of generating novel CNT-dispersed ZrO_2 nanocomposites with exceptional features.

2.1.1.1. Mechanical properties

According to the literature, most of the specialized efforts have been concentrated on making improvements in fracture toughness of SPSed zirconia along with enhanced or maintained hardness through CNT incorporation [39]. The fracture toughness (K_{Ic}) of such ceramic systems are evaluated using the direct crack measurement (DCM), indentation strength in bending (ISB) and single edge notched beam (SENB) methods. Conventionally, the fracture toughness of CNT-reinforced ceramic matrix nanocomposites is measured by using a Vickers indentation test and reported as “indentation fracture toughness”. This method is based on the size of median radial cracks emanating from the corners of the indent at loads beyond the critical load required for crack initiation. In this technique, the fracture toughness could be calculated using Anstis equation (Eq. 2) [40]:

View Article Online
DOI: 10.1039/C7NR01878A

(Eq. 2) $$K_{Ic} = 0.016\left(\frac{E}{H}\right)^{1/2}\left(\frac{P}{c^{3/2}}\right)$$

where c is the crack length from the centre of the indentation imprint, E is the elastic modulus, P is the indentation load and H is the hardness obtained using Eq. 3:

(Eq. 3) $$H = \frac{P}{2a^2}$$

where a is half diagonal of the indent. At low crack-to-indent ratios, the following relation (Niihara equation or Eq. 4) [41] can be applied for Palmqvist cracks:

(Eq.4) $$K_{Ic} = 9.052 \times 10^{-3}.H^{3/5}.E^{2/5}.c^{-1/2}$$

To achieve true K_{Ic}, Melk et al. [42] created a sharp shallow notch on the surface of prismatic bars by ultra-short pulsed laser ablation and determined K_{Ic} by the strength in four-point bending test using Eq. 5 given by Munz and Fett [43]:

(Eq. 5) $$K_{Ic} = \frac{3F(S_1-S_2)}{2BW^2}Y\sqrt{a}$$

so that $$Y = \frac{1.1215\sqrt{\pi}}{\beta^{3/2}}\left[\frac{5}{8} - \frac{5}{12}\alpha + \frac{1}{8}\alpha^2\beta^6 + \frac{3}{8}\exp(-\frac{6.1342\alpha}{\beta})\right]$$

where S_1 and S_2 are the outer and inner spans, respectively. B is the thickness, W is the width, F is the applied load, a is the crack length, $\alpha = a/W$ and $\beta = 1 - \alpha$. They concluded that the true fracture toughness values are lower than those obtained by Vickers indentation. It is possibly attributed to the sharpness of the notch and crack length propagating ahead of the notch.

Nanoindentation test is also a prevailing method for measuring the nanoindentation hardness and the elastic modulus of CNT-zirconia nanocomposites as a function of the penetration depth [42, 44]. Melk et al. [42] reported that unlike K_{Ic}, both hardness and elastic modulus of the nanocomposites are diminished with increasing CNT content.

The first attempt made by Sun et al. [45] to enhance the mechanical properties of SPSed zirconia by addition of both SWCNT and MWCNT, was abortive. This was attributed to the insufficient load transfer from the matrix to CNTs due to the weak interfacial bonding, low bulk density at the presence of nanotubes because of their agglomeration in the grain boundary, and pores formation at the grain boundary due to the presence of the CNT agglomerates acting as defect sources. To obtain a uniform distribution of CNTs in zirconia matrix with no bundle formation, Datye et al. [46] utilized a CVD method for in situ growth of CNTs on the surfaces of the 3Y-TZP particles (Fig. 2a) and reported 30% increase in bending strength of 4.25 wt.% CNT-zirconia SPSed at 1600 °C compared to pure zirconia. Also, a slight decrease in hardness was observed due to the

View Article Online
DOI: 10.1039/C7NR01878A

reduction in grain size. The results showed that the fracture surface of these composites (Fig. 2b) undergoes a mixed mode of intergranular and transgranular fracture, an effective CNT/zirconia interfacial bonding and low porosity along with broken CNTs. In general, low initial density of the CNT–zirconia compacts compared to the pure zirconia, weak CNT-zirconia interfacial bonding and retained porosities after sintering as microstructural defects are the major reasons why CNTs incorporation in zirconia matrix leads to the degradation of its mechanical properties.

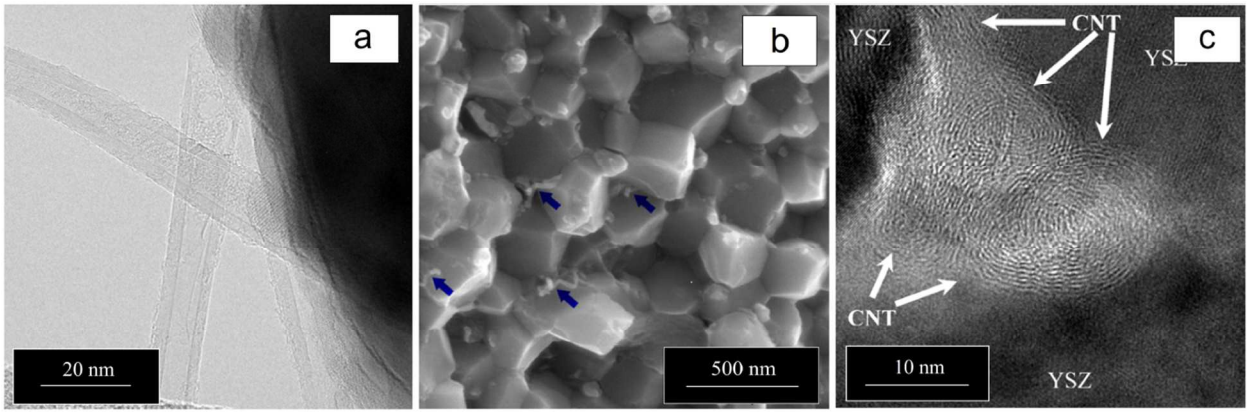

Fig. 2. (a) HRTEM image of in situ grown CNTs on zirconia particles by CVD technique (Reproduced from ref. 46 with permission from Elsevier [46]); (b) SEM image of fracture surface of 2.5 wt.% CNT-zirconia nanocomposite SPSed at 1400 °C (Reproduced from ref. 46 with permission from Elsevier [46]); and (c) HRTEM image of grain boundary of SPSed 5 wt. % CNT-YSZ nanocomposite (Reproduced from ref. 47 with permission from Elsevier [47]).

Among successful research works, most favorable report was published by Mazaheri et al. [47, 48] in which 5 wt.% CNT-yttria stabilized zirconia (YSZ) nanocomposites was fabricated by a fast SPS process at 1350 °C, and 88% increase in indentation fracture toughness up to 10.9 MPa.m$^{1/2}$, 30% in Young's modulus, 38% in shear modulus and 5.7% in hardness were observed predominantly due to the satisfactory CNT/zirconia interfacial adhesion. According to TEM images (Fig. 2c), structurally unchanged CNTs are randomly oriented within the grain boundaries and CNT/zirconia interfaces are flawless with no sign of amorphous carbon. The underlying mechanisms explaining simultaneous improvement in fracture toughness, strength, and hardness in these composite systems include crack deflection (Fig. 3a), uncoiling and stretching of entangled CNTs during intergranular crack propagation. The CNT-induced crack resistance often leads to crack bridging (Fig. 3b) and promotes the energy dissipation at the crack tip and increased toughening. It is noteworthy that CNT pull-out toughening mechanisms are out of question in these composites because the nanotubes are laid at grain boundaries, not inside the

View Article Online
DOI: 10.1039/C7NR01878A

ceramic grains. Also, a strong interfacial adhesion is observed between CNTs and matrix to preclude nanotubes from pull-out.

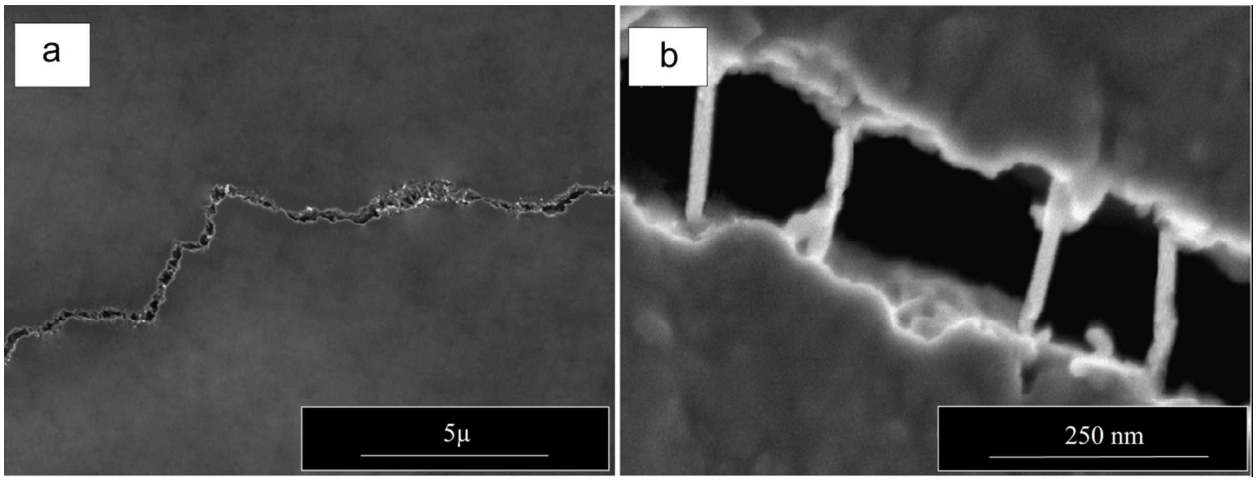

Fig. 3. SEM micrographs of a SPSed CNT-dispersed ZrO_2 nanocomposite showing (a) crack deflection and (b) crack bridging mechanisms (Reproduced from ref. 48 with permission from Elsevier [48]).

Zirconia exhibits superplastic deformation at high temperatures according to grain boundary sliding (GBS) accommodated by grain boundary diffusion [49]. For 3Y-TZP specimens, segregation of yttrium at grain boundaries develops a local electric field and consequently increases the activation energy for grain boundary diffusion [50]. To investigate the high temperature mechanical behavior of SPSed CNT-zirconia nanocomposites, Mazaheri et al. [48] performed the compressive creep tests at constant stress and reported a significant reduction in plastic strain at high temperatures due to CNT pinning to suppress GBS in spite of grain size refinement. Creep commences with a slight rearrangement of grains to arrive at a relaxed state and decreases with CNT entanglement and eventually terminates. The higher CNT content the lower the creep rate will be. In contrast, Castillo-Rodrıguez et al. [50-52] revealed that the CNT incorporation into 3Y-TZP matrix increases the strain rate at high temperatures compared to monolithic zirconia. Improvement in CNT dispersion results in lighter CNT agglomeration as well as high content of CNTs embedded at zirconia grain boundaries. In fact, CNTs act as lubricant agent, render GBS easier during creep deformation and lead to a decrease in the creep resistance of the nanocomposites. The preservation of CNTs and no microstructural evolution during the creep imply that the high-temperature deformation mechanism in CNT-3Y-TZP nanocomposites is GBS accommodated by grain-boundary diffusion same as in monolithic zirconia. CNT bundles embedded between 3Y-TZP grains influence the yttrium segregation and

View Article Online
DOI: 10.1039/C7NR01878A

facilitate the grain-boundary diffusion with lower activation energy compared to monolithic 3Y-TZP. It seems that further investigation is required for this controversial issue to shed light on the real mechanisms by which CNTs can affect creep behavior of SPSed CNT-zirconia nanocomposites.

The incorporation of CNTs into SPSed zirconia matrix leads to a decrease in coefficient of friction (CoF). Melk et al. [44] reported that the wear resistance lessens slightly with CNT addition up to 1 wt. %, while it grows for 2 wt. % CNT. At small load, low CoF and low wear rate are attributed to the exfoliation of the CNTs because of the high shear stresses induced during sliding and to the formation of a lubricating tribofilm over the contact area during the reciprocating sliding. At lower loads, CNT addition up to percolation value (2 wt. %) leads to an increase in CoF and significant reduction in wear rate, while at higher loads, an increase in CNT content gives birth to chipping and brittle fracture of these nanocomposites due to the weak CNT/zirconia interfacial bonding and tensile stresses generated during the scratch test.

2.1.1.2. Electrical and thermal properties

In general, the inclusion of uniformly dispersed unbundled nanotubes in zirconia matrix increases the electrical conductivity of SPSed nanocomposites [53]. To achieve a uniform dispersion and minimize CNT agglomeration, a broad spectrum of methods are proposed particularly sol-gel [54] and aqueous colloidal processing [55]. These techniques can include acid treatment [11], freeze drying [55, 56] and ultrasonication [51].

The electrical conductivity of CNT-ceramic nanocomposites with a percolation network is controlled by a variety of charge transport mechanisms such as charge transport along the CNT shells and hopping conduction across the nanotube-nanotube junctions (for CNT-Si_3N_4 nanocomposites) [57], thermal fluctuation-induced tunneling of the charge carriers through CNT-CNT junctions (for CNT-Al_2O_3 nanocomposites at temperatures higher than 50 K), and three dimensional variable range hopping through MWCNT-induced percolation network (in the alumina matrix at temperatures below 50 K) [58]. The improved electrical conductivity of CNT-dispersed zirconia nanocomposites from an ambient temperature up to ~180 °C is attributed to the thermal fluctuation-induced electron tunneling across nanotube-nanotube junctions [55], while at high temperatures, a combination of ionic and electronic conductivities is suggested [59].

To examine the processing effect on the electrical percolation threshold of the SPSed CNT-zirconia nanocomposites, Poyato et al. [55] fabricated fully dense 3Y-TZP composites with different CNT contents by colloidal processing and SPS. They showed that the CNT agglomeration gives birth to an overestimated amount of the percolation threshold (5.5 vs. 1.5 vol% CNT) due to the lower content of the CNTs really embedded at grain boundaries than the nominal one. The presence of CNT aggregates or large-diameter CNT bundles leads to high nanotube-nanotube junction resistivity and impose some restrictions on the overall composite

View Article Online
DOI: 10.1039/C7NR01878A

conductivity. Therefore, CNT uniform distribution reduces the CNT percolation threshold and enhances the room-temperature conductivity. It was confirmed that the electronic conduction through the nanotubes and a combination of the electronic and ionic conductivities through the zirconia bulk play a major role in the electrical response of these composites within the low and high temperature ranges, respectively. To determine the separate contributions of the individual nanotubes and their junctions in total electrical resistance, the impedance properties were modeled. It was shown that the electrical resistivity of these junctions remarkably decreases with an increment in temperature up to 160 °C due to the thermal fluctuation-induced electron tunneling across nanotube-nanotube junctions.

Limited machinability of ceramic workpieces due to their high hardness and brittleness has aroused interest in using a high precision machining technique called spark/electrical discharge machining (EDM) applicable for hard materials [60]. In this method, as a thermal erosion process, the material is removed from the electrically conductive workpiece by generating a series of recurring electrical discharges between electrode and workpiece immersed in a dielectric liquid [61]. Two approaches are taken to utilize EDM in zirconia as a nonconductive ceramic: (i) applying a conductive layer such as pyrolytic carbon on the surface of the zirconia workpiece referred to as assisting electrode and (ii) the incorporation of a conductive phase such as WC, TiN and CNT [62] into zirconia matrix [63]. Recently, Melk et al. [63] investigated the effect of CNT addition on the electrical and thermal conductivities of SPSed zirconia-based nanocomposites and their machinability using EDM. They obtained 0.5 wt.% CNT-zirconia nanocomposites with highest electrical conductivity equal to 888 S/m. This improvement was attributed to the large aspect ratio of CNTs to contribute in the formation of an entangled network of conductive pathways. These nanocomposites are successfully machined by EDM for which the material removal mechanism was spalling and melting/evaporation. Also, they investigated the thermal conductivity of 2 wt. % CNT-zirconia nanocomposites from room temperature up to 900 °C and found that the nanotubes decrease the thermal conductivity of zirconia due to the increase in porosity. Contrary to SPSed alumina-CNT nanocomposites for which electrical conductivity is highly dependent on CNT content, SPS processing conditions and bulk density, increasing the sintering temperature from 1350 °C to 1500 °C does not have a significant effect on the thermal conductivity of SPSed 0.5 and 1 wt. % CNT-zirconia nanocomposites. Also, a slight rise is observed in the thermal conductivity for 1 wt. % CNT at 1500 °C, originating from the grain growth at elevated temperatures [63].

2.1.1.3. Thermoelectric properties

Thermal-to-electrical energy conversion efficiency in thermoelectric devices depends directly on both parameters: (i) the Carnot efficiency and (ii) thermoelectric figure of merit, ZT, a dimensionless parameter which can be obtained by the following equation:

View Article Online
DOI: 10.1039/C7NR01878A

(Eq. 6) $$ZT = \frac{S^2\sigma}{\kappa T}$$

where S is the thermoelectric power or Seebeck coefficient, σ and **κ** are the electrical and thermal conductivities, respectively, and T is the absolute temperature [64]. Two novel approaches can be taken to enhance the thermoelectric property: (i) nanstructuring to develop lower thermal conductivity due to the higher phonon scattering at the nano-grain boundaries and (ii) compositing with nanodispersoids to reduce the thermal conductivity of a thermoelectric matrix with no significant reduction in electrical conductivity. In the latter case, newly created dispersoids/matrix boundaries stimulate the additional interface scattering and increase the Seebeck coefficient via carrier-energy filtering or quantum confinement of the charge carriers. CNTs are among the most promising nanostructures for thermoelectric applications either in the form of sintered bulk [65] or as an additive[66]. Zhan et al. [67-69] indicated that CNT incorporation into ceramic matrices improves the thermoelectric power of nanoceramics due to its significant effect on increasing electrical conductivity and thermal resistance. Particularly, they found that the SPSed 10 vol% CNT/3Y-TZP nanocomposites could be exploited as a new thermoelectric material with ZT of ~0.02 at 850 K which needs to be enhanced by improving electrical conductivity of the composites using pure metallic CNTs. Variation of σ, S and ZT with temperature is presented in Fig. 4. As seen, increasing temperature up to 545 K decreases the electrical conductivity. It implicitly indicates a metal-like behavior. Afterwards, it gradually increases presumably due to unexplored surface absorption behavior at high temperatures.

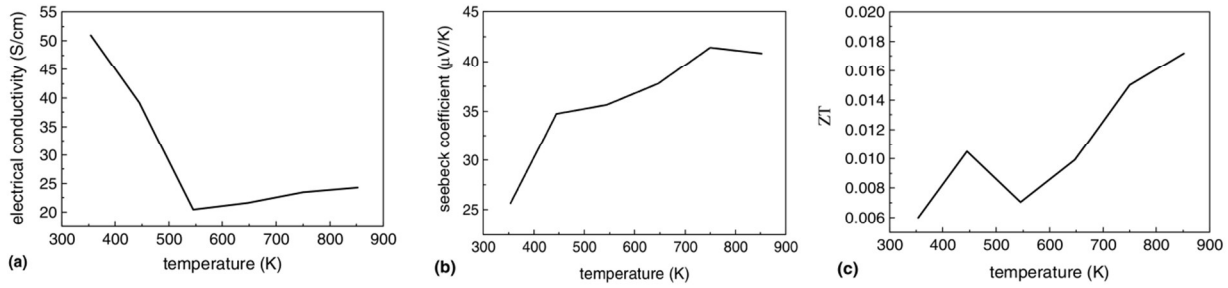

Fig. 4. The variations of (a) σ, (b) S and (c) ZT as a function of sintering temperature (Reproduced from ref. 69 with permission from Elsevier [69]).

2.1.1.4. Physical properties

Grain size refinement as a result of CNT addition to zirconia matrix is generally reported in the literature [47, 70-73]. For instance, Duszová et al. [70] reported 40% decrease in the grain size with

View Article Online
DOI: 10.1039/C7NR01878A

addition of 4 wt.% CNT compared to monolithic zirconia, as well as the reduction in both hardness and indentation fracture toughness. However, Karanam et al. [72] found that 1 wt.% CNT incorporation into YSZ matrix suppresses the densification and grain growth during SPS and results in nonuniform grain size distribution and significantly enhanced hardness. They reported that the nanocomposites with more CNT content underwent an increase in both grain size and hardness (Fig. 5). As another notable research work, Shen et al. [73] reported that the CNT addition in zirconia matrix results in grain refinement, decreased hardness and enhanced fracture toughness. They studied the phase transformation of SPSed CNT-zirconia nanocomposites during Vickers indentation by using Raman spectroscopy and revealed that the tetragonal to monoclinic phase transformation initially decreases with increasing CNT content up to 3 vol% CNT and then increases. It worth noting that Datye et al. [46] reported no evidence of the tetragonal to monoclinic phase transformation in as-SPSed CNT-3Y-TZP samples based on X-ray diffraction results. Contrary to zirconia matrix, no phase transformation or structural damage in CNTs is generally noticed during SPS processing of CNT-zirconia nanocomposites [47, 48].

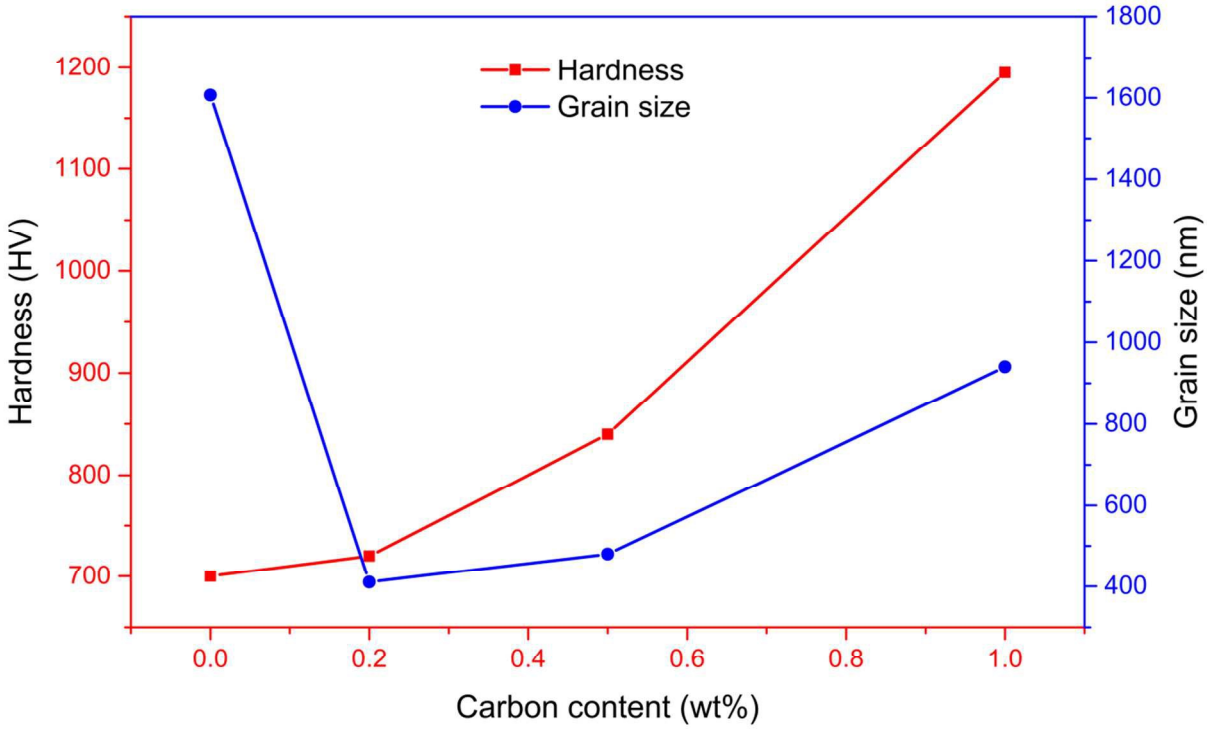

Fig. 5. The possible effects of CNT content on the grain size and hardness of the SPSed CNT-YSZ nanocomposites (Reproduced from ref. 72 with permission from Elsevier [72]).

View Article Online
DOI: 10.1039/C7NR01878A

SPSed CNT-zirconia nanocomposites requires more sintering time and temperature than those of monolithic zirconia [73]. Additionally, the presence of CNTs lowers the densification rate due to hindered GBS or grain boundary migration through cation lattice diffusion which is called "pinning effect". The lower compaction of CNT-containing zirconia powder respect to pristine zirconia could be described with regard to the suppression of the powder sliding and rearrangement by CNTs [47, 48]. In contrast, Milsom et al. [71] demonstrated that addition of 2 vol.% CNT in zirconia matrix significantly reduces the sintering activation energy through the formation of a CNT-based percolation network and developing a lower energy diffusion pathway. In fact, the nanotubes act as a sintering aid presumably through enhancing cation diffusion along the necking regions. Furthermore, they proclaimed that the sintering mechanism for the zirconia matrix nanocomposites is grain boundary diffusion and the presence of the nanotubes does not influence the sintering mechanism. In contrast, Shen et al. [73] affirmed that the CNT addition changes the active sintering mechanism from grain rotating and sliding to grain boundary diffusion as a consequence of pinning effect of CNTs. They also observed surface spalling at high CNT content and indentation force probably due to weak CNT/zirconia interfacial cohesion and CNT agglomeration. More recently, Zahedi et al. [74] concluded that the densification behavior of SPSed CNT/8Y-YSZ is controlled by the CNT dispersion. At CNT contents lower than 2 vol%, better initial packing enhances the densification process; while the formation of the agglomerates at higher CNT content suppress the sintering.

2.1.1.5. Biocompatibility

A tremendous amount of experimental data is released around CNT toxicity and biocompatibility, but inconsistent and conflicting [75]. For instance, Pulskamp et al. [76] reported no sign of acute CNT toxicity in pulmonary epithelial and macrophage cell lines, while Lam et al. [77] remarked that the nanotubes are prone to producing inflammation, fibrosis, epithelioid granulomas and biochemical/toxicological alterations in the lungs. These contradictions could be unraveled by taking several critical effective parameters into consideration such as impurities, surface functionalization and modification, exposure routes and structural characteristics including shape, number of CNT walls, length and agglomeration [78].

Zirconia-CNT nanocomposites are recognized as a promising biomaterial in various applications such as orthopedic implants [79], dental implants [80] and biosensors [81] owing to their satisfactory mechanical properties, proper biocompatibility and trivial amount of biodegradability. Mohamed et al. [79] investigated the possible effect of CNTs on the biocompatibility, biodegradation and cell attachment of SPSed CNT/3Y-TZP nanocomposites with satisfactory mechanical properties proposed as an alternative for conventional zirconia hip implants. The vitality and osteoblast surface proliferation monitored by MTT assay revealed that the CNT incorporation into 3Y-TZP matrix has no considerable effect on cells vitality and cells are proliferated as high as pristine

View Article Online
DOI: 10.1039/C7NR01878A

zirconia. Additionally, CNT-containing zirconia specimens provide better cell attachment (Fig. 6), proper biocompatibility, no acute toxicity and paltry amount of degradation at low temperatures.

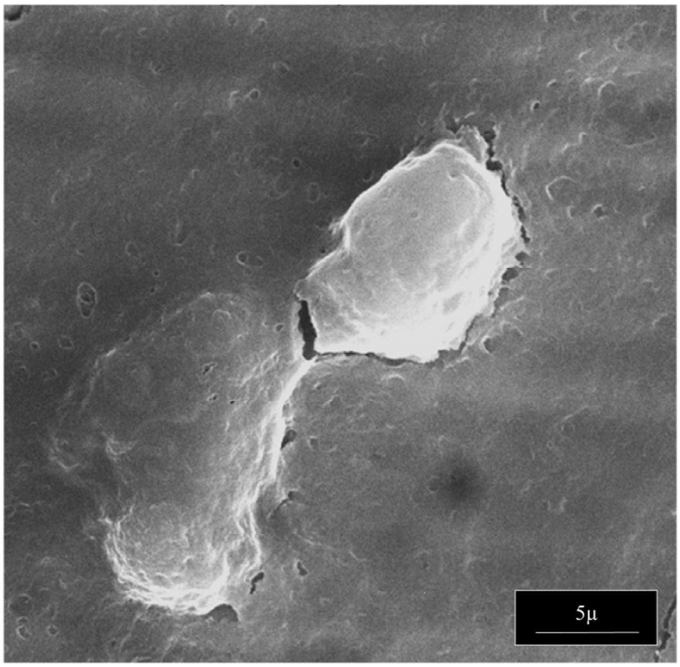

Fig. 6. Cell attachment of CNT-containing zirconia specimens (Reproduced from ref. 79 with permission from Elsevier [79]).

2.1.2. CNT- Al_2O_3 nanocomposites

Among the engineering ceramics, alumina is one of the most popular materials in industrial applications due to its thermal/electrical insulation properties, excellent mechanical strength and chemical inertness. However, low fracture toughness and weak thermoelectric characteristics restrain some of critically novel applications of these ceramics. Hence, a great deal of technical effort has been conducted over the past decade to transfer the extraordinary toughness, mechanical superiorities, and fabulous thermal / electrical conductivities of CNTs to the brittle and insulator alumina [39]. However, these exceptional features cannot be fully obtained due to some serious challenges including weak Al_2O_3-CNT interfacial adhesion and non-uniform distribution of CNTs within the ceramic matrix [39]. The recent research works have strived to develop novel strategies to overcome the aforementioned challenges with the aim to enhance the pertinent properties from mechanical, thermal, electrical, and physical points of views.

View Article Online
DOI: 10.1039/C7NR01878A

2.1.2.1. Physical and Mechanical properties

In general, the presence of impurities, porosities and cracks formed during the fabrication of alumina are the main causes for its low fracture toughness. This shortcoming can be eliminated by using appropriate additives [82-84]. For example, Chakravarty et al. [85] investigated the effect of grain size and content of MgO particles as well as SPS parameters on the hardness, strength and fracture toughness of Al_2O_3. In conformity with the results, the highest density value was obtained for 100 nm MgO, while 15 nm MgO particles gave the better strength (600 MPa), hardness (25 GPa) and fracture toughness (4.5 $MPa.m^{1/2}$). Moreover, it was shown that the compaction capability of SPS technique at much lower temperatures in short times results in protection of a small grain size to provide the sintered samples with a higher strength and hardness.

Other suitable additive for improving the characteristic features of alumina is carbon materials. Maensiri et al. [86] studied on the fabrication and mechanical properties of hot-pressed alumina reinforced with 2.5 vol% carbon nanofibers (CNFs). They observed an improvement in fracture toughness as high as 13% compared to pure alumina. It is while the hardness and bending strength of the nanocomposites were decreased by increasing CNF volume fraction. It was concluded that the main toughening mechanism in this binary system is the crack-bridging effect of CNFs during the crack propagation. Beyond the nanofibers, CNTs are also employed in this regard. Recently, Ahmad and coworkers [87] have concentrated on the mechanical properties of CNT-Al_2O_3 nanocomposites fabricated by hot-pressing. Their results showed that the fracture toughness, hardness and flexural strength of the nanocomposites may improve by 94%, 13% and 6.4% respectively, compared to monolithic alumina. In these systems, Al_2O_3 undergoes a carbothermal reduction in the presence of CNTs and forms an oxycarbide (Al_2OC) layer at the Al_2O_3/CNTs interface under a reducing atmosphere and elevated processing temperatures. This layer benefits from a high chemical compatibility with nanotubes and Al_2O_3 and enables the matrix to effectively transfer applied load into the CNTs. Therefore, the composite structure inherits its superior toughness from the strong interfacial regions. In another study, Kasperski and coworkers [88] explored the microstructure and mechanical properties of MWCNT-Al_2O_3 composites compacted by SPS. They investigated the potential effects of wall number on the microhardness, bending fracture strength and fracture toughness. According to their results, the crack propagation through the grain boundary decohesion phenomenon drives the CNTs to become progressively unfolded and taut. All the unfolded CNTs do bridge the crack at a certain point and enhance the overall fracture toughness. In contrary, the fracture energy is decreased due to breakage of some bridging CNTs. It is noted that the elastic deformation energy absorbed by an individual nanotube during the unfolding is low, but the cumulated energy required for the fracture of all bridging CNTs is much higher and this would thus likely limit the crack propagation [88].

View Article Online
DOI: 10.1039/C7NR01878A

The recent findings indicate that SPS parameters such as processing temperature may bilaterally affect the fracture toughness of these material systems. Jiang et al. [89] studied the potential effects of SPS temperature on the mechanical properties of 10 vol% CNT-Al_2O_3 systems. Microscopic observations confirmed that CNTs are agglomerated within the Al_2O_3 matrix even after ultrasonication and ball milling. It was shown that the sample sintered at 1150 °C shows the best combination of toughness (9.7 MPa $m^{1/2}$) and hardness (1610 kg mm^{-2}). While the hardness is decreased by an increment in the sintering temperature above 1150 °C, the fracture toughness is steadily decreased as a function of temperature but remains at least twice as high as that of monolithic alumina. This temperature-controlled reduction is attributed to the in situ conversion of CNTs to graphite sheets during an allotropic phase transformation. Moreover, as the processing temperature begins to rise, the increased porosity in the matrix structure leads to degradation of fracture toughness and hardness.

Another effort is associated with a research work by Zhang and coworkers [90] who investigated the mechanical properties of CNT-Al_2O_3 nanocomposites synthesized by chemical vapor deposition (CVD) and densified by SPS at 1150 and 1450 °C. Their findings were completely different from those reported by Jiang et al. They indicated that the relative densities of all CNT-Al_2O_3 composites sintered at different temperatures are lower than that of the pristine Al_2O_3. The density of the CNT-Al_2O_3 system is increased with an increment in CNT content to a maximum, and then decreased with a descending trend. For example, the maximum fracture toughness of 8.25 wt.% CNT-Al_2O_3 composite after sintering at 1150 °C is somewhat 1.74 $MPam^{1/2}$, exactly equivalent to half of that for pure Al_2O_3 sample at the same temperature. In addition, the hardness of these nanocomposites becomes lower than that of pure Al_2O_3 when the CNT content is higher than the optimum value (5-8 wt.%) [90]. Similar results are reported by Puchy et al. [91] who studied the microstructure and indentation toughness of SPSed binary CNT-Al_2O_3 systems with different CNT contents. In conformity with their results, the monolithic alumina was fully dense but the SPSed CNT-Al_2O_3 systems were porous due to CNT agglomeration. In fact, as the CNT content increases, the intensity of agglomeration becomes worsened. The nanocomposite with 5 wt.% CNT bears a maximum fracture toughness of 4.14 $MPam^{1/2}$, while the fracture toughness of 3.24 $MPam^{1/2}$ can be obtained for monolithic Al_2O_3 sample. It shows that a better control over the agglomeration of CNTs is required to tailor the mechanical characteristics and obtain the superior properties in SPSed CNT-Al_2O_3 composites. Otherwise, an enhancement in mechanical properties will not be observed as a result of CNT incorporation.

2.1.2.2. Electrical and Thermal properties

It is possible to reduce the amount of amorphous carbon after the allotropic phase transformation of CNTs under SPS by controlling the processing conditions. If practical, the electrical conductivity improves as electrical current easily flows between nanotubes. Inam et al. [92] explored the electrical conductivity of SPSed CNT-Al_2O_3 nanocomposites and put an emphasis on carbon black and its influence on the electrical behavior. They claimed that the electrical

View Article Online
DOI: 10.1039/C7NR01878A

conductivity of SPSed CNT-Al_2O_3 nanocomposites is very high compared to carbon black-dispersed Al_2O_3 nanocomposites. It is attributed to the fibrous nature and high aspect ratio of the nanotubes. In addition, the electrical conductivity of these ceramics is enhanced by an increase in Al_2O_3 grain size due to increased density of CNTs at the grain boundaries [92]. In this work, the highest obtained electrical conductivity was 576 S/m for 5 wt% CNT-Al_2O_3 nanocomposites. In another study, to investigate the effect of CNT content on the electrical conductivity, Kumari et al. [93] studied the synthesis, microstructure and electrical behavior of SPSed CNT-Al_2O_3 nanocomposites. They reported that the CNT addition enhances this property. The measurements were determined using a four-point-probe technique [93]. Based on the results, the electrical conductivity increases with the CNT content at predetermined SPS temperatures. This event is attributed to more CNTs inside the composites to stimulate the formation of continuous CNT-based percolation networks in the matrix structure. Moreover, the electrical conductivity increases with sintering temperatures. This enhancement can be attributed to the nanocomposite bulk density as a direct function of the sintering temperature [93].

One of the effective parameters to manipulate the electrical behavior of SPSed CNT-added Al_2O_3 systems is the way sintering procedure occurs. For example, Sikder et al. [94] have observed that in these systems, electrical conductivity values are almost the same as obtained for green specimens. However, an increase in electrical conductivity beyond 0.6 vol.% CNT is observed compared to the green samples. Also, applying the pressureless sintering (PLS) approach produces the samples with higher electrical conductivity rather than pressure-assisted SPSed samples and green specimens. Another aspect of electrical conductivity is its dependence on the structural direction. To provide clarification, Zhan et al. [67] compared the thermal conductivity of SWCNT-dispersed alumina composites for transverse and in-plane directions. It was found that unlike the transverse thermal conductivity, the incorporation of SWCNT ropes improves the in-plane one, while maintains the in-plane thermal diffusivity of the matrix. It is explained by the electronic nature of these systems.

2.1.3. CNT- SiO_2 nanocomposites

Although brittle, silica-based materials has potential applications in optical and optoelectronic devices [95] owing to their great ability to form various polymorphs with outstanding physical, mechanical, thermal and optical properties [96]. Incorporation of CNT is proposed to be a promising approach to enhance fracture toughness as well as electrical and thermal conductivity of bulk silica. Silica-CNT nanocomposites, as electromagnetic shielding materials [97], exhibit low dielectric constant [98] and have photonic applications such as optical switching and optical waveguides [99]. Several approaches have been taken in order to improve homogeneity of CNT dispersion in silica matrix by SiO_2/CNT interface modification including surfactant utilization [100], chemical functionalization [101], milling of CNT in colloidal silica [102], in situ synthesis of silica

View Article Online
DOI: 10.1039/C7NR01878A

using organic [103] or inorganic [104] sol-gel process. Since CNT incorporation in silica matrix decelerates its sintering kinetics, several consolidation techniques for densification of SiO_2/CNT powder blends is employed including conventional sintering [104] hot press [105] and SPS [106]. SPS process benefits from several advantages especially minimization of CNT damage as a result of very short sintering time, so that the SPSed silica-CNT nanocomposites have enhanced mechanical, thermal and electrical properties due to densified microstructure to the theoretical level. Guo et al. [107] homogeneously dispersed MWCNTs in colloidal silica via attrition milling and consolidated the obtained powder blends using SPS. They investigated the mechanical properties of SPSed silica-CNT nanocomposites as well as their thermal [108] and electrical [102] conductivities. SEM images from fracture surface of these composites (Fig. 7a) showed the adhesion of silica matrix on the surface of protruded CNTs indicating the presence of strong SiO_2/CNT interfacial bonding. Fully dense silica-CNT nanocomposites exhibit an increase of 275% in fracture toughness and 38% in elastic modulus compared to SPSed pure silica. The jagged path of crack propagation and CNT pullout and bridging in silica-CNT nanocomposites (Fig. 7b) specify that the crack deflection and elastic/frictional CNT bridging are active toughening mechanisms [107]. Recently, Dillon et al. [106] fabricated silica-CNT nanocomposites through coating of mesoporous silica on nitrogen-doped and boron-doped CNTs by sol-gel process (Fig. 7 (c-e)). This process enjoys various advantages including: (i) homogenous distribution of CNTs in silica matrix; (ii) improved SiO_2/CNT interface due to surfactant modification of CNTs; (iii) no need to SiO_2/CNT powder blend pre-treatment and (iv) CNT damage prevention during consolidation due to coating prior to sintering. However, with the exception of the boron-doped CNT-silica nanocomposites, an increase in hardness up to 50% is reported for silica-CNT nanocomposites, indicating a stable CNT dispersion. Also, according to TEM observations (Fig. 7f), good SiO_2/CNT interfacial bonding is supervened upon improved dispersion. CNTs were engulfed in an amorphous silica coating (Fig. 7g) in which the metallic nanoparticles are embedded (Fig. 7h) as a result of catalyst remnants migration from CNTs into the silica layer and their crystallization during annealing.

View Article Online
DOI: 10.1039/C7NR01878A

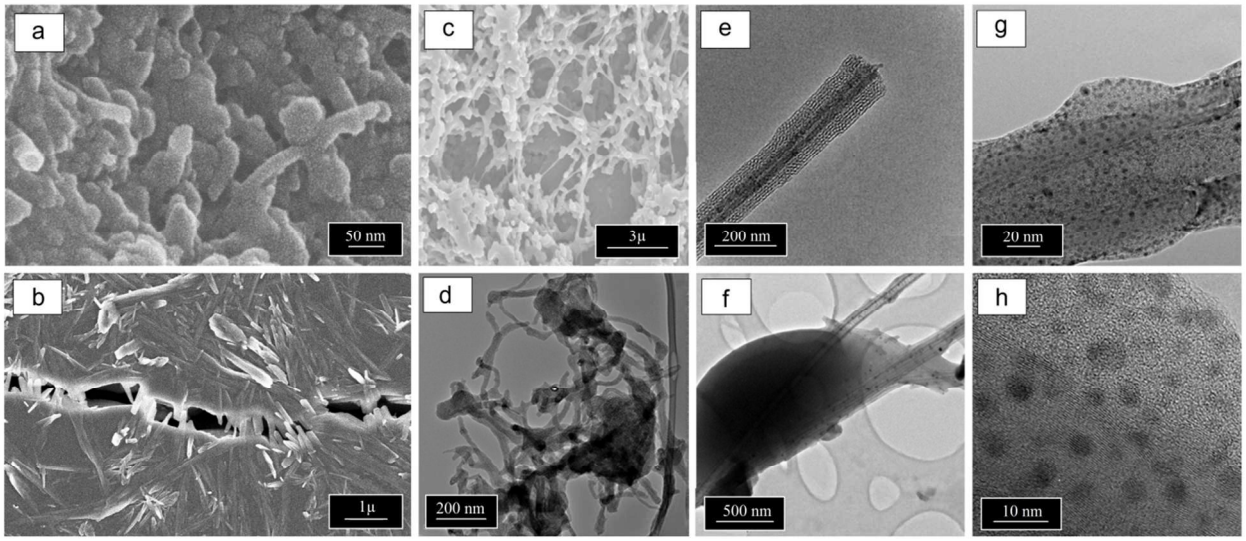

Fig. 7. SEM/TEM images of (a) fracture surface of 5 vol% CNT-silica nanocomposites SPSed at 1050 °C for 5 min under pressure of 50 MPa, (b) crack propagation path through SPSed silica-CNT nanocomposites (Reproduced from ref. 107 with permission from Elsevier [107]), (c) mesoporous silica with interconnected wheat-like structures, (d) silica coating on CNTs, (e) mesoporous ordering of the coating, (f) SPSed CNT-silica nanocomposite and (g, h) CNT coating with amorphous silica through sol-gel (Reproduced from ref. 106 with permission from Elsevier [106]).

Guo et al. [102, 108] investigated thermal and electrical conductivity of SPSed silica and CNT-containing silica nanocomposites. They reported 65% increase in thermal conductivity due to the incorporation of 10 vol% CNT in silica matrix, much lower than predicted one (4.08 W m^{-1} K^{-1} vs. 102.47 W m^{-1} K^{-1}) according to the suggested model by Nan et al. [109]. This is because of CNT/CNT and CNT/SiO_2 interfacial thermal resistance which was neglected. With taking them into account, the thermal conductivity of the nanocomposites, k_c is given by Eq. 7 [13]:

(Eq. 7) $$k_c = k_m + \frac{k_f L}{2R_i k_f + L}\langle \cos^2\theta \rangle V_f$$

where L is the tubes length and R_i is roughly 8.0×10^{-8} m^2 K^{-1} W^{-1}. According to above formulation, thermal conductivity of 10 vol% CNT-silica SPSed nanocomposites is in the range between 2.67 and 4.47 W m^{-1} K^{-1}, which is in consistent with the measured one.

Also, electrical conductivity of 10 vol% CNT-containing silica nanocomposites are noticeably higher than that of pure silica; 64.49 S/m versus 10^{-13} S/m, indicating the conversion of the nanostructured silica insulator into metallically conductive material [102]. In return, de Andrade et

View Article Online
DOI: 10.1039/C7NR01878A

al. [101] reported a regardless increase in electrical conductivity up to 10^{-4} S/m for 0.35 vol% CNT-silica SPSed nanocomposites.

2.1.4. CNT- HA nanocomposites

Hydroxyapatite (HA) is a synthetic ceramic with a chemical formula $Ca_{10}(PO_4)_6(OH)_2$ and bears a proper bioactivity with human tissues [110]. This ceramic benefits from a broad spectrum of sophisticated applications among which tissue engineering, metallic implants, purification and separation of biological molecules are of prime significance. However, brittle nature and poor strength of HA bulk ceramic prohibit its usage as load bearing materials in clinical areas. Hence, recent research works have concentrated on the modification of HA properties through the incorporation of ceramic fillers such as Al_2O_3, ZrO_2, and SiC. In this regard, CNTs with excellent osteoblast adhesion and biocompatibility have been deemed as a potential candidate to toughen and strengthen HA [111]. A variety of synthesis techniques are developed to fabricate homogenous CNT-HA blends among which laser surface alloying, plasma spraying, electrophoretic deposition, and hot pressing are the most important [112]. Recently, SPS technique has been exploited to densify these binary systems for biological and mechanical applications. Hereof, a concise overview of the related effects is provided.

2.1.4.1. Physical Properties

In SPSed CNT-HA nanocomposites, CNTs often locate along the grain boundaries of the matrix ceramic, prevent grain growth, and accelerate its refinement. Thus, the incorporation of CNTs into HA is reported to decline the grain size. In contrary, the relative density of such nanocomposites increases as a direct function of CNT content. This enhancement is attributed to a homogeneous temperature distribution arisen from intrinsically superior thermal conductivity of CNTs [113].

A review on the literature suggests that there exist some processing and chemical factors to bilaterally affect the physical properties of SPSed CNT-HA ceramic systems. These factors include:

(i) **Agglomeration of CNTs.** The agglomeration or clustering of CNTs potentially gives rise to the in situ formation of large pores. In fact, the present pores tend to fuse around the nanotubes due to the interfacial shrinkage arisen from the large difference between thermal expansion coefficients of HA and CNTs. An increase in sintering temperature provokes this difference and facilitate the formation of micro-pores [113].

(ii) **Sintering temperature.** An increment in sintering temperature results in grain growth of HA matrix, because excellent thermal and electrical conductivities of CNTs (2890 W/mK and 2 ×

View Article Online
DOI: 10.1039/C7NR01878A

10^4 S cm^{-1}, respectively) provide the required energy for grain growth at low processing temperatures. Another possibility with increase in SPS temperature is the thermal deposition of HA matrix. It is confirmed by Wang et al. [114] who observed the allotropic conversion of HA to β-TCP after SPS at 1200 ºC for 10 min. Moreover, elevated sintering temperature simultaneously with high pressure and current density can induce some defects such as kink, onion, and grahene induced in CNT strands (Fig. 8).

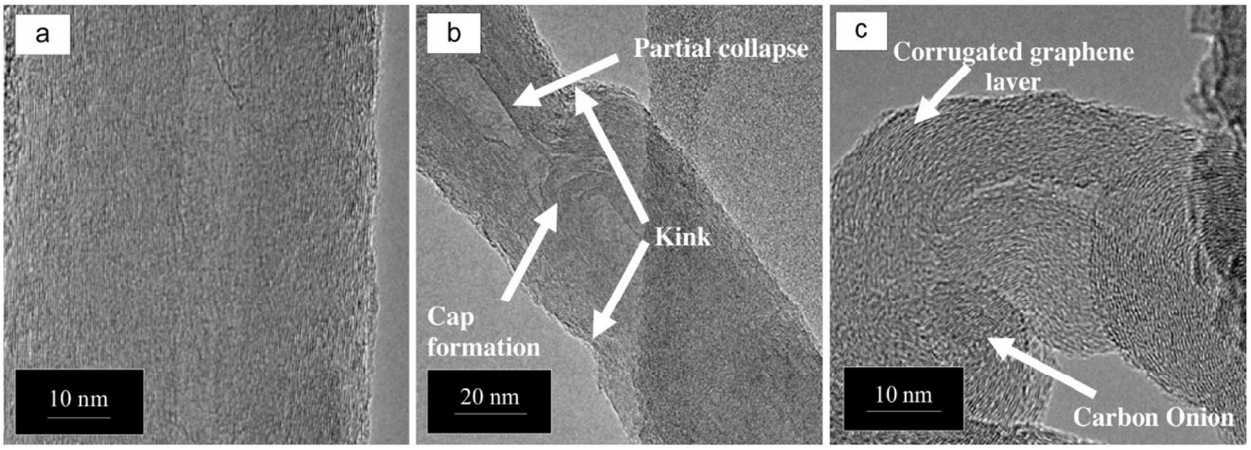

Fig. 8. High resolution TEM photographs of as-received CNT(a) and CNTs in HA-CNT nanocomposite which SPSed at 1373k under 60MPa pressure for 5 min which shows induced defects to CNTs (b and c) (Reproduced from ref. 115 with permission from Elsevier [115]).

(iii) **Incorporation of third material.** Herkendell et al. [116] showed that the addition of Ag nanoparticles to 4 wt% CNT-dispersed HA composites decreases grain size and increases the final relative density thank to its lower melting point (~960 °C).

2.1.4.2. Mechanical Properties

In general, CNT addition to HA ceramics increases their bending strength due to the activation of some toughening mechanisms namely CNT pull-out, crack deflection and crack bridging. It can also enhance the hardness and elastic modulus of HA-based ceramics by inhibition of grain growth and intrinsically high mechanical features of CNTs. Similar to physical behavior, the mechanical properties of SPSed CNT-filled HA nanocomposites may be affected by several processing parameters. These factors include:

(i) **Sintering temperature.** Generally believed, with an increment in SPS temperature, some mechanical characteristics such as fracture toughness, elastic modulus and hardness will increase first, and after a maximum peak, undergo a descending trend [114, 117, 118]. In fact, a temperature

View Article Online
DOI: 10.1039/C7NR01878A

variation in SPS process may switch the active fracture mechanisms depending on the applied temperature range. It is shown that the fracture mechanism of CNT-dispersed HA systems switches from transgranular to intergranular mode by increasing the sintering temperature. Also, further temperature increment may restore that to its initial mode (Fig. 9) [119]. In transgranular mode, residual pores with no CNT pull-out are visible, but in intergranular one, pull-outs form and inhibit the crack propagation. As to high-temperature mechanical behavior, the nanotubes form a continuous percolation network within HA matrix and prevent the grain growth at elevated temperatures. A new adverse scenario can be stimulated at high temperatures. Sintering of these ceramics at high temperatures may change the crosslinks and weaken the reinforcing effects of the nanotubes [119, 120]. Some researchers reported different temperatures at which the highest mechanical properties are achieved for SPSed CNT-HA composites with different content of CNTs [120].

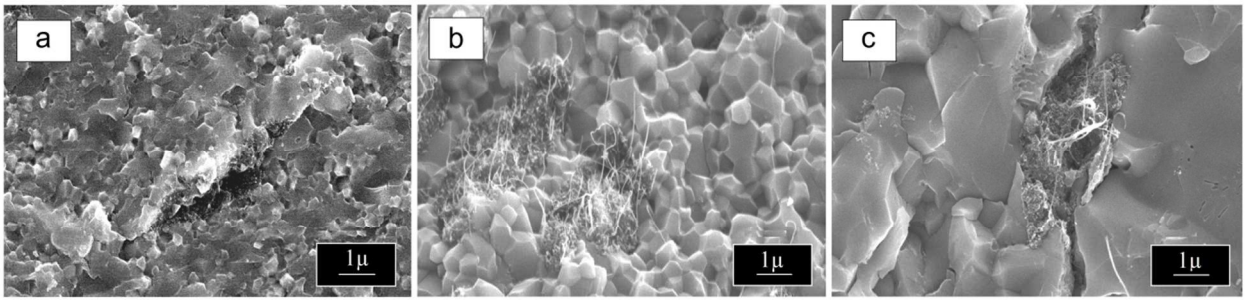

Fig. 9. SEM photographs of CNT-HA nanocomposite fracture surfaces SPSed at (a) 1000°C, (b) 1100°C, and (c) 1200°C. (a) and (c) show a flat surface implying the transgranular mode as the main fracture mode, and (b) exhibits a rough surface implying the intergranular mode as the main fracture mode (Reproduced from ref. 119 with permission from The Royal Society of Chemistry [119]).

(ii) **Agglomeration of CNTs.** The excessive addition of CNTs to HA-based ceramics can result in a heavy agglomeration of the nanotubes and increase the pores around them. These pores may degrade the high-temperature hardness and fail the optimal properties [111].

(iii) **Incorporation of third material.** It is shown that the addition of Ag nanoparticles to binary CNT-dispersed HA systems enhance the fracture toughness by virtue of their capability for easy plastic deformation and easy energy absorption [116].

Recently, some research works have addressed the tribological properties of SPSed CNT-HA nanocomposites. It is found that wear resistance is increased by the inclusion of CNTs. It is ascribed to the superior mechanical characteristics of the nanotubes and their lubrication behavior. In fact, during the macro-wear, superficial regions of CNTs are transformed into

View Article Online
DOI: 10.1039/C7NR01878A

graphene layers and reduce the coefficient of friction as lubrication agent. It is confirmed by Lahiriat et al. [115] who SPSed the monolithic HA and 4 wt.% CNT-HA system at 1100 °C and investigated their wear behavior in both macro and nano scales. They used nanoindentation and ball-on-disk tests to induce nano and micro wears, respectively. In micro mode, 66% increase in wear resistance and 60% reduction in coefficient of friction (CoF) has been found after CNT incorporation. This reduction is attributed to the surface-released graphenes and their lubrication behavior. However, in the nano-scale, the outcome was different. The empirical results revealed that although 45% improvement in the wear resistance was observed owing to the enhanced mechanical properties, the nano-indentator was unable to release CNTs from surface and induce damage to them. This is why the low degree of lubrication property was observed as well as 14% increase in CoF.

2.1.4.3. Biological properties

The SPSed CNT-HA nanocomposites exhibit excellent bone formation ability because of intrinsically excellent mechanical and structural properties of CNTs [114, 116]. The complex structure of CNTs (i.e. sidewall and the end cap) positively affects proteins bound to the surface of these composites [121]. Furthermore, HA may decompose into β-TCP (beta tri-calcium phosphate) phase during SPS and lead to improved cell attachment and chemical affinity with bone tissue in vivo [120]. In this regard, Xu et al. [121] reported that the addition of 2 vol% CNT to SPSed-HA matrix can increase the concentration of bounded proteins from 7.16 to 10.06 ug/ul. This favorable effect on protein bonding maintains constant at high CNT content and even 10 or even 80 vol% CNTs does not have unfavorable effect on the cell attachment [113, 114].

2.1.5. CNT- MgO nanocomposites

Magnesium oxide (MgO) as an eco-friendly and inexpensive ceramic benefits from a broad spectrum of engineering applications among which catalysis, plasma display panels, recycling of waste materials, and superconductors are the most significant [122]. The incorporation of CNTs into MgO structure is claimed to induce some interesting electrical characteristics and suggest them as the positive electrodes in asymmetric supercapacitors (ASCs) owing to MgO role in improving the electrochemical performance. However, MgO has a large band gap to render it electronically inactive and restrict its usage in energy storage applications. CNTs as secondary additive may solve this problem as well as improve mechanical characteristics [122]. In fact, CNT addition can transfer the strength and stiffness of nanotubes to MgO and control the size and morphology of MgO nanoparticles [123]. However, there exists a key drawback to compactability of MgO powder blends. It is observed that adding CNTs gives rise to lower densification in common sintering techniques. To tackle this problem, an elevated sintering temperature is required to adversely result in the thermal damages of the nanotubes [124]. Therefore, the SPS

View Article Online
DOI: 10.1039/C7NR01878A

technology as a novel process is considered as an appropriate alternative and recently addressed to eliminate this deficiency.

Generally, CNT incorporation in MgO-based systems declines the final relative density and grain size due to the inhibition of grain growth and changes the finished mechanical properties. In this regard, the fine dispersion of nanotubes plays a pivotal role. It is indicated that if the dispersion of CNTs and CNT-matrix bonding are in excellent fashion, the hardness may be enhanced. Also, CNT addition can increase fracture toughness of MgO matrix with the intergranular mode as the main fracture mechanism. In fact, the nanotubes locate at intergranular sites and elevate the fracture toughness due to the activation of some toughening mechanisms including pull-out, crack-deflection, and crack-bridging. Other physical features also may be manipulated by CNT addition. For instance, the electrical conductivity of MgO can be changed from insulator to conductive material due to the excellent electrical properties of the nanotubes [125]. These potential influences strongly depend on the SPS parameters. An increment in applied pressure can result in two significant events: (i) the densification enhancement owing to the rearrangement of grains blocked by CNTs, and (ii) the pulverization of matrix agglomerates. In addition, better densification will be obtained with an increase in dwell time, especially for lower pressures and higher temperatures [126].

Less attention is paid to SPSed MgO-CNT nanocomposites. In a simple study, Peigney et al. [125] processed (0, 2.3, and 7.1 wt %) CNT-MgO composite systems at 1650 °C by catalytic chemical vapor deposition (CCVD) method and studied the effects of CNT addition on the properties of SPSed MgO systems. As to physical properties, the relative density calculations show higher values for monolithic MgO (98.3%) than composite forms, and it is reduced with CNT content (93.4% for 7.1 wt% CNT-containing sample). Also, the grain size reduces from 31 μm to 60-70 nm by addition of 7.1 wt% CNT and favorably enhances the fracture toughness from 3.4 $MPam^{1/2}$ for pure MgO to 6.7 $MPam^{1/2}$ for 2.3 wt% CNT. In these binary composites, the microstructure observations clear some toughness mechanisms such as CNT bundle pullout (i.e. sticking out bundles from the surface and cutting them near the grain surface), crack-deflection (Fig. 10c) (owing to low grain size of MgO), and crack-bridging. The intergranular fracture mode is the common one in these composites (Fig. 10 a and b). The possibility of crack bridging depends on the propagating crack width. It is shown that if this parameter ranges between 300 and 500 nm (Fig. 10 f and g), this mechanism is more likely to occur. Meanwhile, the chance of crack bridging declines, if the crack width is reduced down to 100 nm (Fig. 10d and e).

View Article Online
DOI: 10.1039/C7NR01878A

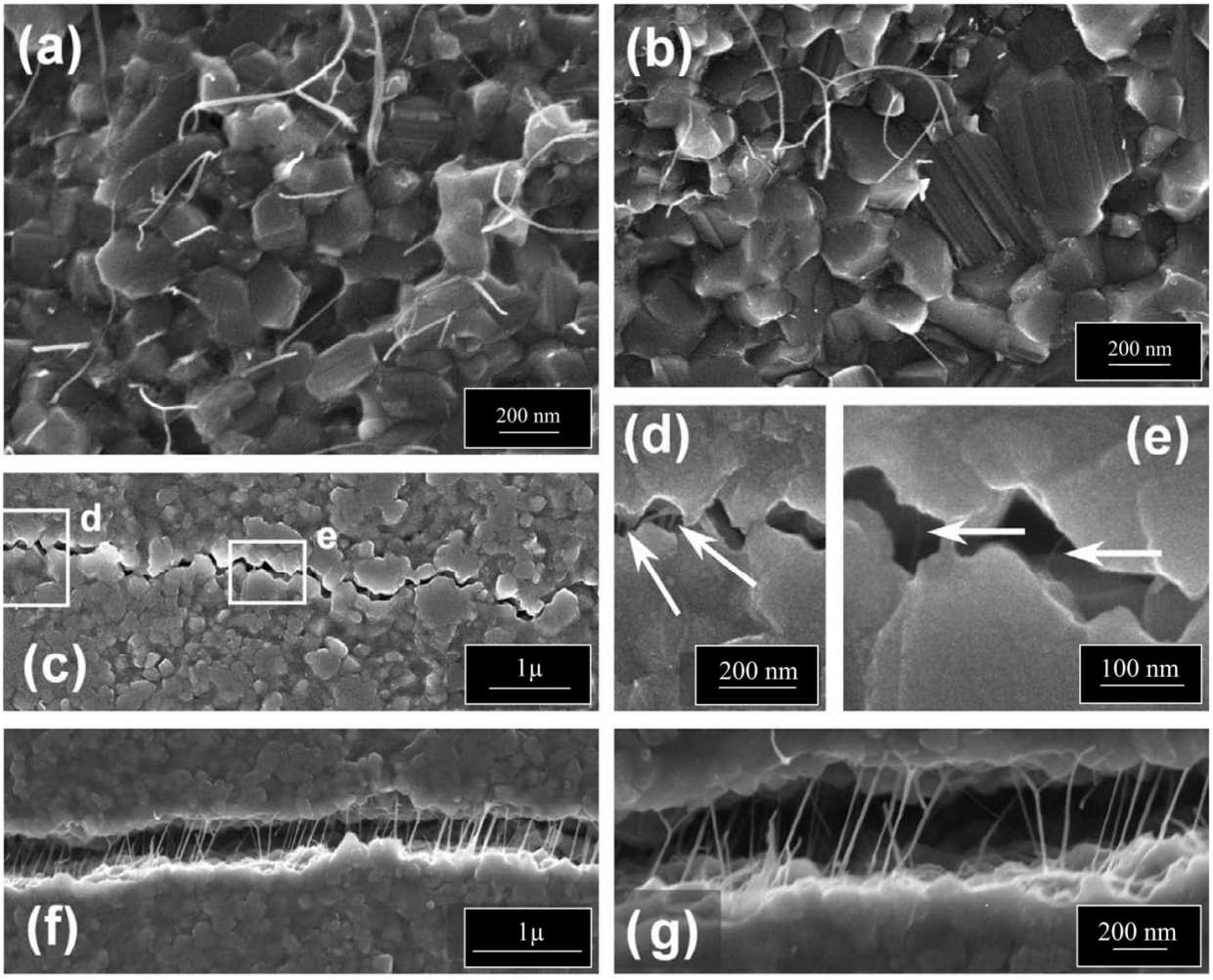

Fig. 10. FESEM images of SPSed 2.3wt% CNT-MgO systems: (a) and (b) fracture surfaces, (c) crack deflection of a microcrack with 100 nm in width, (d and e) higher magnification of CNT-induced crack bridging phenomenon, and (f and g) crack bridging with 300-500 nm in width (Reproduced from ref. 125 with permission from Elsevier [125]).

The Vickers microhardness of pure MgO (i.e. 7.5 GPa) is higher than that of 7.1 wt% CNT-filled sample (i.e. 7.4 GPa) and lower than that of 2.3 wt% CNT-dispersed one (i.e. 12.2 GPa). The grain size refinement and the strength of chemical bonding between CNTs and matrix can be considered as compelling reasons for this superior characteristic in 2.3 wt% CNT-filled sample. However, low grain growth of MgO, low relative density, and insufficient grain boundaries cohesion are responsible for inferior hardness value in 7.1 wt% CNT-containing sample. Similar results are reported by Garcia et al. [126].

View Article Online
DOI: 10.1039/C7NR01878A

2.1.6. CNT- Mullite nanocomposites

In recent years, mullite (Al_2O_3/SiO_2:3/2) has attracted a great deal of attention from researchers due to its excellent mechanical properties such as high creep and thermal shock resistance, low thermal expansion and electrical conductivity, high thermal and oxidation resistance, and superior dielectric properties. These advantages make mullite an efficient ceramic for high-temperature structural or electronic packaging, sophisticated composite industry, and optical applications [127-129]. However, its low toughness [128, 130], weak stiffness [131] and poor sinterability [132] have severely limited its applications.

Many research works have been done to improve the shortcomings of mullite by adding oxide materials (such as Al_2O_3 and ZrO_2), nonoxide ones (such as Si_3N_4 and SiC), and metals or by synthesizing layered structures [127, 129]. Recently, CNTs as a promising non-oxide component benefits from a good compatibility with mullite matrix and serves its industrial requirements [131]. In these material systems, some primary challenges i.e. non-uniform CNT distribution and poor bonding between CNTs and mullite are still remained thoroughly unsolved [129]. However, some techniques are employed to overcome these challenges. For instance, Jing Wang et al. [131] functionalized CNT and dispersed them in mullite by ultrasonication for better CNT-mullite bonding and appropriate CNT homogeneity. In good agreement with the results, adding 1 vol% CNT can decrease the electrical resistivity by 9 orders of magnitude. Such an improvement is ascribed to high volume percolation network arisen from high aspect ratio of functionalized CNTs, albeit the relative density is decreased due to the CNTs-induced porosities. Also, an improvement is reported for the mechanical properties of CNT-added mullite due to the stimulation of some toughening mechanisms including crack deflection, CNT pull-out, and CNT bridging. It is expected that a better densification will give rise to higher toughening and electrical behavior. Hence, some researchers have used the SPS technique to produce fully dense CNT-mullite bulk materials. For instance, fully dense SPSed CNT-mullite composite systems with superior mechanical properties are obtained by Wang et al. [133]. In another study, Weibel et al. [130] prepared a uniform CNT-iron-mullite ($Fe_{0.6}Al_{5.4}Si_2O_{13}$) composite powder by an in-situ catalytic chemical vapor deposition (CCVD) and consolidated that by SPS at 1500 °C. It was found that this novel dispersion procedure does induce no mechanical mixing-arisen damages in the synthesized CNTs and pave the way for effective performance of CNTs in the mechanical behavior of SPSed CNT-iron-mullite nanocomposites. Although no improvement was observed in fracture toughness, SENB[1] toughness was doubled. This effect was ascribed to the activation of some toughening mechanisms i.e. crack-bridging (Fig. 11-a) and bundle pull-out (Fig. 11-b). More importantly, the presence of 3 vol% carbon filament effectively reduces the electrical resistivity of mullite. Similar results are obtained by Cascales et al. [129].

[1] single-edge notch beam (SENB)

View Article Online
DOI: 10.1039/C7NR01878A

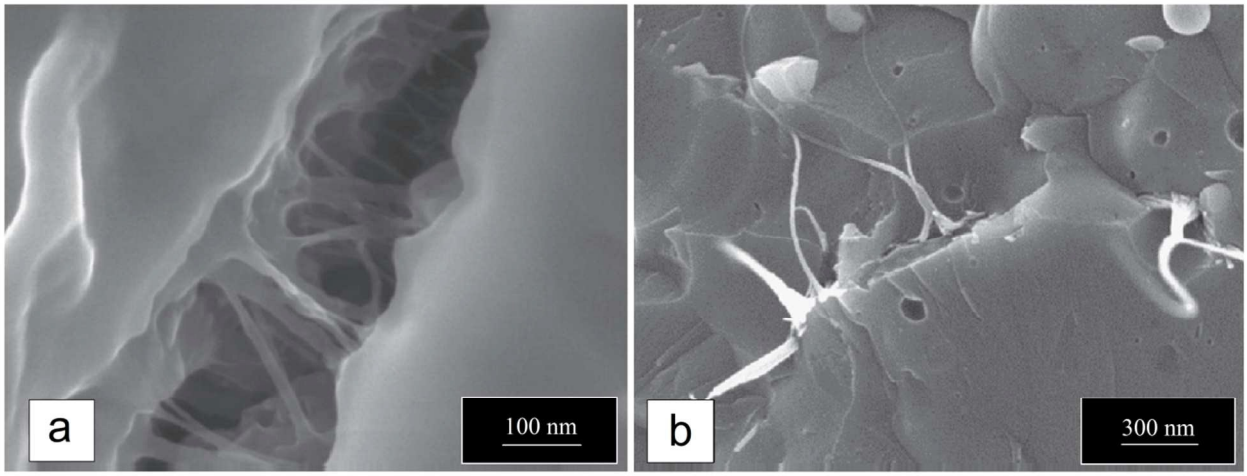

Fig. 11. SEM photographs of fracture surface of SPSed CNT-iron-mullite composites (Reproduced from ref. 130 with permission from Elsevier [130]).

2.1.7. CNT- TiO_2 nanocomposites

Recently, a wide variety of sophisticated applications are developed for TiO_2 both in powder and bulk forms. These applications often rely on functional properties of titanium oxide among which excellent photocatalytic behavior and superior photoreactivity are of prime significance. The recent studies have confirmed that anatase as an affluent polymorph of titania, benefits from better photocatalytic activity than rutile due to its better charge-carrier mobility [134]. Moreover, mixed-phase of TiO_2 shows increased photoreactivity by the virtue of formed solid-solid interfaces to enhance charge-carrier transfer, suppress the recombination of charge carriers, and provide a high density of interfacial defect sites as catalytic hole spots [135].

Some researchers have suggested that CNT particles can improve some functional properties of titania-based ceramics such as photocatalytic behavior and photoconversion efficiency [136]. For instance, one of the most significant factors in photocatalyic processes to remove pollutants is adsorption efficiency. It can be promoted by CNT addition to TiO_2–based particles and composites, because these nanotubes bear a high surface area to enable higher photoreactivity beyond the anatase or mixed phases in titania [134]. A large number of recent research works are concentrated on the novel densification methods of TiO_2-based ceramics [137]. A review on the literature reveals that SPS has been introduced as a superior process for sintering of pure TiO_2 and its CNT-reinforced ceramics. However, there are few works on these nanocomposites for which SPS technique has been used as a main sintering process. In one of the reported studies, Seo et al. [138] thoroughly investigated the electrical behavior of CNT-TiO_2 composites processed by SPS at 1173 K. It was found that CNT addition results in lower grain size as well as homogeneously distribution of CNTs between nano-grains. Also, an increase in CNT content up

View Article Online
DOI: 10.1039/C7NR01878A

to 8 wt % gives rise to a remarkable increment in electrical conductivity from 7×10^{-5} to 16.7 S/m at 300 K.

The electronic behavior of SPSed CNT-added TiO_2 nanocomposites has been recently addressed. The findings show that Seebeck coefficients are negative for all these composites, although holes are the prominent charge carriers in CNT-insulator ceramics. It means that electrons serve as the great majority of charge carriers in CNT-TiO_2 systems. Such an effect is related to the fact that excited electrons in TiO_2 grains can transfer from valence band into the electronic structure of nanotubes because of the band alignments between CNTs and matrix. The valence and conduction bands of TiO_2 are positioned at -7.4 and -4.2 eV, respectively, which result in 3.2 eV bandgap. On the other hand, CNTs have the electron affinity of 4.4 eV with a narrow bandgap (<1.1ev). As a result, excited electrons in TiO_2 can freely transfer to CNTs and holes remain in electronic structure of TiO_2 grains for maintaining the electrical balance (Fig. 12a). This event, which leads to the electron flow through CNTs, is presented in Fig. 12b. As seen, conductivity in these systems is generated by a series of steps. It is noteworthy that in step 3, where the continuity of CNT network is interrupted, electrons are transferred by variable-range hopping (VRH) model.

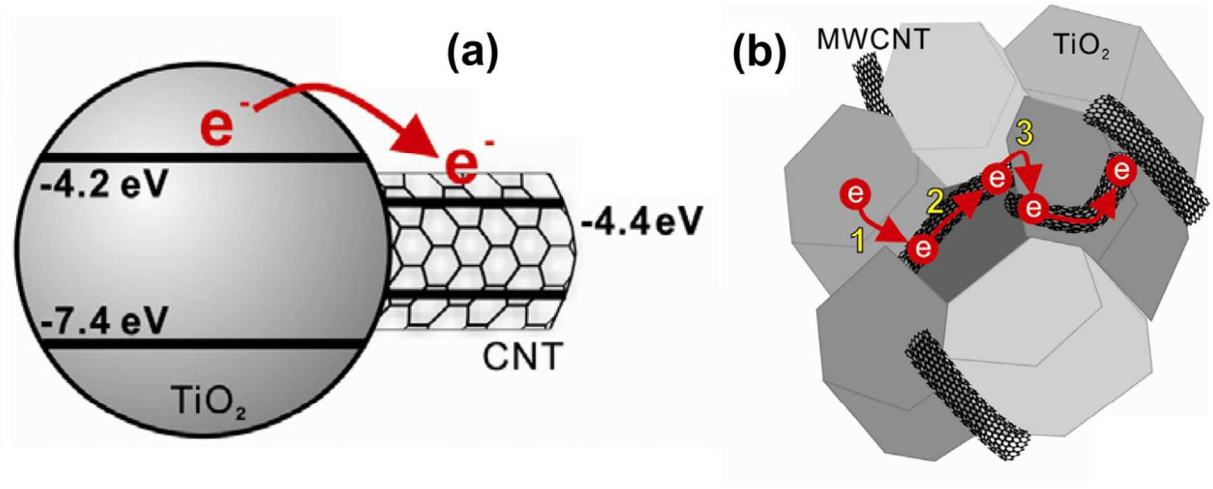

Fig. 12. (a) A representative schematic of electron transfer from TiO_2 matrix to CNTs; and (b) A schematic diagram of electron transfer in a SPSed CNT-TiO_2 nanocomposite. Electron transfer occurs in several steps: (1) Electrons transfer from TiO_2 matrix to a CNT, (2) electrons pass across a single CNT, and (3) electrons transfer to another non-contact nanotube by variable-range hopping model (Reproduced from ref. 138 with permission from Elsevier [138]).

The potential effects of CNTs on the physical, mechanical and photocatalytic properties of SPSed titania are also studied in a novel study by Debalina and coworkers [139]. In good agreement

View Article Online
DOI: 10.1039/C7NR01878A

with the results, CNT addition to titania increases densification rate, because nanotubes act as paths for electricity and generate much heat. However, the relative density of SPSed binary CNT-TiO_2 systems is same to that of pristine titania (98%). As to phase transformations, the thermodynamically irreversible anatase-to-rutile allotropic transformation fully occurs during SPS due to elevated processing temperatures (>400°C). CNT addition increases the grain growth and broadens size distribution of matrix grains due to higher thermal conductivity and agglomeration of carbon nanotubes.

From the viewpoint of mechanical behavior, fine contact between CNTs and matrix grains intensifies load transfer and gives rise to better mechanical properties. It is shown that addition of 2 wt% CNT to titania results in 22% and 5.4% enhancement in hardness and elastic modulus, respectively.

As a summary, to date, numerous CNT-TiO_2 systems have been developed with promoted photocatalytic activity due to CNTs contribution. In fact, the incorporation of CNTs into TiO_2 ceramic is proved to enhance this behavior due to activation of three mechanisms: (i) the increase of active surface reaction sites for adsorbance of reactants, (ii) the inhibition of electron-hole recombination or reduction in its rate, and (iii) the extension of excitation wavelength to visible light by using photosensitizers and/or band gap engineering [140]. Furthermore, CNTs act as dispersing agent and suppress the agglomeration of TiO_2 particles and provide higher active surface area [141]. To identify the influence of fabrication method and obtained morphology of CNT-TiO_2 systems on photocatalytic activity, relevant concentration profiles of methylene blue during photocatalytic degradation are often examined (Fig. 13). The observations show that the photocatalytic performance drastically varies with CNT content and dispersion, particles size, CNT/TiO_2 interfacial bonding, and morphology-controlled process parameters including time and temperature. As seen in Fig. 13, the presence of CNTs in SPSed TiO_2 systems enhances the photocatalytic activity. Nevertheless, some research works have reported that CNTs introduction to TiO_2 powder degrades its photocatalytic performance supposedly due to process-related events [142]. As a significant point, the SPSed sample shows slower photocatalytic rate among the graphitized data in Fig. 13 mainly due to the lower porosity content [143]. Therefore, the utilization of free pressureless SPS, known as a partial sintering method, could be suggested to fabricate porous CNT-TiO_2 photocatalysts with faster kinetics of photocatalytic reactions compared to highly dense SPSed ones. This subject is open to research.

View Article Online
DOI: 10.1039/C7NR01878A

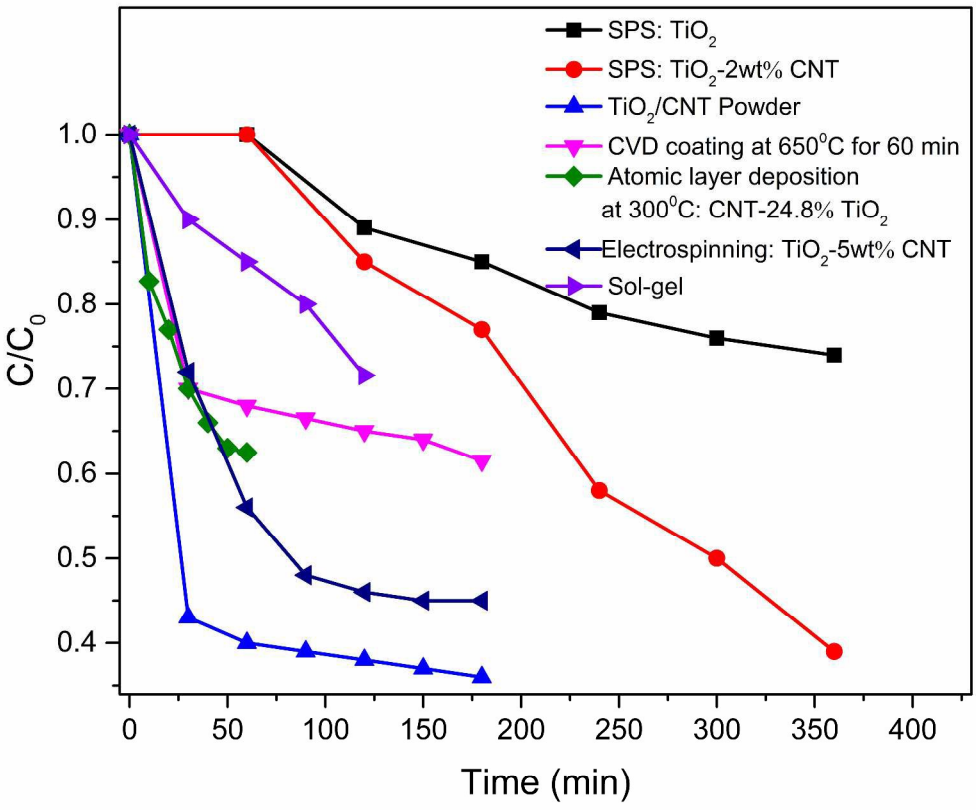

Fig. 13. Concentration profiles of methylene blue during photocatalytic degradation using CNT-TiO_2 composites fabricated by different methods (Reproduced from ref.s 142 and 144-147 with permission from Elsevier, Springer, and IOP Publishing [142, 144-147]).

2.1.8. Summary of properties

The relative density of different SPSed CNT-ceramic oxides is depicted as a function of CNT content in Fig. 14. Generally, the incorporation of CNTs into the SPSed ceramic oxides results in lower densification due to the inhibition of grain growth by individual nanotubes and pores induced by CNT agglomeration [125]. However, some experimental works are reported in which the addition of CNTs has resulted in comparatively higher densification of SPSed ceramic oxides. For instance, adding low amount of uniformly dispersed CNTs is capable of enhancing the relative density of SPSed CNT-ZrO_2 ceramics. In contrary, the inclusion of CNTs does not decrease the relative density of SiO_2, Mullite, and TiO_2. The highest relative density (i.e. 100%) is reported for SPSed pure SiO_2, SiO_2-CNT, and ZrO_2-CNT systems (in low amounts of

View Article Online
DOI: 10.1039/C7NR01878A

nanotubes). Such favorable effects are originated from the homogeneous dispersion of CNTs within oxide ceramic matrices and the formation of electrical/thermal flow paths generated throughout the ceramic powders. This CNT-induced percolation network can enhance the densification capacity and its rate [129, 139].

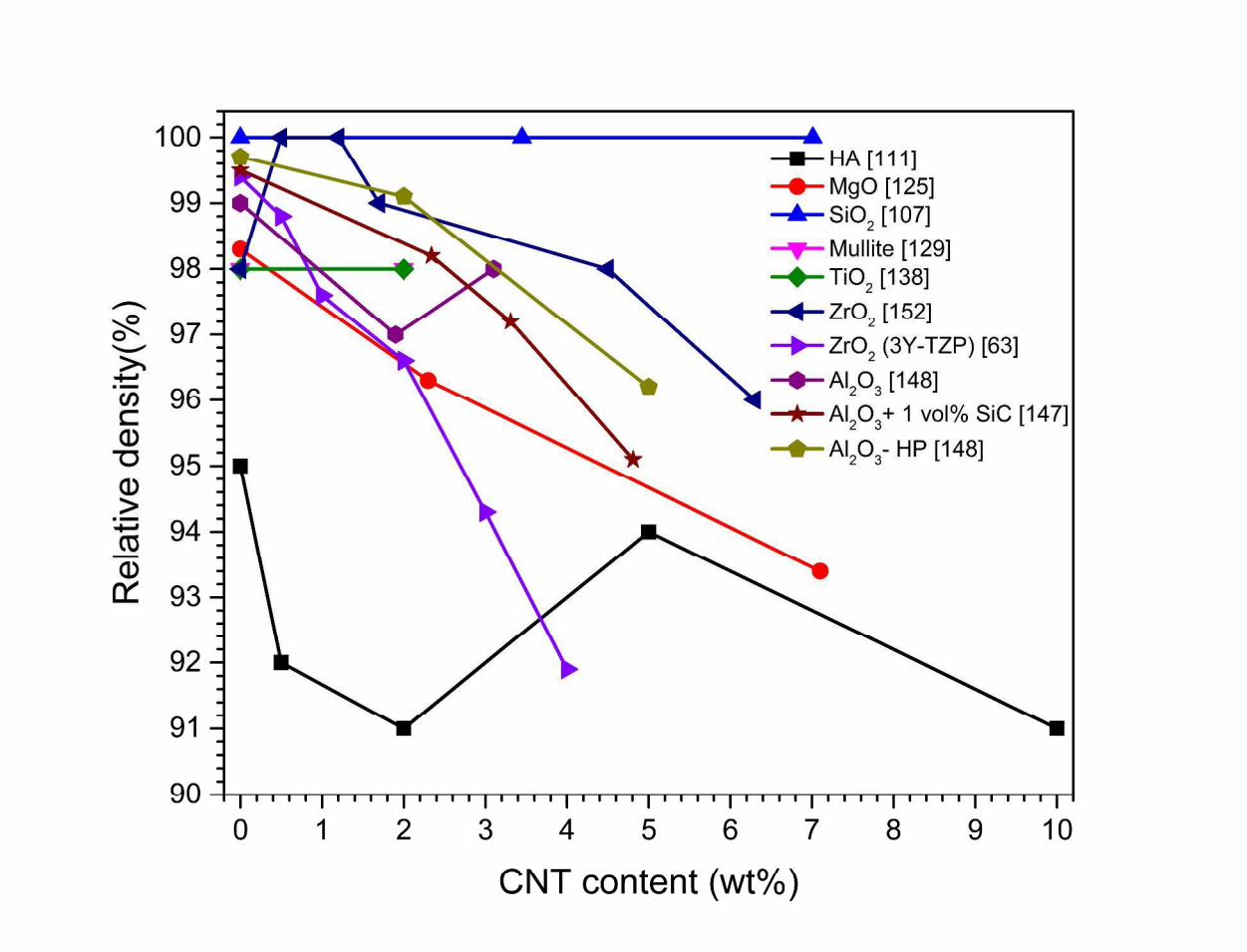

Fig 14. The relative densities of SPSed CNT-oxide ceramics as a function of CNT content.

The hardness of different SPSed CNT-ceramic oxides versus CNT content is shown in Fig. 15. Generally, an increment in CNT content up to a critical level results in higher values of hardness in these binary nanocomposites due to the intrinsically high hardness of individual nanotubes. However, further addition of CNTs gives rise to their agglomeration and reduction of hardness values as well as relative density. Moreover, poor adhesion of nanotubes to ceramic oxide matrixes is another adverse parameter to drastically decrease hardness [111, 125, 129, 139]. For example, the inclusion of CNTs in HA matrix below 5 wt% may significantly increase its hardness (approximately 1.5 times higher than that of SPSed pure HA), but it decreases this

View Article Online
DOI: 10.1039/C7NR01878A

property at higher contents due to the heavy CNT agglomeration [111]. The highest hardness belongs to SPSed Al_2O_3 due to its high natural hardness. However, according to the literature, CNT addition in most cases leads to a considerable decrease in hardness of SPSed CNT-Al_2O_3 nanocomposites. On the other hand, adding low amounts of SiC particles can decrease such an adverse effect. Reportedly, the highest hardness values of SPSed oxide ceramic matrices with relatively high CNT content (>5wt%) are related to SPSed CNT-SiC-SiO_2 nanocomposites [148, 149].

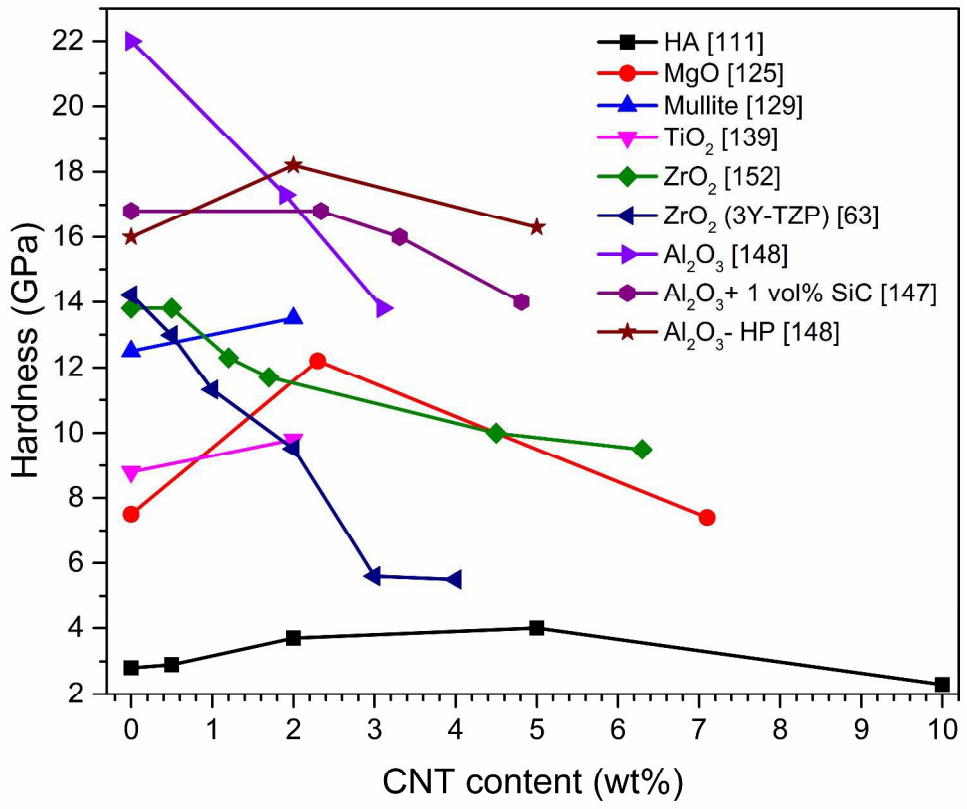

Fig.15. The hardness values of SPSed CNT-oxide ceramics versus CNT content.

The fracture toughness variation of different SPSed CNT-ceramic oxides with nanotube content is shown in Fig. 16. Expectedly, in these systems, the fracture toughness will increase by the activation of toughening mechanisms, provided that CNTs are homogeneously dispersed, remain intact during SPS, and benefit from a good binding with matrix. However, adding CNTs more than a critical value may decrease the fracture toughness by the poor interfacial adhesion

View Article Online
DOI: 10.1039/C7NR01878A

between CNTs and oxide matrix and formation of heavy CNT agglomerates and ubiquitous pores. As seen in Fig. 16, the highest fracture toughness values are related to ZrO_2 due to its natural high fracture toughness. However, adding CNT decreases its K_{IC}. In contrast, adding CNTs up to some degree in other matrices results in better fracture toughness due to the aforementioned reasons. The highest CNT content up to which the fracture toughness of SPSed CNT-oxide matrix nanocomposites increases is approximately 7 wt% for SiO_2 matrix. Table 1 presents a list of toughening mechanisms reported for CNT-filled oxide ceramic matrix nanocomposites. As seen, CNT pullout and crack-bridging are the most conventional toughening mechanisms in these materials systems.

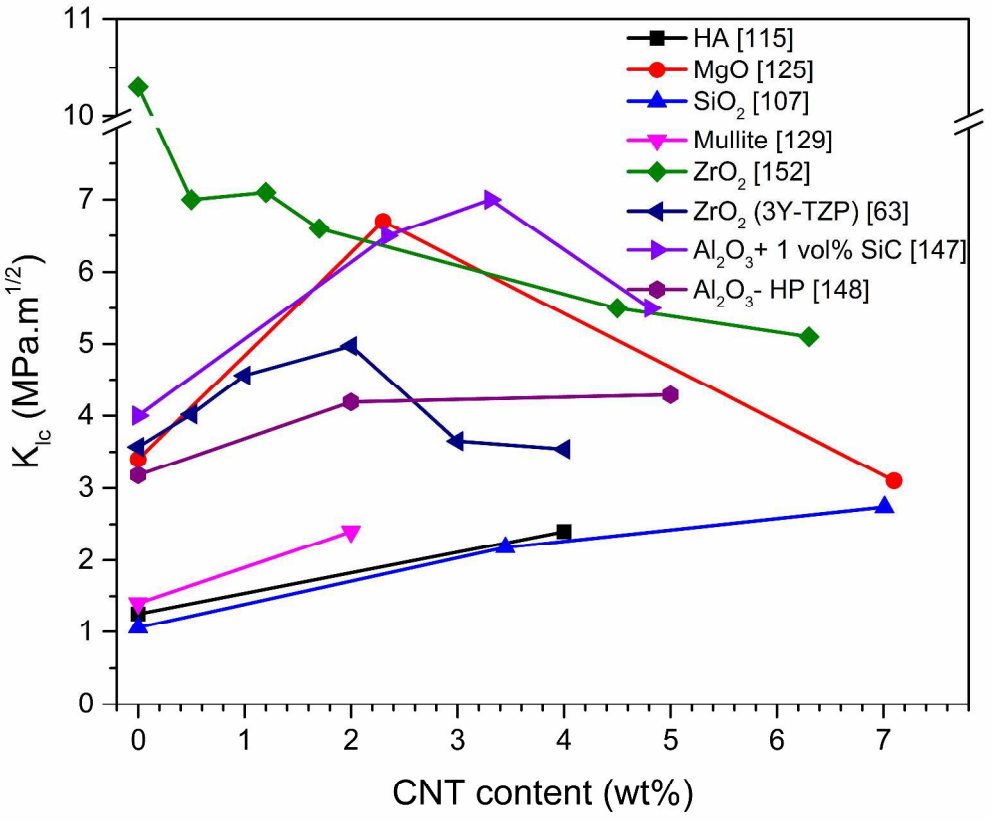

Fig.16. The fracture toughness of SPSed CNT-oxide ceramics versus CNT content.

View Article Online
DOI: 10.1039/C7NR01878A

Table 1. A review on toughening mechanisms in CNT-containing oxide ceramic nanocomposites

Composite system	CNT volume (vol %)	Active Toughening mechanism	Reference
SiO_2-CNT	Pure silica	typical brittle crack propagation	102, 107, 108
	5-10	nanotube elastic bridging and frictional nanotube bridging	102, 107, 108
Mullite-CNT	3 (wt%)	CNT pull-out and Crack bridging	130
HA-CNT	4	Fine grain and resistance to crack propagation	115
	0.5-2 wt %	Nanotube pullout, crack bridging, and crack deflection	117
	4 wt.% (1,2, 5, 10 wt% Ag)	Volumetric toughening of Ag and interfacial strengthening of CNT	116
ZrO_2-CNT	Pure zirconia	R-curve behavior	38
	0.1-1 wt. %	Interfacial load transfer	45
	Pure zirconia	Intergranular mode of fracture	46
	2.5-4.25 wt. %	Mixed mode of intergranular and transgranular fracture	46
	Pure zirconia	diffusional creep and grain boundary sliding at high temperatures	47, 48
	0.5-5 wt. %	Frictional bridging, uncoiling and stretching of CNTs	47, 48
Al_2O_3-CNT	Pure Al_2O_3	crack propagation -crack bridging	150
	Al_2O_3-0.5CNT (wt.%)	crack propagation -crack bridging	150
	Pure Al_2O_3	Intergranular cracks	150

View Article Online
DOI: 10.1039/C7NR01878A

		Transgranular cracks	
	Al_2O_3-4CNT (vol%)	Intergranular cracks Transgranular cracks	150
	Pure Al_2O_3	crack propagation -crack bridging	150
	Al_2O_3-2.5CNT (wt.%)	crack propagation -crack bridging	150
	Pure Al_2O_3	Intergranular cracks Transgranular cracks	150
	Al_2O_3-2.5CNT (vol%)	Intergranular cracks Transgranular cracks	150
	Pure Al_2O_3	crack propagation -crack bridging	150
	Al_2O_3-1CNT (vol%)	crack propagation -crack bridging	150
	Al_2O_3-10 CNT (vol%)	crack propagation -crack bridging	150
	Pure Al_2O_3	the breakage and pull-out of CNTs	151
	Al_2O_3-7.39CNT (wt.%)	the breakage and pull-out of CNTs	151
MgO-CNT	2.3, 7.1 wt%	CNT pullout, crack-bridging, crack-deflection	125

View Article Online
DOI: 10.1039/C7NR01878A

Fig. 17 and 18 exhibit the variation of bending strength and elastic modulus with CNT content for different SPSed CNT-ceramic oxides, respectively. As clearly seen, adding CNTs enhances these mechanical properties due to the intrinsically high mechanical strength of CNTs. This increment is fully guaranteed whenever CNTs are homogeneously dispersed and the binding between nanotubes and oxide matrix is not poor. As an interesting point, the empirical data show that adding CNTs in oxide matrices with low elastic modulus and bending strength results in a pronounced increment in mechanical properties of these binary material systems. In contrary, adding CNTs in oxide matrices with intrinsically high elastic modulus and bending strength gives rise to a decrement in their mechanical properties.

In addition to the mentioned properties, electrical and thermal properties of CNT-filled oxide ceramic nanocomposites are examined. Table 2 gives a list of measured values of thermal and electrical characteristics reported in the literature for these binary systems. As seen, depending on used dispersion method, CNT incorporation can enhance or degrade the thermal and electrical conductivities. Therefore, correct selection of dispersion technique will guarantee increased properties.

To compare the potential capabilities of the SPS process with other conventional powder metallurgy methods such as hot pressing and conventional sintering, typical properties of CNT-Al_2O_3 nanocomposites processed by hot pressing at 1600 ^oC for 60 min [87, 152] are given in Fig. 14-17. As seen, SPS can achieve the same level of physical and mechanical properties of oxide ceramics even for lower sintering temperatures and times. Additionally, it is possible for SPS to achieve higher properties of CNT-oxide ceramic nanocomposites in many cases. However, a review on the literature confirms that a careful and systematic control over SPS conditions is required to obtain the sintered components with superior physicomechanical properties.

View Article Online
DOI: 10.1039/C7NR01878A

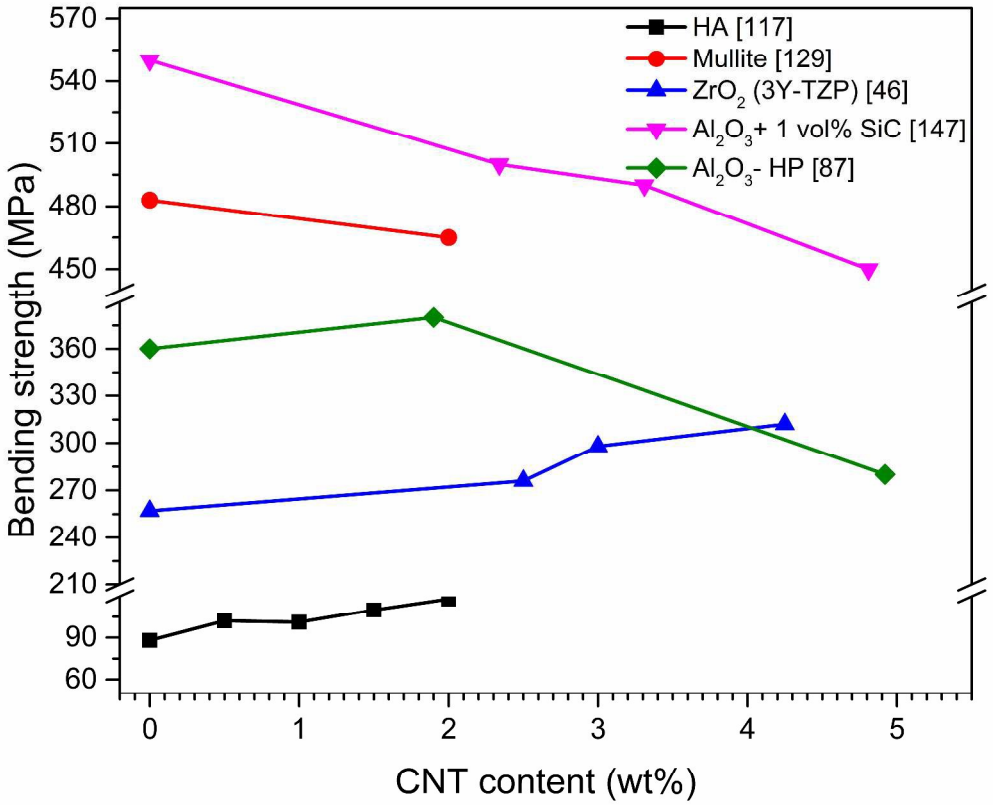

Fig.17. The bending strength of SPSed CNT-oxide ceramics versus CNT content.

View Article Online
DOI: 10.1039/C7NR01878A

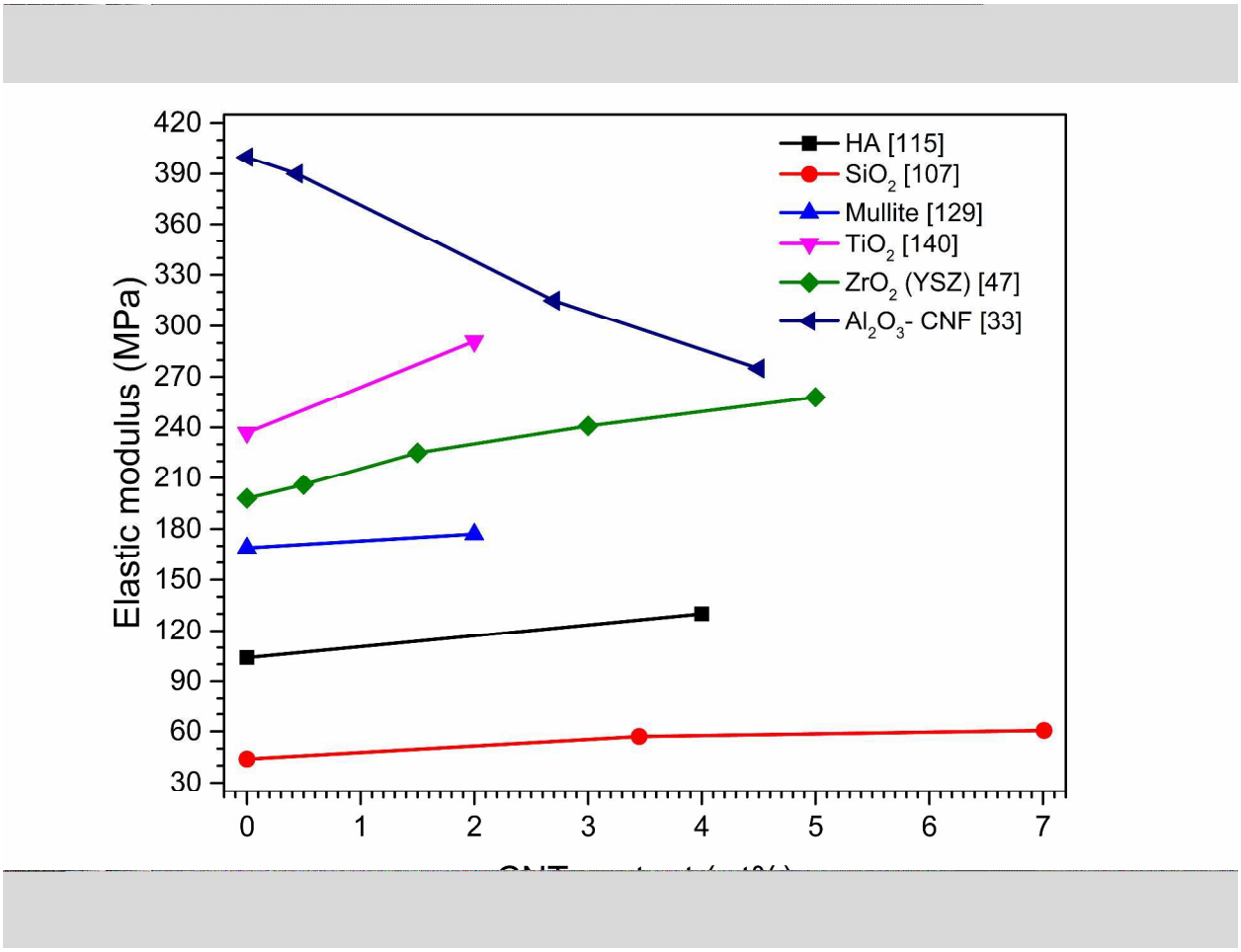

Fig.18. The elastic modulus of SPSed CNT-oxide ceramics versus CNT content.

Table 2. Thermal and electrical conductivities of SPSed CNT-containing oxide ceramic matrix nanocomposites

Composite system	CNT volume (vol%)	Dispersion method	Fabrication conditions	Thermal conductivity (W/mK)	Electric conductivity (Ω.cm)	Reference
SiO_2-CNT	Pure silica	-	SPS (1050 °C, 5 min, 50 MPa)	2.47 ± 0.05	10^{-13} S/m	102, 107, 108
	5-10	attrition milling of CNT in colloidal silica	SPS (950-1050 °C, 5-10 min, 50 MPa)	4.08 ± 0.01	64.49 S/m	102, 107, 108
	0.35	Sol-gel process	SPS (1000 °C, 5 min, 50 MPa)	-	10^{-4} S/m	101

View Article Online
DOI: 10.1039/C7NR01878A

Mullite-CNT	3 (wt%)	In-situ catalytic chemical vapor deposition (CCVD)	SPS (1500 °C, 5 min, 150 MPa)	4.08 ± 0.01	2.4 S/m	[130]
ZrO_2-CNT	10	Ultrasonication → ball milling	SPS (1150-1250 °C, 3-4 min)	-	51 S/cm	[69]
	Pure zirconia	-	SPS (1250-1350 °C, 2 min, 50 MPa)	-	10^{-11} S/m	[47, 48]
	0.5-5 wt. %	attrition milling	SPS (1250-1350 °C, 2 min, 50 MPa)	-	~100 S/m	[47, 48]
	Pure zirconia	-	SPS (1350-1450 °C, 5 min, 30 MPa)	-	10^{12}	[153]
	0.4-3.4	sonication	SPS (1350-1450 °C, 5 min, 30 MPa)	-	0.4	[153]
	Pure zirconia	-	SPS (1300 °C, 3 min, 60 MPa)	-	1.95×10^{-9} S/m	[73]
	1-10	Ball milling	SPS (1300 °C, 3 min, 60 MPa)	-	2.58×10^{-3} S/m	[73]
	Pure zirconia	-	SPS (1350-1500 °C, 5 min, 50 MPa)	2-3	-	[42, 44, 63]
	0.5-4 wt. %	Ultrasonication → ball milling	SPS (1350-1500 °C, 5 min, 50 MPa)	1-3.25	888 S/m	[42, 44, 63]
	0.5-1.5	hetero-agglomeration method	SPS (1250 °C, 5 min, 75 MPa)	-	2.8×10^{-4} S/m	[53, 55]
	Pure zirconia	-	SPS (1200 °C, 10 min, 100 MPa)	-	$< 5\times10^{-12}$ S/m	[154]
	0.5-6.3 wt.%	CNT	SPS (1200-1350	-	0.88 S/m	[154]

View Article Online
DOI: 10.1039/C7NR01878A

		functionalization → sonication	°C, 10 min, 100 MPa)			
	1	CNT Surface functionalization → Surface charging → ultrasonication	SPS (1250 °C, 5 min, 75 MPa)	-	2.5±0.5 S/m	[155]
Al_2O_3-CNT	Pure Al_2O_3	bath sonication + Attrition milling	SPS (1300 °C, 60 min, 10MPa)	-	$1x10^{-15}$ S/m	[150]
	Al_2O_3-0.6CNT (wt.%)	bath sonication + Attrition milling	SPS (1300 °C, 60 min, 10MPa)	-	$1x10^{-8}$ S/m	[150]
	Al_2O_3-19CNT (vol%)	bath sonication + milling	SPS (1450 °C, 10 min, 100MPa)	-	$2.6x10^{3}$ S/m	[150]
	Pure Al_2O_3	ultrasonic	SPS (1375 °C, 5 min, 40 MPa)	-	$1x10^{-12}$ S/m	[150]
	Al_2O_3-2.5CNT (wt.%)	ultrasonication	SPS (1375 °C, 5 min, 40 MPa)	-	10 S/m	[150]
	Pure Al_2O_3	ultrasonication + Ball milling	Hot Pressing (1550 °C, 1h, 30MPa	-	10^{-4}-10^{-5}	[150]

View Article Online
DOI: 10.1039/C7NR01878A

	Al_2O_3-2.5CNT (vol%)	ultrasonication + Ball milling	Hot Pressing (1550 °C, 1h, 30MPa	-	1	[150]
	Pure Al_2O_3	ultrasonication + stirring	pressureless sintering (1500°C/2h)	-	$>10^{15}$ Ω.cm	[150]
	Al_2O_3-1CNT (vol%)	ultrasonication + stirring	pressureless sintering (1500°C/2h)	-	$4.6x10^{13}$ Ω.cm	[150]
	Al_2O_3-5CNT (wt.%)	DMF sonication +ball milling	SPS (1800 °C, 3 min, 100MPa)	-	580 (S/m)	[156]
	Pure MgO	-	SPS (1700 °C, 30 min, 150 MPa)	-	insulator	[126]
MgO-CNT	14 DWCNT	CCVD synthesizing	SPS (1700 °C, 30 min, 150 MPa)	-	12	[126]
	2.3, 7.1 wt%	CCVDsynthesizing	SPS (1650 °C, 5 min, 150 MPa)	-	1.9-2.1 (for 2.3wt), 6.3-6.9 (for 7.1 wt%)	[125]
	Pure MgO		SPS (1650 °C, 5 min, 150 MPa)	-	insulator	[125]
TiO_2-CNT	Pure TiO_2	high energy ball milling	SPS (1000 °C, 10 min, 50 MPa)	-	7×10^{-5}	[138139]

View Article Online
DOI: 10.1039/C7NR01878A

	0-8	Ball milling	SPS (1173 K, 5min, 50-70 MPa)	-	16.7 (at 300 K)	[138]

2.2. CNT-Carbide ceramic matrix nanocomposites

2.2.1. CNT- SiC nanocomposites

SiC-based ceramics are vastly used in high-temperature applications due to their excellent elevated-temperature properties such as outstanding strength, creep, oxidation, and shock resistance [18, 150, 157]. However, this ceramic suffers from low fracture toughness and poor sinterability due to its low self-diffusion coefficient [151, 158] and strong covalent bonds between Si and C atoms [18, 19]. It is generally agreed that using sintering aids such as boron, carbon, and alumina in conventional methods (pressureless solid-state sintering) or employing advanced sintering techniques such as HIP and SPS are proposed to solve the aforementioned problems and yield the superior mechanical and physical properties [17].

2.2.1.1. Physical properties

A broad spectrum of studies has concentrated on potential effects of CNFs and CNTs on microstructure properties of SPSed SiC-based nanocomposites. It is generally reported that CNT/CNF addition can efficiently increase the relative density of SiC-based ceramics. Rocha et al. [19] prepared different SPSed CNF-SiC samples with various CNF contents and achieved a relative density of 91.6% for 80% CNF after SPS at 1800 $^{\circ}$C compared to 73% for pure SiC. It shows that CNT addition is not sufficient to enhance the relative density of SiC ceramic up to a desirable level and a more effective sintering additive such as Al_2O_3 [151] is required along CNTs and CNFs. In a good agreement with Rocha et al. report, CNT addition can increase the relative density up to 99%. This effect is attributed to highly thermally and electrically conducting nanotubes present in nanocomposite powder packs to provide a percolation network for better transfer of electric current and heat flow and intensify local heating between powder particles. Additionally, self-lubrication of CNTs/CNFs and size differences between them and matrix powder result in better arrangement of these additives in batches, and produce higher relative density [150, 151].

Alongside an increment in relative density, CNT/CNF addition gives rise to comparatively larger and equiaxial SiC grains [17, 151], because CNFs/CNTs facilitate the heat transfer along the grain boundaries due to appropriate conditions for atomic diffusion and then lessen sintering activation energy [151]. The effect of CNTs on lattice parameter (L_C) and lattice strain (ε_C) of SPSed SiC matrices are investigated by Sarkar et al. [151] by Eq. 8:

View Article Online
DOI: 10.1039/C7NR01878A

(Eq. 8) $$\beta \cos\theta = \frac{k\lambda}{L_C} + 4\epsilon_C \sin\theta$$

where B, θ, and k are integral breadth, Bragg angle, and Scherrer's constant (0.9), respectively. Also, λ = 1.5406 °A. The parameter ε_C is found to vary from positive values for pure SiC to negative ones for CNT-SiC nanocomposites, and decreases following an increase in CNT content due to the acceleration of heat transfer arisen from high conductivity of CNTs. Also, lattice parameter steadily increases with an increment in CNT content.

2.2.1.2. Mechanical and tribological properties

CNTs and CNFs may increase SiC matrix brittleness due to refining grains. On the other hand, these materials can intensify the toughness by acting as bonding agents between matrix grains [159]. Such an event occurs when the present CNTs inside the grain boundaries get an opportunity to bridge the progressing cracks and prevent their propagation, until they finally undergo a brittle fracture far behind the crack tip.

Recently, a great number of research works have investigated the possible effects of CNTs and CNFs on the mechanical properties of SPSed SiC-based ceramics. A review on the literature suggests that these properties include elastic modulus, fracture toughness, and hardness, and may be bilaterally affected by CNTs and CNFs. Xie and coworkers [150] utilized a two-step SPS process to avoid the temperature gradient across the sample and overcome its counterproductive influences on mechanical properties of SiC-CNT nanocomposites. B_4C compound was selected as a sintering aid and SiC-1 wt% B_4C-4 wt% CNT nanocomposite was SPSed at 1800 °C for 10 min. It was shown that addition of CNT particles in SiC matrix can effectively increase elastic modulus of SiC matrix up to 32%, while the hardness is dropped from 28.1 GPa (for pure SiC) to 26.7 GPa. This effect is repetitively claimed by other researchers [17, 160].

An improvement in fracture toughness is reported by Sarkar et al. [151] through CNT addition to SiC matrix. In this study, the mainly-increasing effect of CNFs on mechanical properties of SiC-based nanocomposites is ascribed to their high tensile strength and Young's modulus [17, 150]. Also, the homogeneous dispersion of CNFs and their survival at elevated temperatures and pressures are considered as the required conditions to achieve this synergetic effect. In conformity with TEM images and their correlation with mechanical properties, the presence of structurally intact CNTs with a uniform distribution inside SiC matrix and the formation of 3-4 nm thick interface between CNTs and SiC matrix with no adverse chemical byproduct (Fig. 19) render CNT particles an effective reinforcement to stimulate some efficient toughening mechanisms such as bridging, CNT pull-out, crack deflection, and branching, and consequently facilitate fracture energy dissipation as well as early arrest of the propagating cracks (Fig. 20).

View Article Online
DOI: 10.1039/C7NR01878A

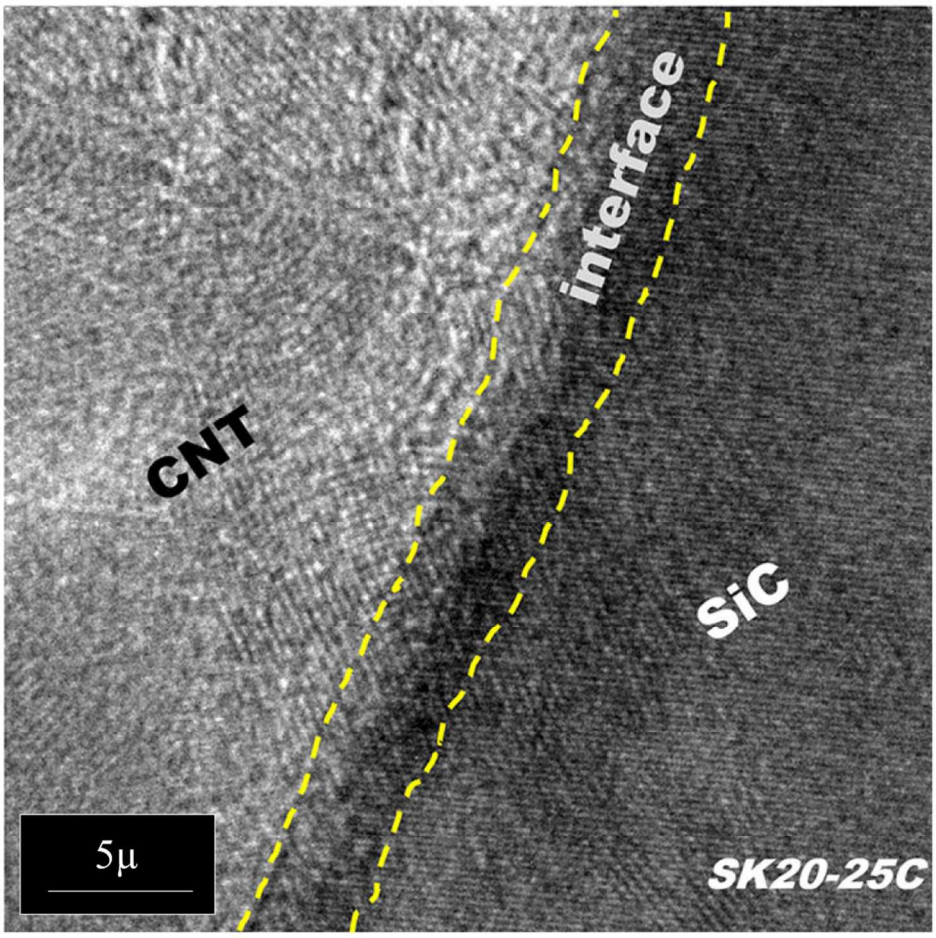

Fig. 19. TEM image of SPSed CNT-SiC composite showing the presence of CNT-rich region along SiC grain boundaries (Reproduced from ref. 151 with permission from Springer [151]).

View Article Online
DOI: 10.1039/C7NR01878A

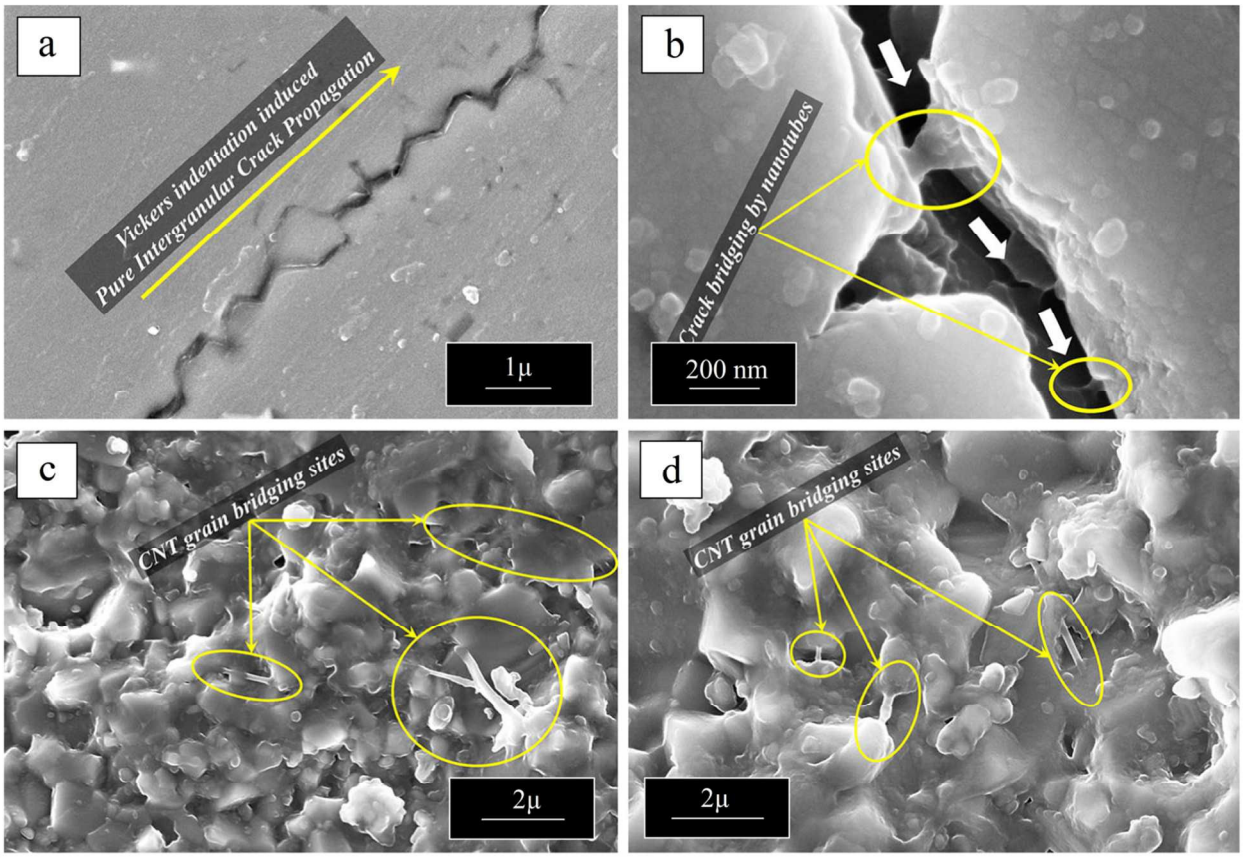

Fig. 20. FESEM images of SPSed 1.2 wt% CNT-SiC composite: (a) crack propagation, (b) crack bridging, (c) and (d) grain bridging by dispersed CNTs (Reproduced from ref. 151 with permission from Springer [151]).

The wear resistance and steady-state friction coefficient of SPSed SiC-CNT nanocomposites are also investigated in some research works. The essential mechanism of wearing in such nanocomposites is abrasion of SiC matrix, and carbon ingredients serve as lubricants on the interfaces. In a clear manner, CNT addition to SiC matrix may reduce the wear rate owing to synergetic effects of CNT-induced toughening and lubrication by which the propagation and combination of short cracks are hindered and the severity of sliding-contact conditions are alleviated [159, 160]. In summary, self-lubrication capacity of sp2-hybridized carbons such as CNTs and CNFs increases the friction coefficient of SPSed SiC-based bulk materials and improves SiC wear resistance [151].

A review on the obtained experimental results confirms that developing novel approaches to enhance mechanical properties of SPSed CNT-SiC nanocomposites is required. This challenge has been addressed in some recent papers. One approach is the utilization of appropriate

View Article Online
DOI: 10.1039/C7NR01878A

additives. Xie and Wosu [150, 156, 157] added TaC compound to SiC ceramic and investigated the mechanical characteristics of SPSed TaC-added CNT-SiC nanocomposites. Unlike the hardness, no improvement in densification was observed. They showed that higher melting temperature of TaC compound results in a need for higher sintering temperature to achieve a full relative density. In contrary, the oxidation behavior improves significantly and TaC addition contributes to CNTs for stimulation of some efficient toughening mechanisms involving particle shearing, crack deflection, and pull-out of CNT strings. Another approach is to develop new techniques for better dispersion of CNTs in SiC matrix. Yoshiaki Morisada et al. [4] coated CNT particles by a nano-sized SiC polycrystalline layer and proved a uniform CNT distribution in B_4C-dispersed SiC ceramic after SPS at 1800 °C. It was found that such a surface modification can enhance the mechanical behavior and relative density of SPSed CNT-SiC components. A meticulous overview on fracture surfaces of these composites confirms the pull-out of CNT strings in uncoated CNT-containing samples, arisen from poor adhesion of CNT-SiC interfaces (Fig. 21).

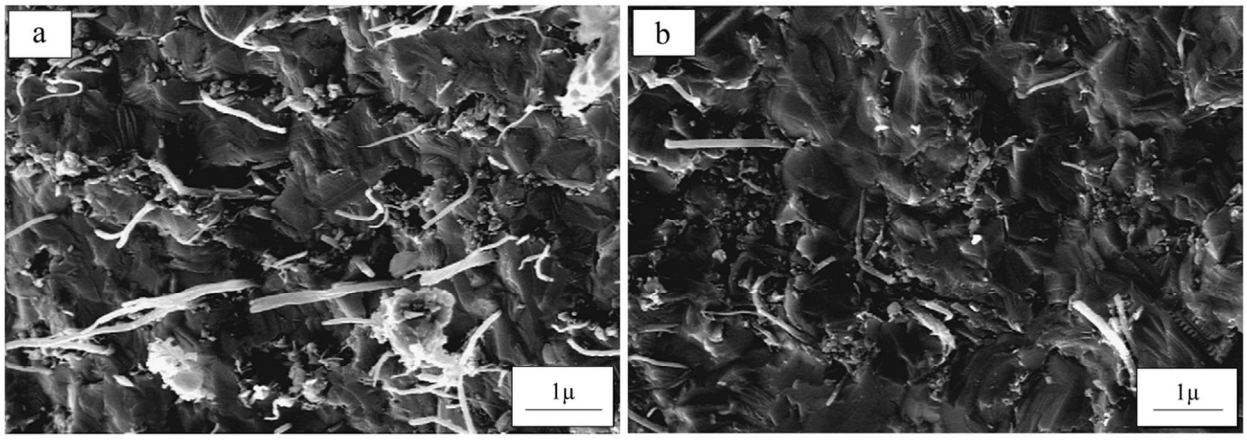

Fig. 21. SEM images of the fracture surface for (b) CNT-SiC composite, and (c) SiC-coated CNT/SiC composite processed by SPS (Reproduced from ref. 158 with permission from Elsevier [158]).

2.1.1.1. Effect of SPS process parameters

The main parameters of SPS procedure (i.e. heating rate, processing time, temperature, and applied pressure) can bilaterally affect physical and mechanical properties of SPSed CNT-SiC bulk materials. Xie and Wosu [150] explored the potential effects of SPS parameters on microstructure and mechanical behavior of CNT-SiC nanocomposites. It was found that an increment in heating rate leads to a reduction in densification, grain size (i.e. low grain growth), elastic modulus and hardness. In fact, it degrades the atomic diffusion and mobility of grain

View Article Online
DOI: 10.1039/C7NR01878A

boundaries, resulting in higher porosity and prevention of grain growth. However, the rapid heating rate leads to inhomogeneous densification and deteriorates mechanical properties by inducing local temperature gradients. In conformity with the results, an increase in sintering temperature leads to higher densification and grain size due to enhanced diffusion, but at temperatures higher than 1900 °C gives rise to lower densification owing to the surface vaporization of SiC matrix and melting or even deterioration of CNTs. In Addition, higher applied pressures increase sintering driving force and lead to lower gradient temperature, and better contact between particles by which relative density, grain size, modulus, and hardness are enhanced. Rocha et al. [19] investigated the effect of holding time on free-sintering additive CNF-SiC composites. It was found that an increment in holding time from 1 to 30 minutes does not change the relative density and porosity due to the absence of diffusion, but fracture toughness is improved because of harder necks at SiC particles contacts.

2.1.2. Others

TaC and ZrC are known as the ultra-high temperature ceramics (UHTCs) with elevated temperature mechanical properties and high melting point due to their covalent-metallic bonds. These remarked characteristics besides high erosion resistance render UHTCs appropriate for high-temperature applications such as spaceplanes and rocket engines. However, low fracture toughness, low self-diffusivity, and inferior covalent bond-induced compactability, restrict their properties [161, 162].

In the case of TaC, long sintering times lead to decreased mechanical properties owing to grain growth and the formation of instable Ta_2C. Although this new phase benefits from high flexure strength, it restricts its thermal stability [161]. For example, only 94% relative density can be achieved during hot pressing at 2300 °C for pure TaC [163]. One of the applicable methods for achieving higher density in ZrC- and TaC-based ceramics is to use fine starting powders. However, unavoidable grain growth and pore entrapment do not allow them to reach near full density. The formation of oxide impurities in powders is another reason to accelerate the microstructural coarsening by the evaporation–recondensation mechanism and intensify the grain growth. These oxides can be removed by reducing agents and contribute to higher densification. Moreover, some researchers have employed SPS process for TaC and ZrC ceramics to effectively increase the relative density. It is reported that full density for TaC is attained by SPS at 1850 °C under high pressures [164]. Other viable alternative is addition of carbon-based nanomaterials such as graphene and CNTs to enhance sinterability and resultant mechanical properties [161]. Hereof, a concise overview is provided on the research works done for SPSed CNT-modified TaC or ZrC nanocomposites and their physical and mechanical properties.

View Article Online
DOI: 10.1039/C7NR01878A

2.2.2.1. Physical properties

CNT addition to these UHTCs can increase relative density through filling the porosities present in between matrix grains and accelerating diffusion through enhanced heat transfer. These nanotubes are shown to settle in intergranular regions, impede grain boundary motions, and hinder grain growth [165]. The dimension and effective length of CNT strands are among determining parameters to control their modification capacity. Bakshi et al. [165] and Lahiri et al.[166] processed various samples of TaC ceramic including 4 wt% short (1-3μm) and long (10-20 μm) CNTs at 1850 °C to investigate the potential influences of applied pressure and nanotube dimensions on the physical behavior of SPSed CNT-TaC nanocomposites. It was shown that short CNTs benefit from a somewhat uniform distribution than long nanotubes due to their shortness and ease of distribution. The measurements confirmed that relative density increases from 89% (for pure TaC) to 94% (for short CNT-dispersed TaC systems) and 95 % (for long CNT-added TaC nanocomposites) after SPS under 100 MPa pressure. It is while an increment in applied pressure up to 255 MPa results in full densification of both monolithic TaC and short CNT-added TaC composites, but long CNT-containing systems do not undergo such an enhancement. It suggests that long CNTs impede grain boundary motions and give rise to hindrance in grain growth and accessibility to full densification. As another advantage of short nanotubes, they can effectively fill the pores and decrease intrinsic resistance of matrix grains against boundary motions. The further rise in applied pressure can change the variation trend. In good agreement with the empirical results, an increase in SPS pressure up to 363 MPa causes relative density of both SPSed CNT-TaC systems to exceed 100% and reach to 104%, since cylindrical CNTs can be deformed to graphite under such a high pressure during a graphitization phase transformation. In the case of grain growth, longer nanotubes are more successful in acting as grain pinning agent than shorter ones, because long CNTs can wrap more intergranular surfaces. CNTs can also increase the relative density by inducing local melting (Fig. 22), because CNTs can act as a source of joule heating. Fig. 22 shows a short CNT encapsulated by a re-solidified TaC particle. This particle is melted by heating through CNT strand. This also proves that CNTs can remain intact in such harsh conditions during SPS [165].

View Article Online
DOI: 10.1039/C7NR01878A

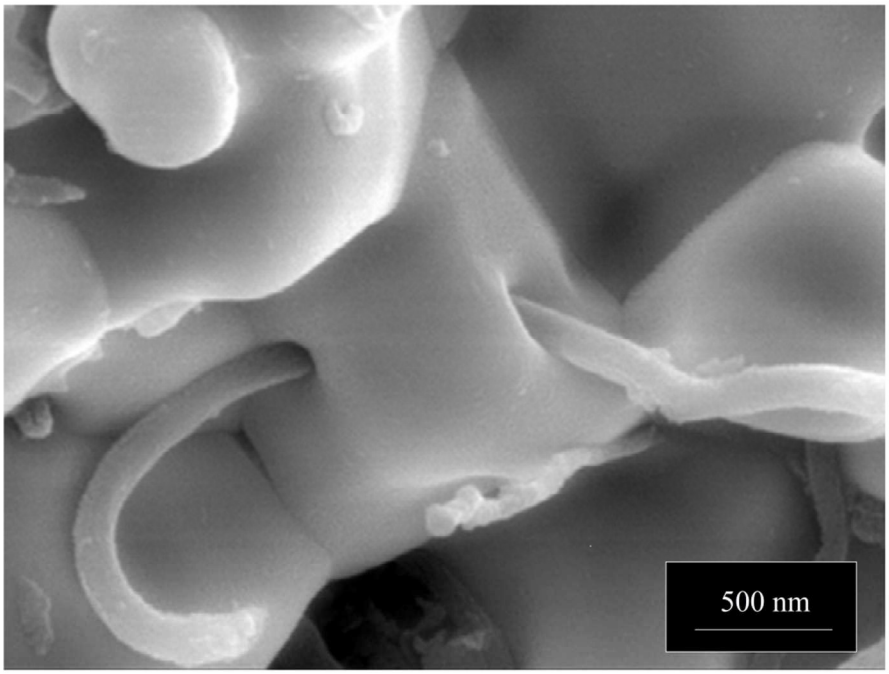

Fig. 22. High resolution TEM image of the fracture surface of CNT-TaC nanocomposite SPSed at 1850 ^{o}C under 100 MPa pressure (Reproduced from ref. 165 with permission from Elsevier [165]).

In contrary, adding CNTs to ZrC-based ceramics does not change the relative density and porosity. This lack of access to enhanced relative density in CNT-added material system is associated with the remaining porosities between the matrix grains and agglomeration of nanotubes, as confirmed by SEM micrographs. Such investigations are only experimental reports and a deep study on the potential reasons of this phenomenon is required.

2.2.2.2. Mechanical properties

It is generally accepted that an increase in relative density of UHTCs can bring about enhancement in mechanical properties involving elastic modulus and fracture toughness. Such an enhancement is arisen from high elastic modulus of CNTs and the stimulation of some striking toughening mechanisms such as crack bridging and crack deflection [165]. However, there exist some key factors to adversely affect mechanical properties of these composites among which the thermal degradation of nanotubes during SPS process is of prime significance. In accordance with some observations, CNTs need a pressure around 3GPa at ambient temperatures to structurally decompose. This pressure may be greatly dwindled in SPS process by the virtue of plasma generation. [165] This is the reason why CNTs can be transformed into a wide variety of carbon allotropes such as graphene nanosheets [167], graphite [15], diamond [168], and n-diamond (a

View Article Online
DOI: 10.1039/C7NR01878A

metallic form of carbon with FCC structure) [169] during SPS process. Regarding TaC-based ceramics, it is shown that if SPS temperature and pressure are high enough to deform CNTs into graphite flakes, the hardness will be decreased due to lower hardness of graphite compared to TaC matrix. Moreover, CNTs denote a beneficial effect to fracture toughness than graphite byproducts.

Albeit an enhancement in hardness and elastic modulus of TaC-based composites is observed owing to addition of 4 wt% short and long CNTs before SPS, employing short CNTs or applying exceedingly high pressures culminate in lower hardness and inferior elastic modulus. This reduction can be ascribed to the thermomechanical damages in SPSed short CNT-dispersed TaC nanocomposites. Overall, in SPSed CNT-TaC nanocomposites, short CNTs are more capable to fill porosities and increase the final density, but more susceptible to get damaged compared to long nanotubes. It is due to the fact that short CNTs have a length similar to that of TaC grains and feel maximum pressure during SPS where grain boundaries are highly loaded. In contrast, long nanotubes bear comparatively large size than grains and remain twisted and unzipped due to SPS-induced thermomechanical loads (Fig. 23). Unlike unzipped CNTs, intact nanotubes can promote fracture toughness and rupture strength more and more due to further activation of toughening mechanisms such as crack bridging [166]. These results are in agreement with work done by Khaleghi et al.[170].

Fig. 23. A representative scheme of CNT-to-graphite phase transformation for short and long CNTs during SPS of CNT-TaC nanocomposites (Reproduced from ref. 166 with permission from Elsevier [166]).

View Article Online
DOI: 10.1039/C7NR01878A

Simultaneous utilization of CNTs and other additives can have a synergetic effect on the mechanical behavior of SPSed CNT-TaC binary ceramics. As a practical example, Nisar et al. [171] added SiC to SPSed CNT-dispersed TaC systems and investigated their physical and mechanical properties. It was shown that CNTs and SiC have a synergetic effect on pure TaC and increase its relative density from 93.1 to 98.2%. This is the case for the hardness: Adding SiC and CNTs increases and decreases this property, respectively. The former is attributed to obtained high density and grain refining of ceramic matrix and the latter is ascribed to agglomeration of nanotubes and their thermomechanical damages, as proven by Raman and microscopic spectroscopies. However, an increase in fracture toughness from 8.9 to 11.4 MPa $m^{1/2}$ is reported after addition of SiC to CNT-dispersed TaC nanocomposites. Apart from CNT-induced toughening mechanisms, this enhancement is attributed to the reduction of interfacial residual tensile stress after incorporation of SiC particles. A similar trend is reported for ZrC-based ceramics [172].

2.2.2.3. Oxidation behavior

CNTs and other additives such as SiC are shown to enhance the oxidation behavior of SPSed TaC-based ceramics. Indeed, for TaC and SiC-TaC composites, oxygen molecules prefer to transport through sharp boundaries of TaC and SiC grains than intragranular regions. Additionally, the incorporation of CNTs into TaC-SiC grain boundaries creates a torturous diffusion path for oxygen molecules, impedes oxygen transport, and protects grains from oxidation. Besides, SiC forms a protective SiO_2 layer and increases the oxidation resistance [173].

2.2.3. Summary of properties

In general, CNT have bilateral effects on relative density of SPSed CNT-carbide ceramic nanocomposites. As seen in Fig. 24, CNTs can increase, decrease, or do not change the relative density of these binary systems. However, they generally possess high relative density values (usually over 97%). Expectedly, CNTs up to a critical amount can enhance the densification and increase the relative density of SPSed carbide systems such as SiC and B_4C by generating a better thermal dispersion in the ceramic matrix due to intrinsically high thermal conductivity of nanotubes. However, further addition of CNTs more than the critical value may degrade the relative density and induce pores by CNT agglomerates, as seen in Fig. 24 for B_4C [151, 174]. It is noteworthy that the geometrical size of nanotubes can have a great effect on the densification capacity of SPSed carbide ceramics. Compared to short CNTs, long ones suffer from more difficulty in dispersion and can hinder the grain growth. Therefore, long nanotubes usually result in lower densification than short ones [165].

View Article Online
DOI: 10.1039/C7NR01878A

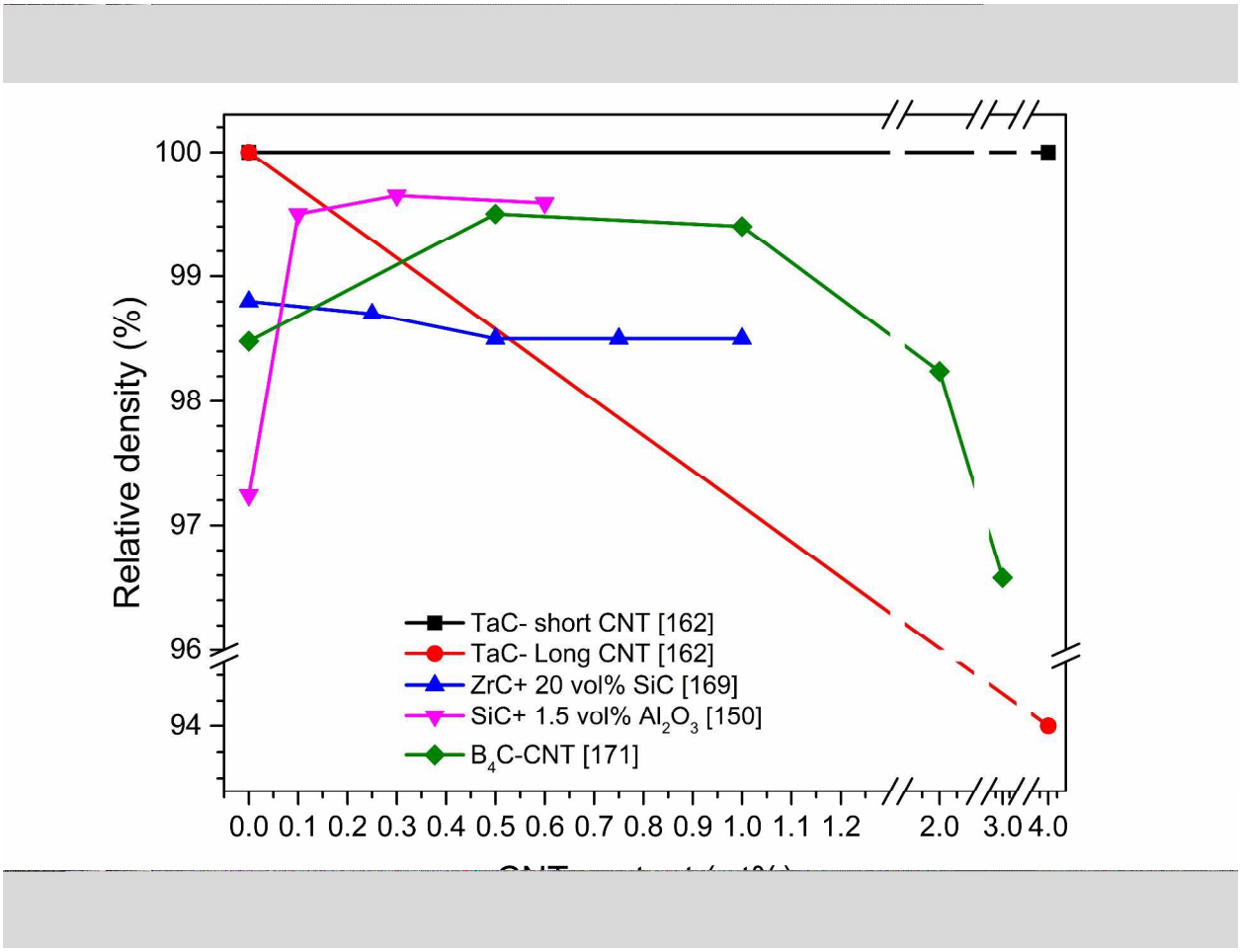

Fig. 24. The relative density of SPSed CNT-carbide ceramics as a function of CNT content.

Fig. 25 shows the hardness variation of SPSed CNT-carbide ceramics as a function of nanotube content. Generally, adding CNTs more than a defined value will enhance the hardness of these materials by suppressing the grain growth, provided they are homogeneously dispersed. Further addition of nanotubes may give rise to a drastic reduction in hardness due to the formation of CNT agglomerates and pores [151, 172]. Another factor which directly dictates the effect of CNTs on the hardness of SPSed carbide ceramics is the interfacial bonding between nanotubes and carbide matrix. If the interfaces are strong enough, the addition of CNTs can increase the hardness. One way to create such interfaces is coating CNTs by other appropriate materials. As seen in Fig. 25, coating CNTs by SiC can reinforce the hardness of SPSed CNT-SiC nanocomposites by strengthening their interfaces [158].

View Article Online
DOI: 10.1039/C7NR01878A

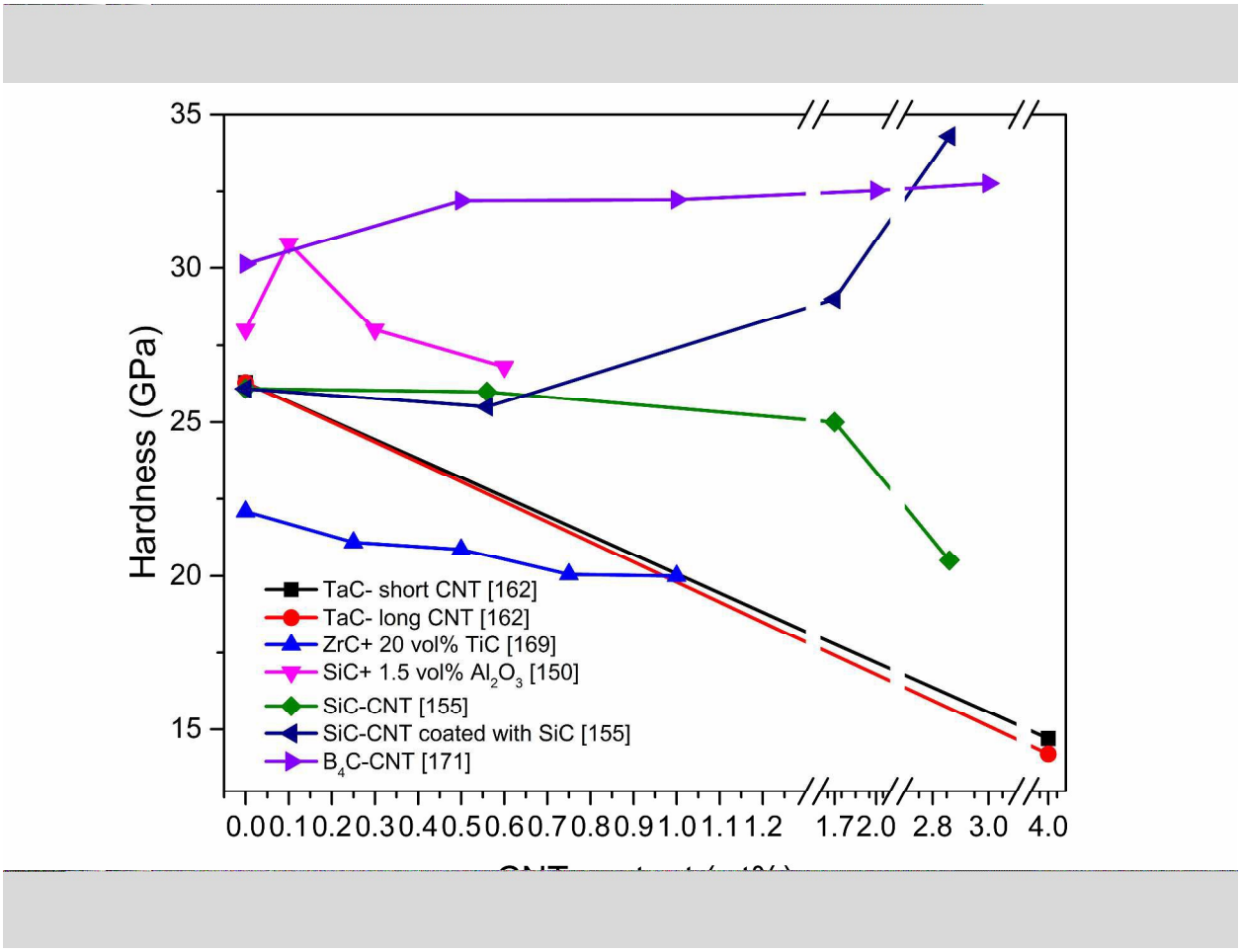

Fig. 25. The hardness of SPSed CNT-carbide ceramics versus CNT content.

The fracture toughness variation of SPSed CNT-carbide ceramics with nanotube content is shown in Fig. 26. Generally, adding CNTs in SPSed carbide ceramics activates some of toughening mechanisms including bridging and pull-out, and enhances their fracture toughness This improvement is valid until CNTs are homogenously dispersed in the matrix. Whenever the CNT agglomerates form, the grain growth is persuaded and toughening is degraded [151, 172]. The surface modification of nanotubes can strengthen the CNT/carbide ceramic interfaces, facilitate the better transfer of forces, and enhance the fracture toughness [158]. Table 3 lists the dominant toughening mechanisms for several CNT-filled carbide ceramic matrix nanocomposites.

View Article Online
DOI: 10.1039/C7NR01878A

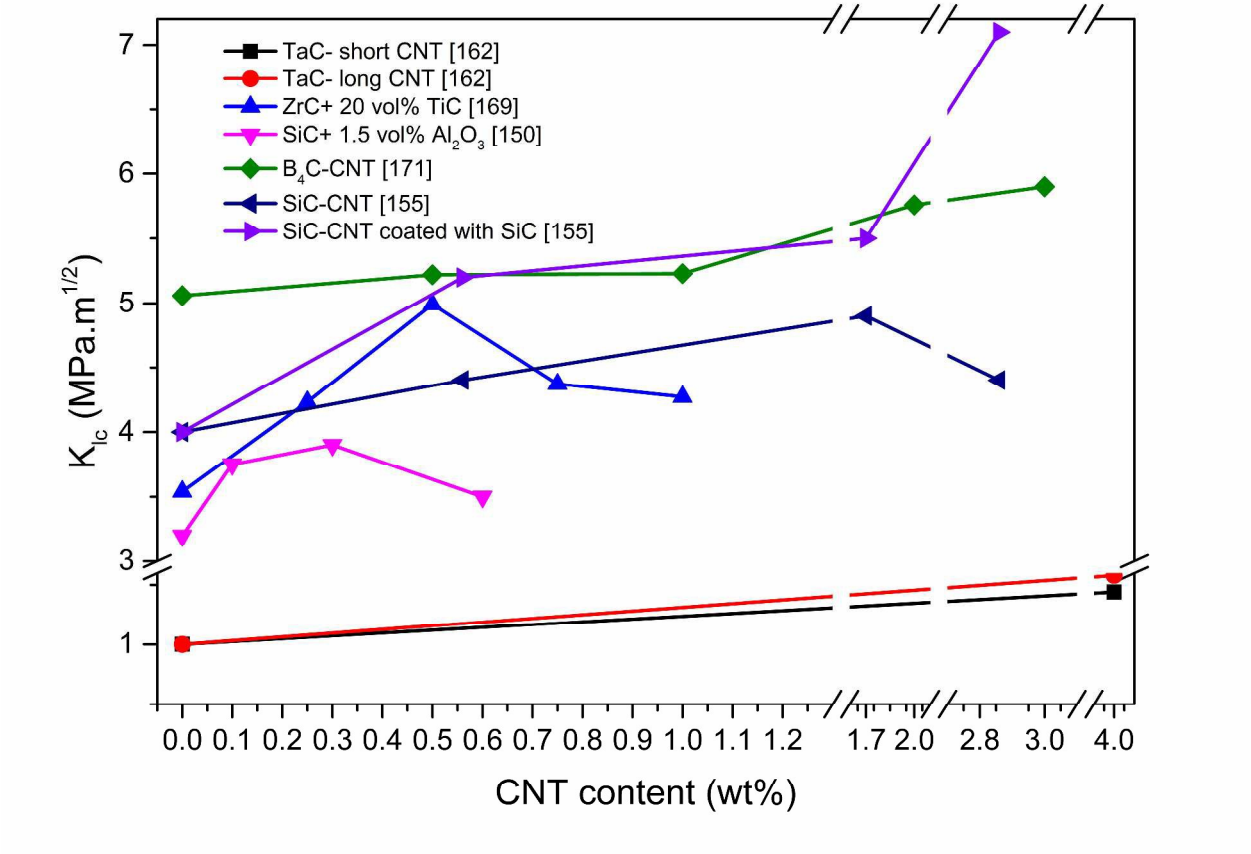

Fig. 26. The fracture toughness of SPSed CNT-carbide ceramics versus CNT content.

Table 3. Dominant toughening mechanisms in some CNT-filled carbide ceramic matrix nanocomposites

Composite system	CNT volume (vol%)	Active Toughening mechanism	Reference
SiC-CNT	MWCNT 0.1-1.2 wt% + 1.5 wt% Al_2O_3	-crack propagation -crack bridging -grain bridging	151
CNT-TaC and/or CNT-ZrC	4wt% Long (10-20 µm) Or short (1-3µm)	Crack bridging	165, 166

View Article Online
DOI: 10.1039/C7NR01878A

TaC + 15 % CNT	energy dissipating mechanisms such as crack branching, CNT bridging, and crack-deflection	[171, 173]
15%CNT +15% SiC	the reduction of interfacial residual tensile stresses	[171, 173]

2.2. CNT- Nitride ceramic matrix nanocomposites

2.2.1. CNT- Si_3N_4 nanocomposites

Silicon nitride (Si_3N_4) has been used in many industrial applications such as machining tools and electrical circuits due to its superior mechanical properties, thermal conductivity and electrical insulation [175, 176]. Similar to other ceramics, Si_3N_4 suffers from low compatibility as to its strong covalent bonds. To overcome this challenge, a great variety of sintering additives such as MgO, Y_2O_3 and Al_2O_3 have been utilized to date. Additionally, high electrical insulation of these ceramics induces superficial static electricity and subsequent adhesion of impurities to their external surfaces and gives rise to mechanical failure. Some efforts have been done to meet this challenge through the development of Si_3N_4-based conductive ceramics by CNT addition [176]. More importantly, the incorporation of CNTs into Si_3N_4–based ceramics can effectively change their electrical properties due to the high percolation network-arisen electrical conductivity of nanotubes. However, two counterproductive events are reported in association with CNT addition to Si_3N_4 matrix: (i) High temperatures at which sintering of Si_3N_4-based ceramics occurs may thermally degrade the nanotubes; and (ii) CNTs impede the matrix densification and weaken mechanical behavior [176]. For this reason, a large number of research works employed a low-temperature SPS technique as sintering method for Si_3N_4-CNT nanocomposites to meet these challenges and produce fully dense materials with superior electrical and tribological properties, as explained in details hereunder.

2.3.1.1. Physical and mechanical properties

Generally, the incorporation of CNTs into Si_3N_4 matrix results both in inferior physical properties due to lower relative density and large grain size and in weak mechanical behavior (in particular, low fracture toughness and hardness) due to induced porosities. Given its low sintering temperature and processing time, SPS technique can effectively curtail the porosities of binary Si_3N_4-CNT systems and improve their physical and mechanical properties. However, the obtained properties have still maintained lower than those of pristine Si_3N_4 in a vast majority of research works. In one of the related studies, Balázsi and coworkers [29, 177] drew a comparison

View Article Online
DOI: 10.1039/C7NR01878A

between SPS and hot isostatic pressing (HIP) and studied their distinct influences on the physical and mechanical properties of CNT-Si_3N_4 nanocomposites. They used 4 wt% Al_2O_3 + 6wt% Y_2O_3 as sintering additives. In accordance with the results, the samples SPSed at 1500-1650 °C for 3-5 min showed better relative density and superior mechanical properties compared to HIPed ones even at higher temperatures (Fig. 27). Other microstructural discrepancy between SPSed and HIPed specimens was whether an allotropic phase transformation occurs or not. The phase analysis demonstrated that the HIPed samples retain their allotropic phase and remain in β state, but the microstructural composition of SPSed parts varies depending on time/temperature-controlled sintering conditions. In fact, the α→β phase transformation gives birth to elongated grains and enhances fracture toughness and mechanical behavior of Si_3N_4-based ceramics [176] SPSed at 1650 °C. As an interesting result, CNT addition hinders this transformation. However, some contradictory reports are published to reject this theory. Miranzo and coworkers [178, 179] who SPSed a binary CNT-Si_3N_4 system with similar additives at 1585 °C, discovered no meaningful interrelationship between CNT content and type of stable phases (i.e. α or β). In contrast, the incorporation of CNTs into Si_3N_4-based ceramics led to (1) introducing some impurities to the matrix, and (2) increasing conductivity from $3*10^{-13}$ (for pristine Si_3N_4) to 14 S/m (for 5.3 vol% CNT-Si_3N_4 nanocomposites). These factors lower melting temperature of Si_3N_4 and effectively promote the rearrangement of matrix particles. Moreover, the formation of the CNT percolation networks inhibits the grain growth, decreases grain size, and induces fine matrix grains. Such microstructural phenomena give rise to enhanced fracture toughness from 4.5 up to 4.8 $MPa.m^{1/2}$ for 1.8 vol% CNT. This improvement is associated with in-situ toughening to arise from elongated grains of β-Si_3N_4 matrix.

View Article Online
DOI: 10.1039/C7NR01878A

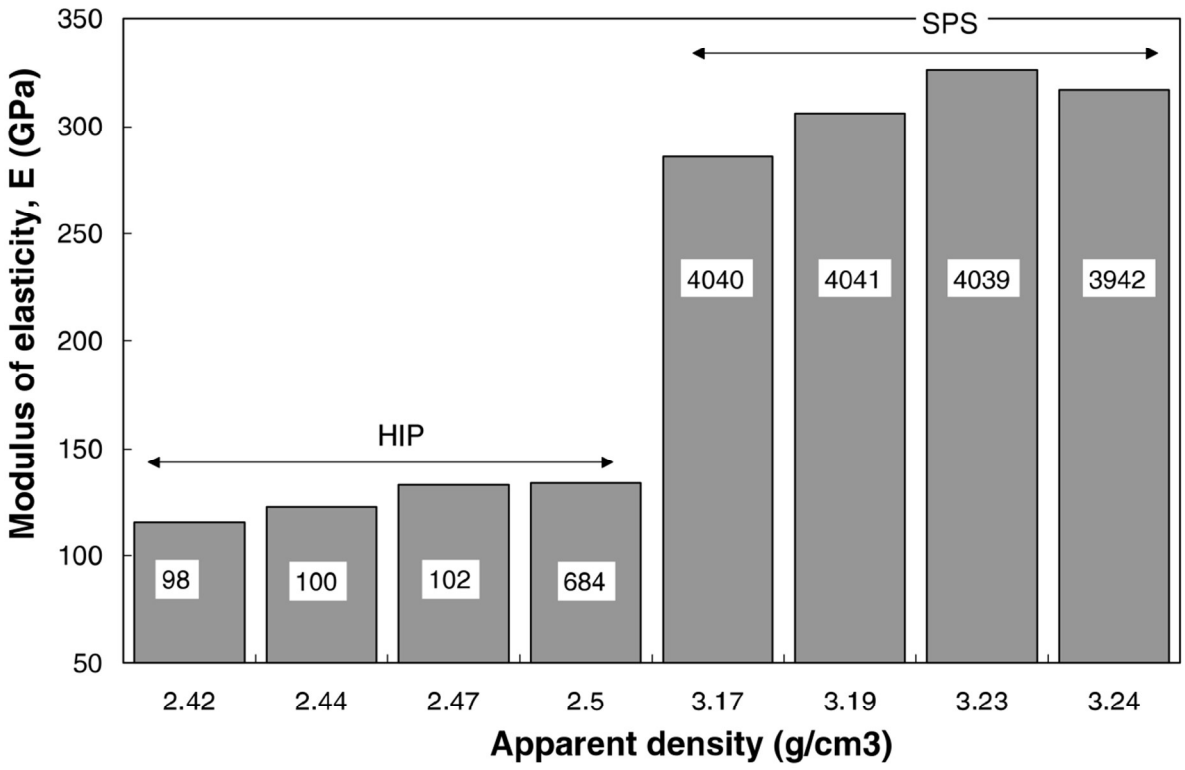

Fig. 27. Elastic modulus versus apparent density for Si_3N_4-CNT samples SPSed at 1500-1650 °C for 3-5 min and HIPed at 123,1700°C for 0,1 hr (Reproduced from ref. 29 with permission from Elsevier [29]).

Similar results are also obtained by Corral and coworkers [180], who found out that CNTs can activate some toughening mechanisms such as pull-out (as seen in Fig. 28) in SPSed CNT-Si_3N_4 systems. However, more microscopic studies are required to explain how CNTs presence can affect the microstructural events especially phase transformation of Si_3N_4 matrix during SPS.

View Article Online
DOI: 10.1039/C7NR01878A

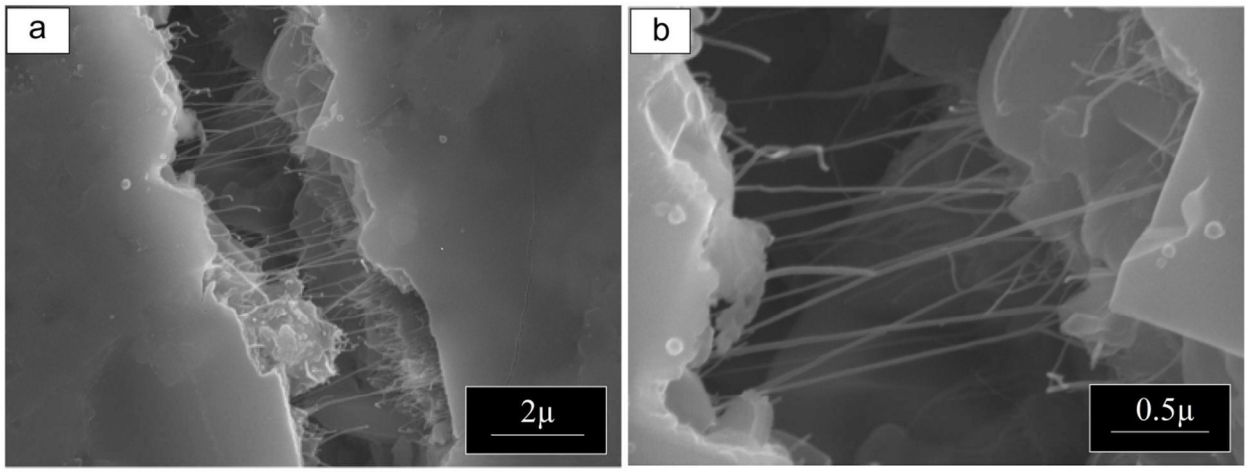

Fig. 28. Crack bridging and CNT pull out in a microcrack generated in a SPSed CNT-Si_3N_4 nanocomposite (Reproduced from ref. 180 with permission from Wiley [180]).

Another factor to strongly influence the physical and mechanical properties of SPSed CNT-added Si_3N_4 nanocomposites is the mixing approach. It is confirmed by Osendi and coworkers [181] who investigated the fracture surfaces of SPSed 1.8 vol% CNT-Si_3N_4 composites produced by (i) ball milling and (ii) blade mixing and subsequent sonication. It was claimed that blade mixing technique has some advantages compared with ball milling as follows: (i) It can effectively disperse CNTs with no pronounced agglomeration, (ii) It does not deteriorate the favorable properties of finished composites which can be observed after surfactant addition during the ball milling, and (iii) It requires short processing times. However, using such a promising mixing procedure does not increase the physical and mechanical properties of the composites over than those of pure Si_3N_4 except for the fracture toughness.

In summary, CNT addition may lead to a reduction in physicomechanical properties of Si_3N_4-based nanocomposites and the SPS technique can alleviate some parts of it. Moreover, if SPS temperature is low enough to hinder the formation of β-Si_3N_4, CNTs can slightly improve the fracture toughness.

2.3.1.2. Tribological properties

The main wear mechanism in Si_3N_4–based systems is micro-abrasion during which the debris detached from superficial regions of the contact surfaces serves as a lubricating agent. This mechanism is different from dry sliding in which hardness and toughening play a significant role. In CNT-Si_3N_4 nanocomposites, CNTs extract from matrix, arise to the surface and typically acts as a lubricant and ultimately reduces the friction coefficient and wear volume. In fact, CNTs settling at grain boundaries can increase wear resistance by inhibiting the growth of long cracks

View Article Online
DOI: 10.1039/C7NR01878A

through redistribution of the stress field. An important factor dictating the effects of CNTs on tribological properties is distribution of CNTs. If the CNTs are well-dispersed and inter-locked between matrix grains, they would act as lubricant at higher levels of friction forces because they need more force to be taken apart from matrix. On the other hand, if dispersion and CNT/matrix interfaces are poor, CNTs would take apart at such a lower force. Therefore, CNTs can acts as lubricant under lower critical force. To study the effect of CNT on tribological properties of CNT-Si_3N_4 composites, Gonzalez-Julian and coworkers [182, 183] fabricated various CNT-Si_3N_4 systems by SPS at 1585 °C and examined their tribological properties under different applied pressures. It was found that friction coefficient and wear volume are effectively decreased by increasing the CNT content. Also, an increment in processing pressure intensifies this enhancement because unlike high pressures, graphite-based debris as lubricating agent is not produced under small loads. In their study, the abrasion-arisen imperfections in nanotubes were clearly revealed by Raman spectroscopy. They reported that the CVD-synthesized inter-locked CNTs with coherent contact interfaces lead to a significant decrease in wear volume down to 65% and 87% compared to pure Si_3N_4 and the samples reinforced with sonication-assisted dispersed CNTs, respectively. In this study, the content of β-Si_3N_4 phase for all samples was in the range of 42-49 vol%. It alleviates the possible effects of β grains on the tribological behavior.

2.3.1.3. Electrical and thermal properties

The incorporation of CNTs into Si_3N_4-based ceramic systems can surprisingly increase the electrical conductivity of insulating Si_3N_4 matrix and render them a conductive material through the formation of a continuous percolation network. In contrast, the thermal diffusivity and conductivity are decreased with CNT content. To investigate the potential reasons of this contradictory behavior, Corral and coworkers [184] processed binary CNT-Si_3N_4 nanocomposites by SPS. While pristine Si_3N_4 is insulator, adding 2 and 6 wt% CNT can dedicate a semiconducting or conducting feature to Si_3N_4, respectively. In this regard, mixing methods play a pivotal role in the way CNTs influence the electrical behavior of these nanocomposites. The observations show that the colloidal processing gives rise to the uniform distribution of nanotubes not only along the grain boundaries, but also inside grains and leads to a lower electrical conductivity than that obtained by other conventional mixing processes. In fact, by conventional mixing, the nanotubes are restricted to the grain boundaries and the percolation threshold becomes reduced. On the other hand, the thermal diffusivity and conductivity are decreased with CNT addtion due to some following reasons [184]:

(i) CNT incorporation decreases the thermal conductivity of Si_3N_4 matrix due to an increase in number of phonon scattering points,

(ii) CNT addition intensifies the phonon scattering by providing CNT/Si_3N_4 interfaces,

View Article Online
DOI: 10.1039/C7NR01878A

(iii) Since the thermal conductivity of CNTs in axial direction is more than that in transverse one, a random and homogeneous dispersion of nanotubes can worsen the thermal behavior of these binary systems,

(iv) There exists a pronounced discrepancy between the thermal behavior of single-walled and bundled CNTs, and

(v) The mixing step and SPS process may induce bending, twisting, and volume distortions in the nanotubes.

As empirically measured, a homogeneous dispersion can lead to equality between axial and transverse thermal diffusivities. Additionally, the thermal diffusivity is decreased with an increase in ambient temperature due to the pivotal effect of Umklapp scattering (i.e. phonon–phonon scattering) to reduce the mean free path length of phonons [184]. Similar results are reported by Osendi et al. [181].

One of the promising properties which CNT addition can induce in Si_3N_4 matrix is electromagnetic interference (EMI) shielding due to attenuation properties and high aspect ratio-induced properties of well-dispersed CNTs. This kind of electromagnetic interference can protect environment and sensitive circuits from the microwave radiation emitting from telecommunication apparatus [185].

2.2.2. Others

Nitride ceramics are refractory compounds with high hardness, thermal stability, chemical inertness, and fascinating electrical and optical properties. These UTHCs are widely used in some sophisticated industries among which aluminum nitride (AlN) and titanium nitride (TiN) are the most conventional [186, 187]. TiN bears the optical properties similar to gold, the hardness higher than alumina, excellent thermal stability up to 3000 °C, appropriate chemical stability in exposure to many etching solutions, high electrical conductivity, and excellent diffusion barrier capability against metals. These properties make TiN useful in integrated circuit manufacturing in which TiN is used as a glue layer for tungsten deposition, and as a diffusion barrier between silicon and metals [187]. Moreover, AlN benefits from some special characteristics such as high thermal conductivity about 10 times greater than that of Al_2O_3, low dielectric coefficient, excellent electrical resistance, and thermal expansion coefficient similar to silicon. Due to these advantageous properties, it is used in various engineering applications and especially, electronic industry [188, 189]. However, the potential applications of AlN and TiN ceramics have been restricted due to their inherent brittleness and comparatively low strength [190]. Recently some researchers have suggested CNTs as modifying agent and SPS technique as the appropriate compaction approach to enhance the mechanical and transportation properties of these ceramics.

View Article Online
DOI: 10.1039/C7NR01878A

Some reports show that the inclusion of CNFs results in the inhibition of grain growth and resultant high flexural strength. In contrary, they inhabit the easy rearrangement of AlN particles during SPS process and decline the final relative density. Also, it increases the fracture toughness of AlN ceramic through activating toughness mechanisms such as crack bridging and pull-out (Fig. 29). This increment in fracture toughness is due to the embedment of CNFs along the grain boundaries of AlN matrix and prevention of intergranular fracture mode. These implications do highly rely on fine CNF dispersion, such that the formation of CNF agglomeration in AlN matrix can degrade interfacial bonding and result in lower mechanical properties. Concerning the electrical effect, the electrical conductivity behavior of these binary systems abides by the percolation theory, so that CNF addition leads to an enhancement in electrical conductivity [191].

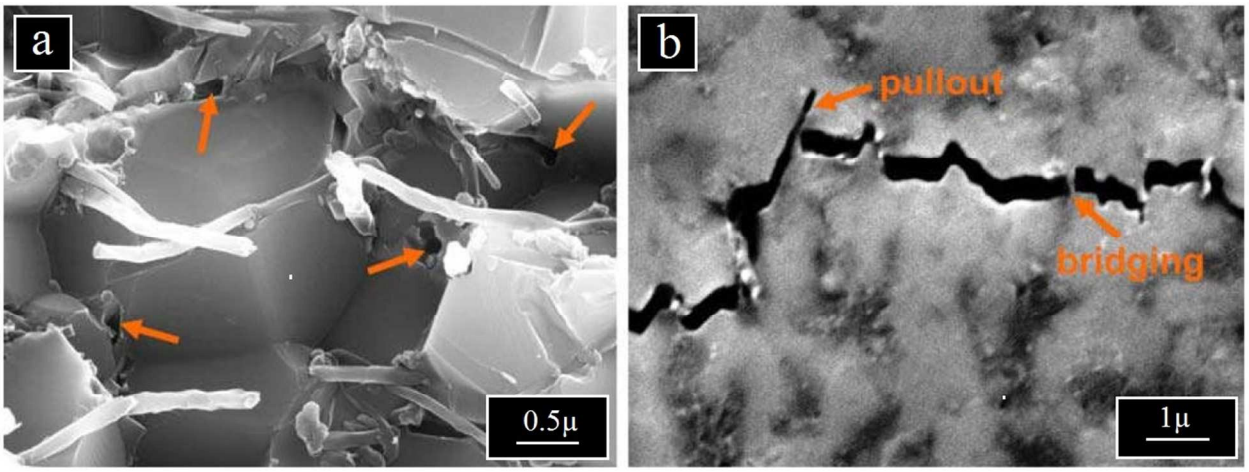

Fig. 29. SEM images of fracture surface of SPSed CNF-AlN nanocomposite. Residual holes caused by CNF pull-out and bridging effects of CNFs are marked by arrows in (a) and (b), respectively (Reproduced from ref. 191 with permission from Elsevier [191]).

In TiN-based nanocomposites, the CNT addition results in a decline in relative density due to the increased volume fraction of interfaces and pores and inevitably a high degree of agglomeration. In contrast, assuming a uniform distribution of nanotubes, binary TiN–CNT systems can benefit from high heat capacity and excellent thermal conductivity with respect to the monolithic matrix. The reasons for these events include: (i) higher thermal conductivity of CNTs compared with the matrix, (ii) decreased interfacial thermal resistance owing to strong covalent bonds between the reinforcements and the matrix, and (iii) fine dispersion of CNTs within the matrix with no phase separation and CNT agglomeration [192].

View Article Online
DOI: 10.1039/C7NR01878A

In one of these rare studies, Shi et al. [191] SPSed a variety of AlN-CNF nanocomposites with 0-7 wt% CNF at 650 °C with a small amount of CaF_2 and Y_2O_3 and investigated the potential effects of nanofibers on their physicomechanical properties. It was found that adding CNF reduces the relative density. As to the mechanical properties, CNF incorporation leads to a considerable increment in flexural strength and fracture toughness of AlN-based nanocomposites. However, CNFs at contents higher than 3wt% tend to agglomerate due to the low efficiency of present mixing techniques and form clusters (Fig. 30). This inhomogeneity may result in poor interfacial bonding between CNFs and the matrix and give rise to the low fracture toughness and flexural strength with respect to monolithic AlN. Moreover, the hardness and elastic modulus of these composites are decreased continuously with CNF due to the poor CNF/AlN interfacial bonding (Fig. 30).

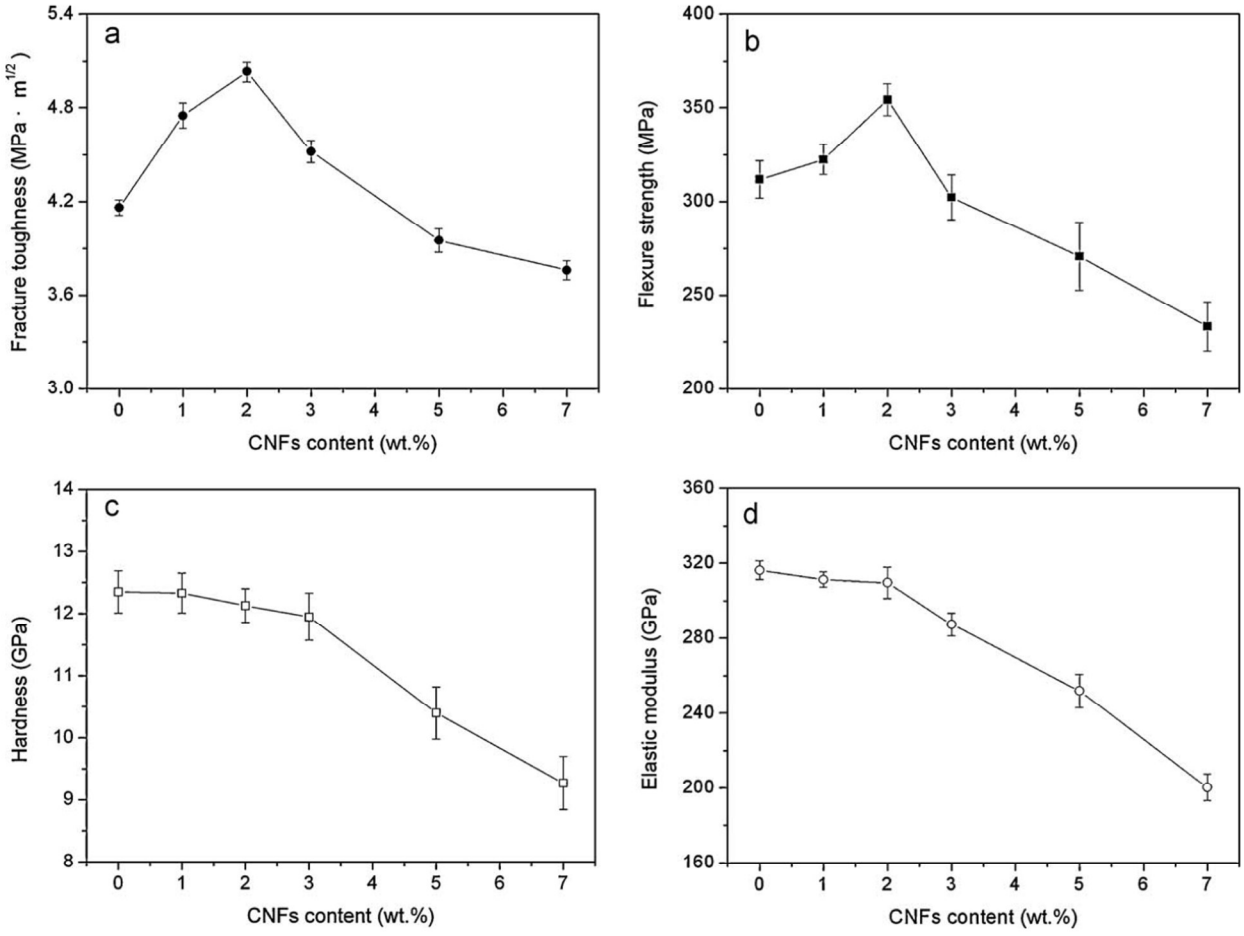

Fig. 30. The mechanical properties of SPSed CNF-AlN nanocomposites with various CNF content (Reproduced from ref. 191 with permission from Elsevier [191]).

View Article Online
DOI: 10.1039/C7NR01878A

In another study, Jiang et al.[192] SPSed TiN-based nanocomposites with 0-5 wt% CNT at 1250 °C and studied the influence of CNTs on physical and thermal properties of this ceramic system. Microscopic and Raman spectroscopy revealed that CNTs are well-dispersed with no thermomechanical degradation and structural damages after SPS process. The results show that the fracture mechanism in monolithic TiN switches partially from intergranular to intragranular mode (Fig. 31). Also, the addition of 0.1 wt% CNT slightly increases the thermal diffusivity due to the formation of CNT-based percolation network. It is while the further increment in CNT content higher than 1 wt% lessens the thermal diffusivity even less than that of monolithic TiN. This phenomenon is related to covalent interactions between CNTs and the matrix. In fact, the centers of phonon distractions begin to increase due to these interactions and warping of nanotubes, and finally decline the mean free path of phonons and resultant thermal diffusivity. In addition to thermal diffusivity, the "thermal conductivity" and heat capacity of TiN increase by adding CNTs due to their extraordinary electrical characteristics. Moreover, an increase in temperature results in higher thermal properties.

View Article Online
DOI: 10.1039/C7NR01878A

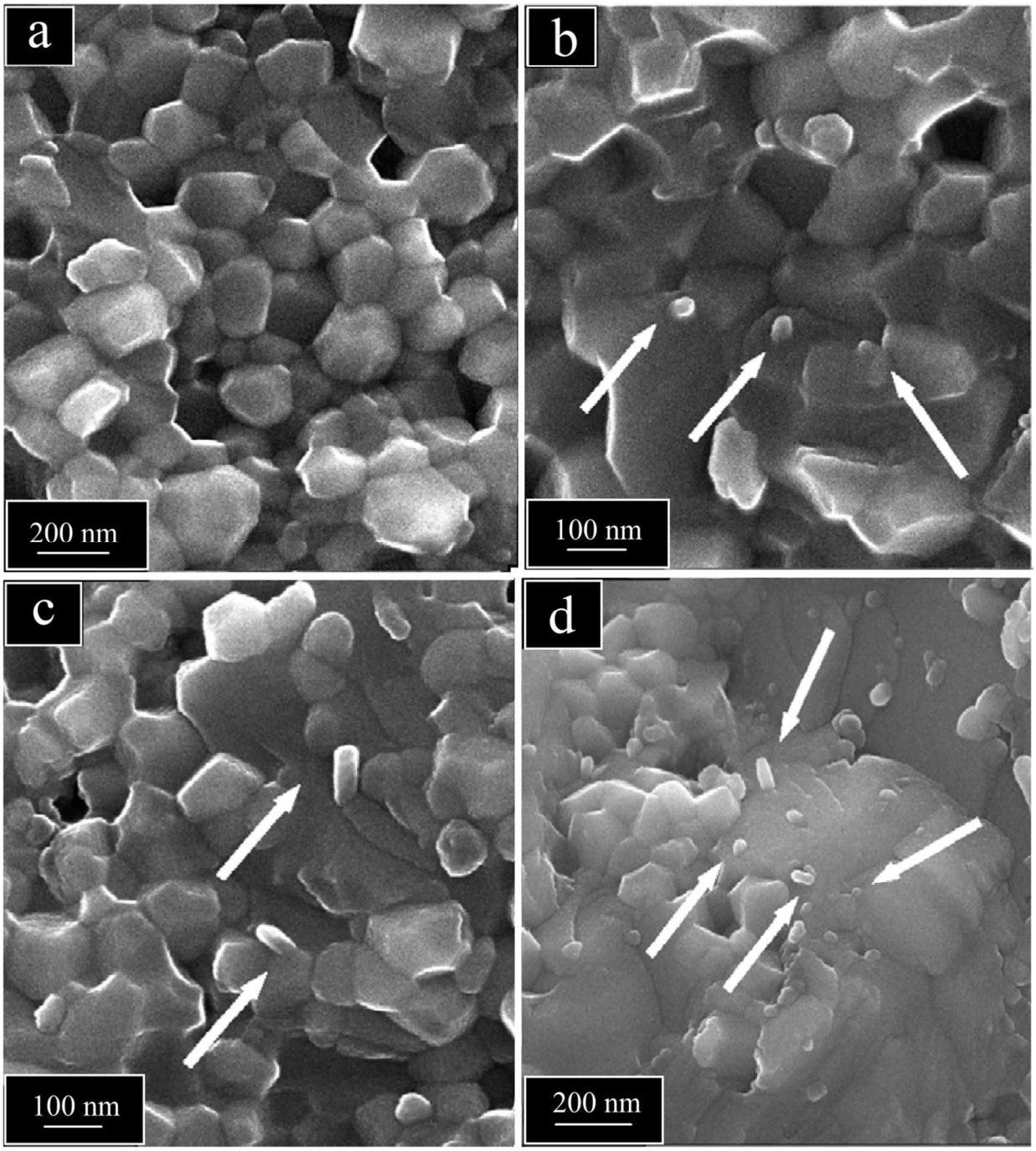

Fig. 31. SEM photographs of (a) pure TiN, and SPSed CNT-TiN nanocomposites with (b) 0.1wt%, (b) 1wt%, and (c) 5wt% MWCNT content. The clear edges and corners in (a) suggest the intergranular fracture mode, while increasing CNT content results in blurred and rugged grain interfaces and suggests both the intergranular and intragranular fracture modes (Reproduced from ref. 192 with permission from Elsevier [192]).

View Article Online
DOI: 10.1039/C7NR01878A

2.2.3. Summary of properties

The relative density of SPSed CNT-nitride ceramics as a function of nanotube content is depicted in Fig. 32. Generally, adding CNT to SPSed nitride ceramics degrades their relative density due to the inevitable formation of pores and CNT agglomerates [192]. However, the selection of an appropriate mixing procedure can maintain the relative density of these nanocomposites at higher amounts (over 97-98%). For instance, the in-situ growth of CNTs in Si_3N_4 matrix with a highly uniform distribution results in higher relative density [183].

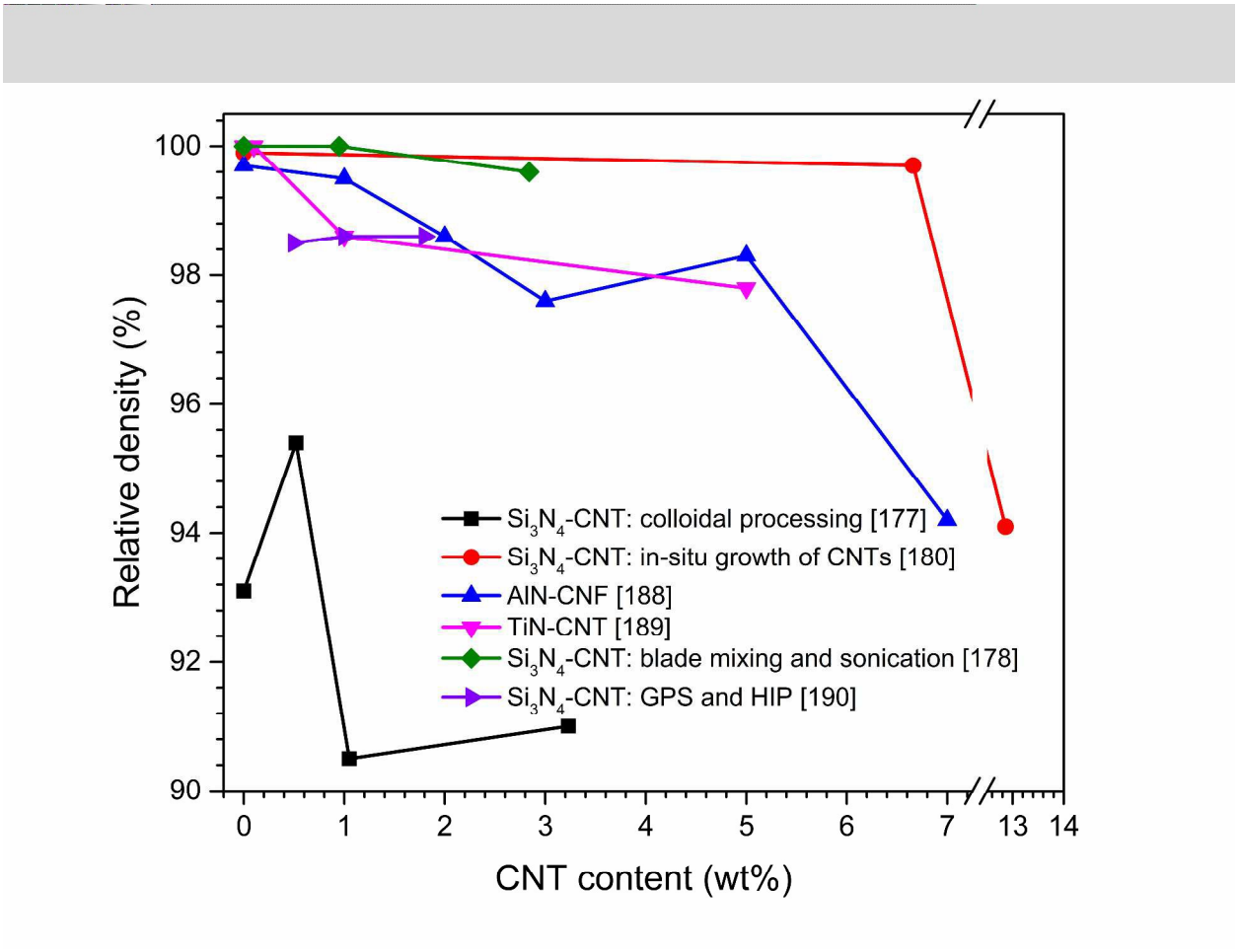

Fig. 32. The relative density variation of SPSed CNT-nitride ceramics as a function of CNT content.

The hardness variation of SPSed CNT-nitride ceramics has the same trend as relative density. As seen in Fig. 33, the incorporation of CNTs into nitride ceramics generally results in lower hardness mainly due to the formation of pores and CNT agglomerates [192]. The highest hardness values belong to SPSed in-situ grown CNT-filled Si_3N_4 nanocomposites due to comparatively high hardness of synthesized α-Si_3N_4 grains and better distribution of CNTs due to in-situ growth [183].

View Article Online
DOI: 10.1039/C7NR01878A

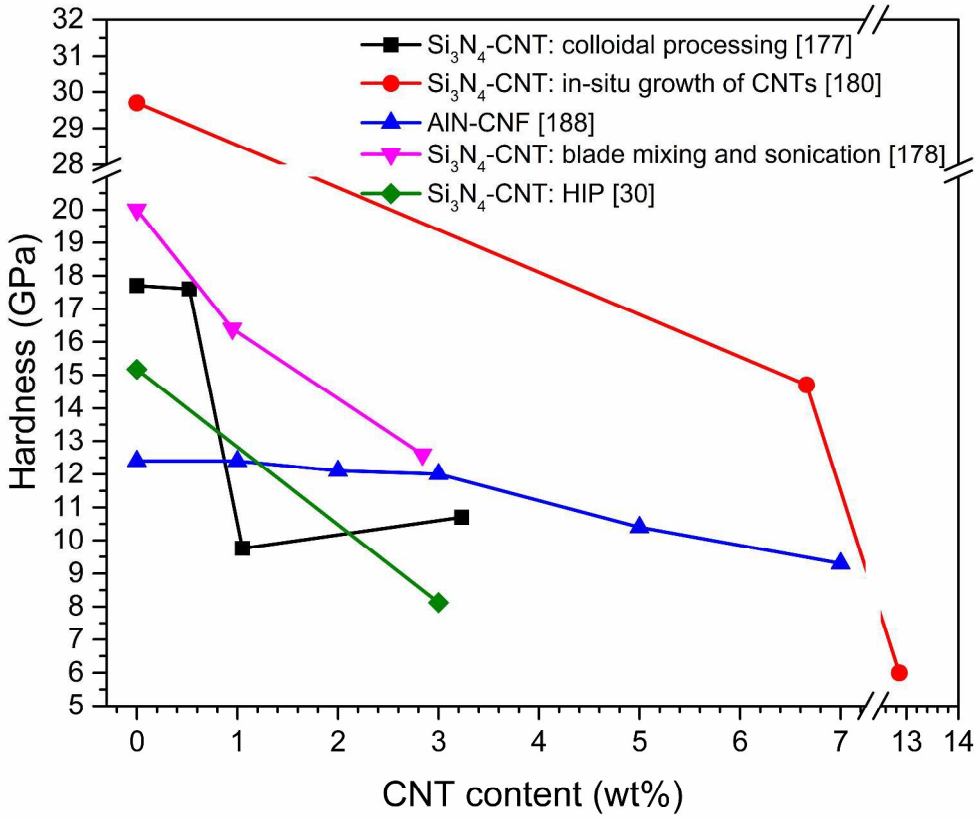

Fig. 33. The hardness of SPSed CNT-nitride ceramics as a function of CNT content.

Fig. 34 presents the fracture toughness variation of different SPSed CNT-nitride ceramics with nanotube content. As clearly seen, adding CNTs to nitride ceramics may decrease or increase their K_{Ic}. For example, the inclusion of CNTs drastically degrades the fracture toughness of Si_3N_4 due to the absence of elongated β-Si_3N_4 and presence of CNT agglomerates and pores [180]. In contrast, the homogenous dispersion of CNFs between AlN grains up to a critical value can increase the toughness through the activation of toughening mechanisms such as bridging and pull out. These mechanisms are activated when the bonding between AlN grains and CNTs are strong enough [191]. Table 4 presents a list of dominant toughening mechanisms in CNT-containing nitride ceramic matrix nanocomposites.

To compare the potential capabilities of the SPS process with other conventional powder metallurgy methods, some typical properties of HIPed CNT-Si_3N_4 nanocomposites processed by gas pressure sintering or/and HIP at 1700 ^oC for 1 [193] or 3 [30] hours are given in Fig. 32-34. As obviously seen, SPS is capable of producing CNT-filled nitride ceramic nanocomposites with higher relative density and superior mechanical properties. However, to achieve this goal, the

View Article Online
DOI: 10.1039/C7NR01878A

optimization of SPS conditions and selection of an appropriate method for homogeneously dispersing CNTs in nitride matrices are critically required.

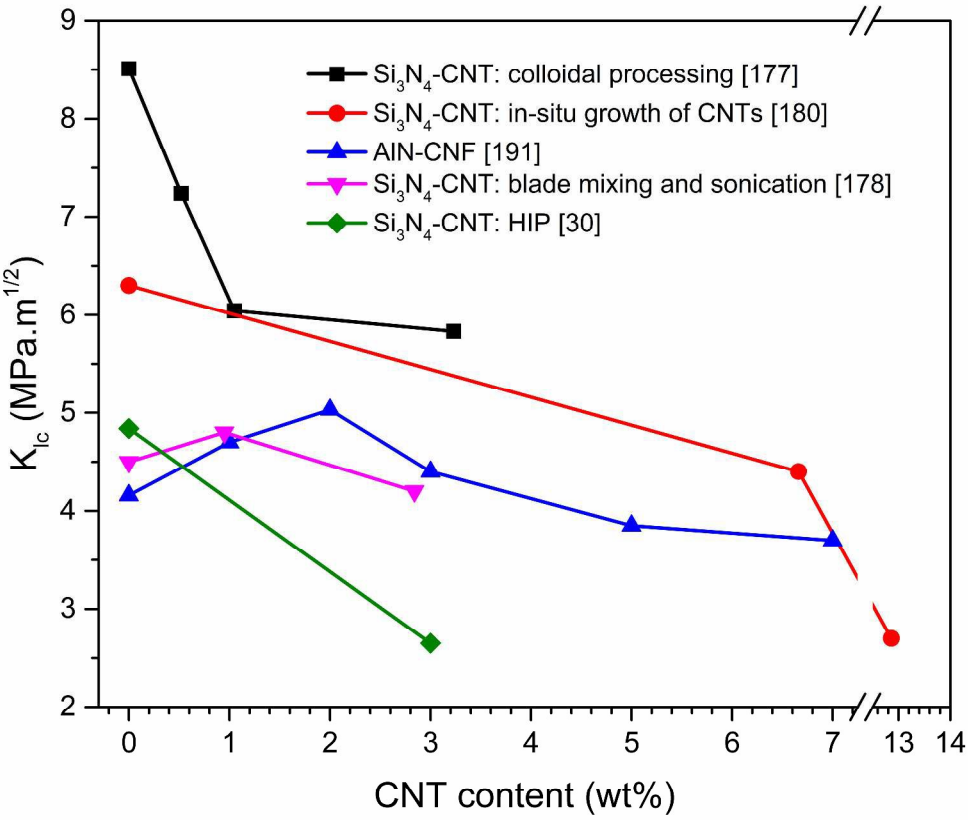

Fig. 34. The fracture toughness of SPSed CNT-nitride ceramics versus CNT content.

Table 4. Dominant toughening mechanisms in some CNT-filled nitride ceramic matrix nanocomposites

Composite system	CNT volume (vol%)	Active Toughening mechanism	Reference
Si_3N_4-CNT	α-Si_3N_4 1wt% MWCNT +4wt% Al_2O_3 +6wt% Y_2O_3	Pull-out	29, 177
	1,2,6% SWNT + +<10mass% Y_2O_3, MgO and Al_2O_3	crack bridging, pull-out, and crack deflection	180, 184

View Article Online
DOI: 10.1039/C7NR01878A

	α-Si_3N_4+ 5wt% Y_2O_3 +2wt% Al_2O_3 +0-22% MWCNT	Pull-out bridging	183
AlN-CNT	Monolithic AlN	-	191
	1-7wt% CNF +2wt%CaF_2 +1wt% Y_2O_3	Crack bridging- Pull out- Crack propagation	191
TiN-CNT	Monolithic TiN	-	192
	0.1-5wt% CNT	-	192

The thermal and electrical conductivities of SPSed CNT-Si_3N_4 and CNF-AlN composites are depicted in Fig. 35. As seen, adding CNTs or CNFs can increase the electrical conductivity of SPSed nitride ceramics. In the case of thermal conductivity, it generally results in lower thermal conductivity due to induced pores and interfaces [184, 191].

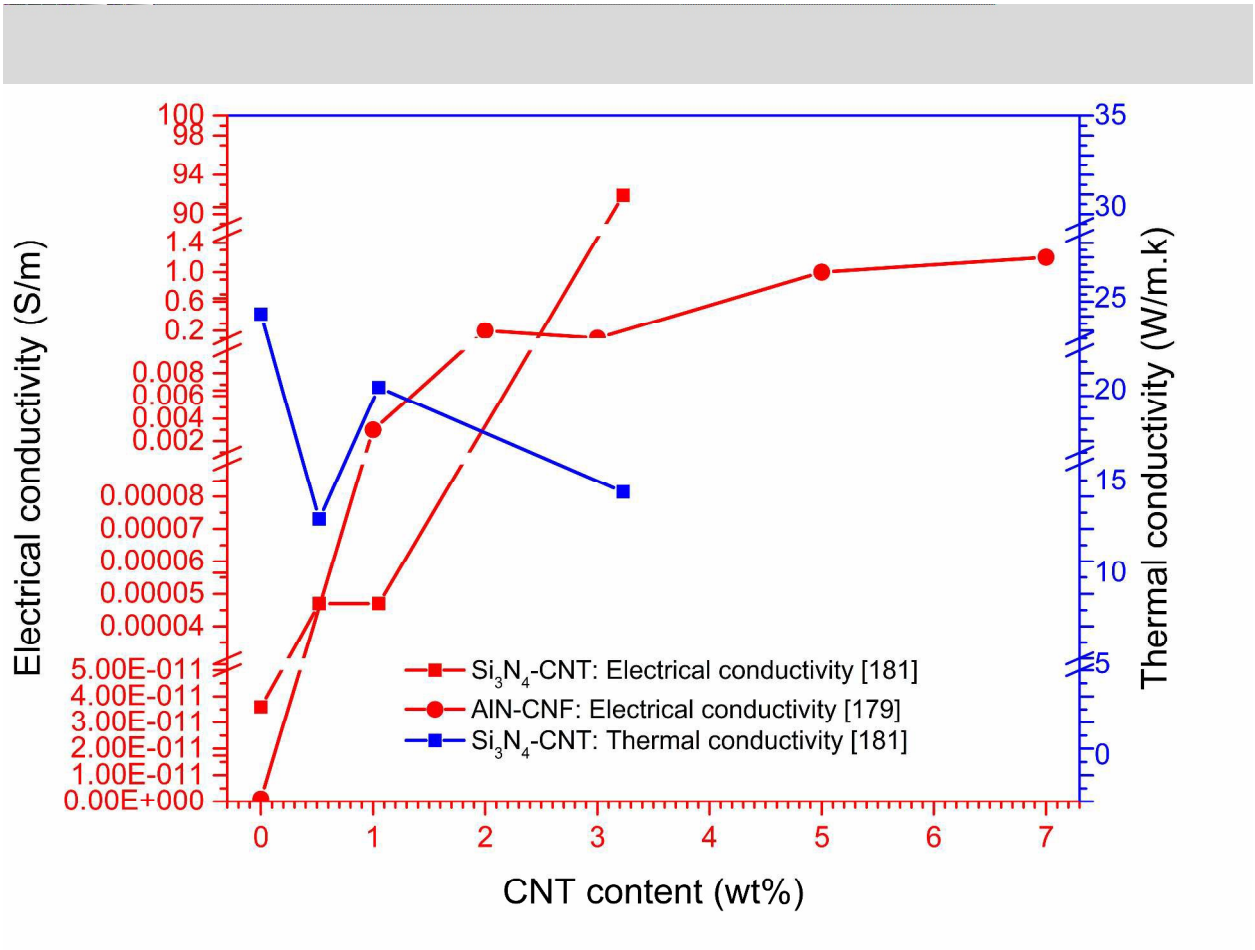

View Article Online
DOI: 10.1039/C7NR01878A

Fig. 35. The thermal and electrical conductivities of SPSed CNT-nitride ceramics versus CNT content.

2.3. CNT- Boride ceramic matrix nanocomposites

2.3.1. CNT- B_4C nanocomposites

Boron carbide (B_4C) as third hardest material benefits from many high-performance applications such as lightweight armour for individual protection, control rods in nuclear reactors and sandblasting nozzles [194-196]. It is characterized by low density, high elastic modulus, extraordinary hardness, excellent chemical and thermal stability and appropriate neutron absorption cross-section [197-200]. However, its practical applications in industry are restricted by weak mechanical stability, especially, low fracture toughness. All attempts to obtain fully dense B_4C ceramic specimens through conventional sintering methods, result in a variety of secondary phases, grain coarsening and residual porosities to deteriorate the physical and mechanical properties of these materials [201-205]. To tackle these challenges, some research works have resorted to SPS technique. Unlike the conventional sintering methods which can produce the samples with relative density of 85%, SPS enables the fabrication of highly dense parts with a relative density of 95%. Other approach to toughen B_4C-based ceramics is the incorporation of carbon derivatives [1, 206]. It can generate the presence of CNTs within the matrix gain boundaries and shorten the crack length [207-209]. In this regard, the first attempts are associated with works by Zhang et al. [210] who employed the SPS technique for first time to densify B_4C ceramic powders reinforced with CNTs. They reported that the hardness and fracture toughness of these composites are increased linearly as a direct function of CNT volume fraction. As shown in Fig. 36-a, the increased hardness of the composites and the monolithic samples are sufficiently low, suggesting that these material systems are not fully dense. In another study, Kobayashi et al. [211] reported that Vickers hardness and elastic modules of B_4C-based ceramics are decreased and fracture toughness of the composites are slightly improved as a function of CNT content provided Al powder is added as a modifier (Fig. 36-b). This additive can be laid into the oxygen sites (i.e. oxygen deficiency) and promotes the increased electrical conductivity in the grain and grain boundaries. Therefore, the relative density of SPSed CNT-B_4C systems are expected to be measured 10% more than that of the monolithic B_4C, which is in good agreement with the results reported by Milsom [212] (Fig. 36-c), Apark and Sahin [213], and Yavas et al. [174]. They found out that such a superior mechanical properties can be attributed to the better homogenous distribution of CNTs, resulting in higher relative density and consequently superior mechanical properties. However, high content of the nanotubes gives rise to the formation of proved micro-cracks between the CNT and B_4C grain boundaries.

View Article Online
DOI: 10.1039/C7NR01878A

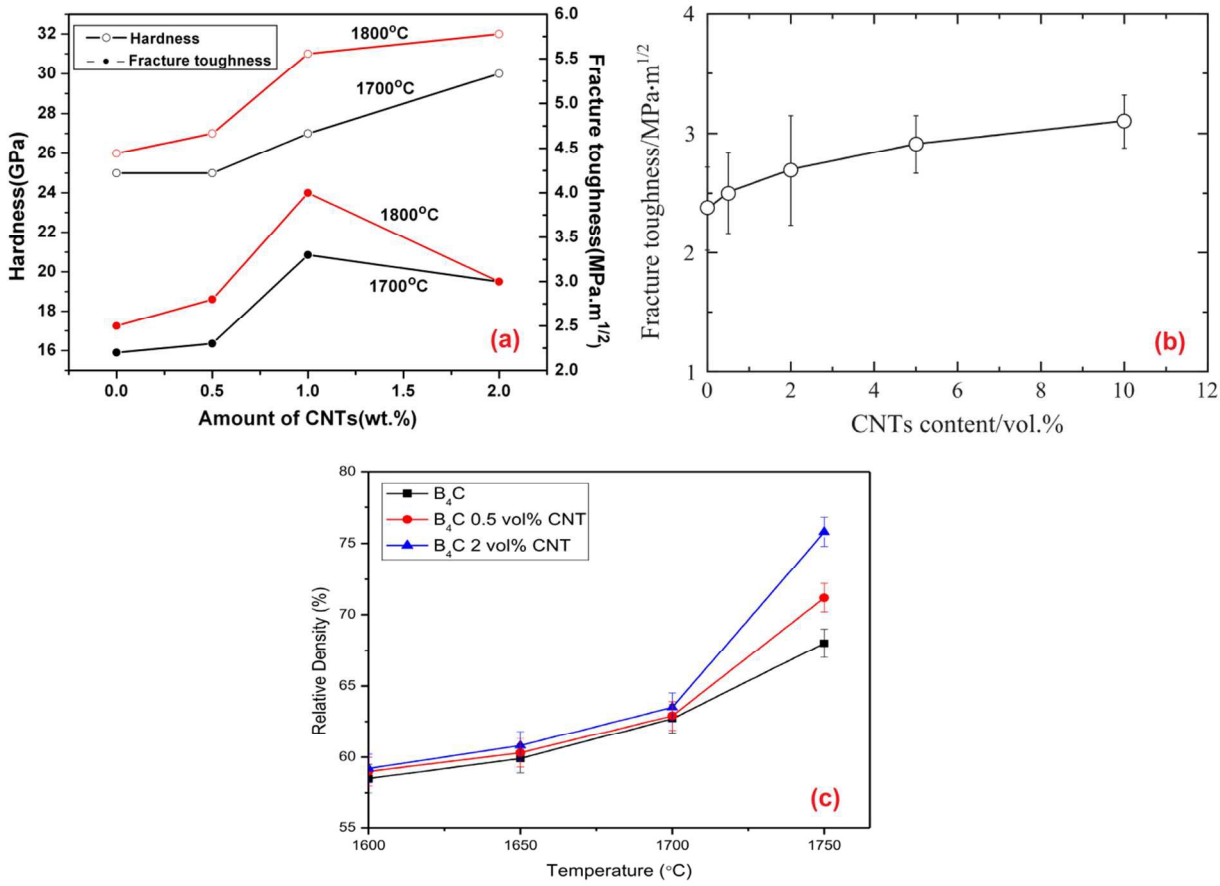

Fig. 36. The variation of hardness (a), fracture toughness (b), and relative density (c) as a function of CNT content and SPS temperature for SPSed binary CNT-B_4C nanocomposites (Reproduced from ref. 210-212 with permission from Elsevier [210-212]).

2.3.2. CNT- ZrB_2 nanocomposites

In the last two decades, ZrB_2 has been considered as one of the most significant UHTCs for thermal production systems in space vehicles and scramjet engine components for hypersonic aerospace vehicles. Nowadays, it is highly demanded owing to its special features [214-216] including high elastic modulus, excellent thermal and electrical conductivities, extraordinary thermal shock resistance and appropriate chemical inertness. However, its fracture toughness is inadequate for these sophisticated applications. Therefore, it is necessary to improve its physico-mechanical properties through the inclusion of a second phase such as SiC and other carbon flakes. For instance, if a ternary ZrB_2-SiC-CNT system is produced by hot pressing at 1900 °C, its fracture toughness will be 15% higher than that of the monolithic ZrB_2 [217], but fails to improve the thermal and mechanical behaviour of the ceramic matrix due to large grain growth and strong interfacial CNT/ZrB_2 reactions. As a result, the SPS technique is required for the

View Article Online
DOI: 10.1039/C7NR01878A

fabrication of tough ZrB_2-based ceramics. Overall, in SPSed CNT-added ZrB_2 systems, some CNT-induced toughing mechanisms may be stimulated among which CNT pull-out, crack bridging and crack deflection are highly observed. For example, Govindaraajan and coworkers [218] modified the SPSed monolithic ZrB_2 by two ways: (i) the addition of 2-4 wt% CNT, and (ii) the incorporation of 10-40 wt% SiC. They reported that almost fully dense samples (>99%) can be achieved in both cases (Fig. 37). Additionally, the fracture toughness values can be improved by 2 and 1.4 times more than that for the monolithic sample (>1.5 MPa $m^{1/2}$), respectively (Fig. 38). However, the hot pressing is comparatively successful in elevating the hardness of these ceramic composites than SPS. In fact, the SPS technique can improve the mechanical properties of CNT-containing ZrB_2 composites through CNT pull-out mechanism at grains and grain boundaries and offer lower grain size compared with hot pressing. Crack propagation in SPSed ZrB_2–based matrices with CNTs or SiC particles is recently examined. The observations show that these particles can deflect cracks and considerably increase the fracture toughness. On the other hand, CNTs do not increase the hardness of SPSed CNT-ZrB_2 (Fig. 37) due to the fact that CNTs do not inhibit the grain growth of matrix in this case. Similar results are obtained by Lin et al. [144, 219]. Table 5 summarizes the experimental results of fracture toughness for CNT-modified B_4C and ZrB_2 nanocomposites.

View Article Online
DOI: 10.1039/C7NR01878A

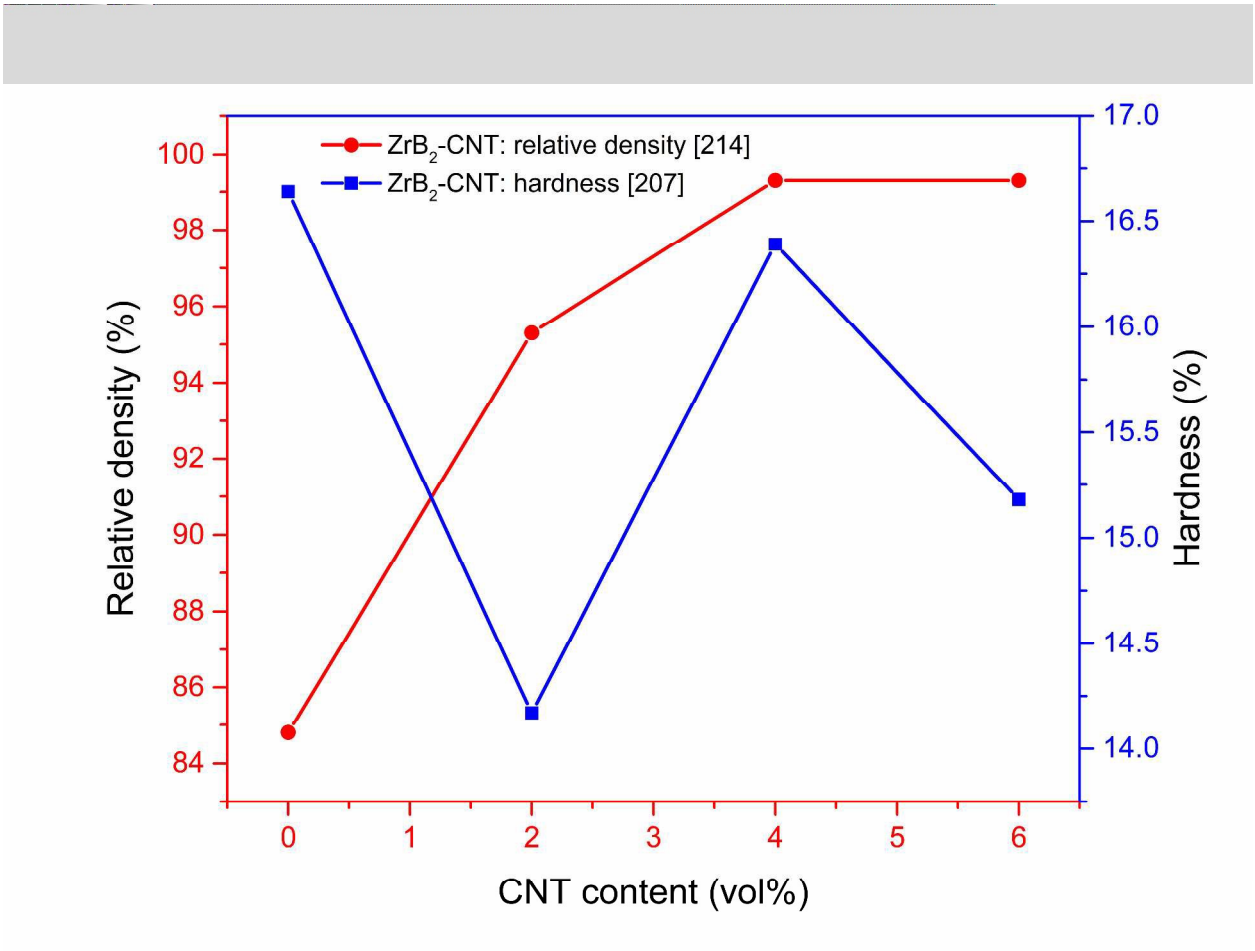

Fig. 37. The relative density variation of SPSed CNT-boride ceramics as a function of CNT content.

View Article Online
DOI: 10.1039/C7NR01878A

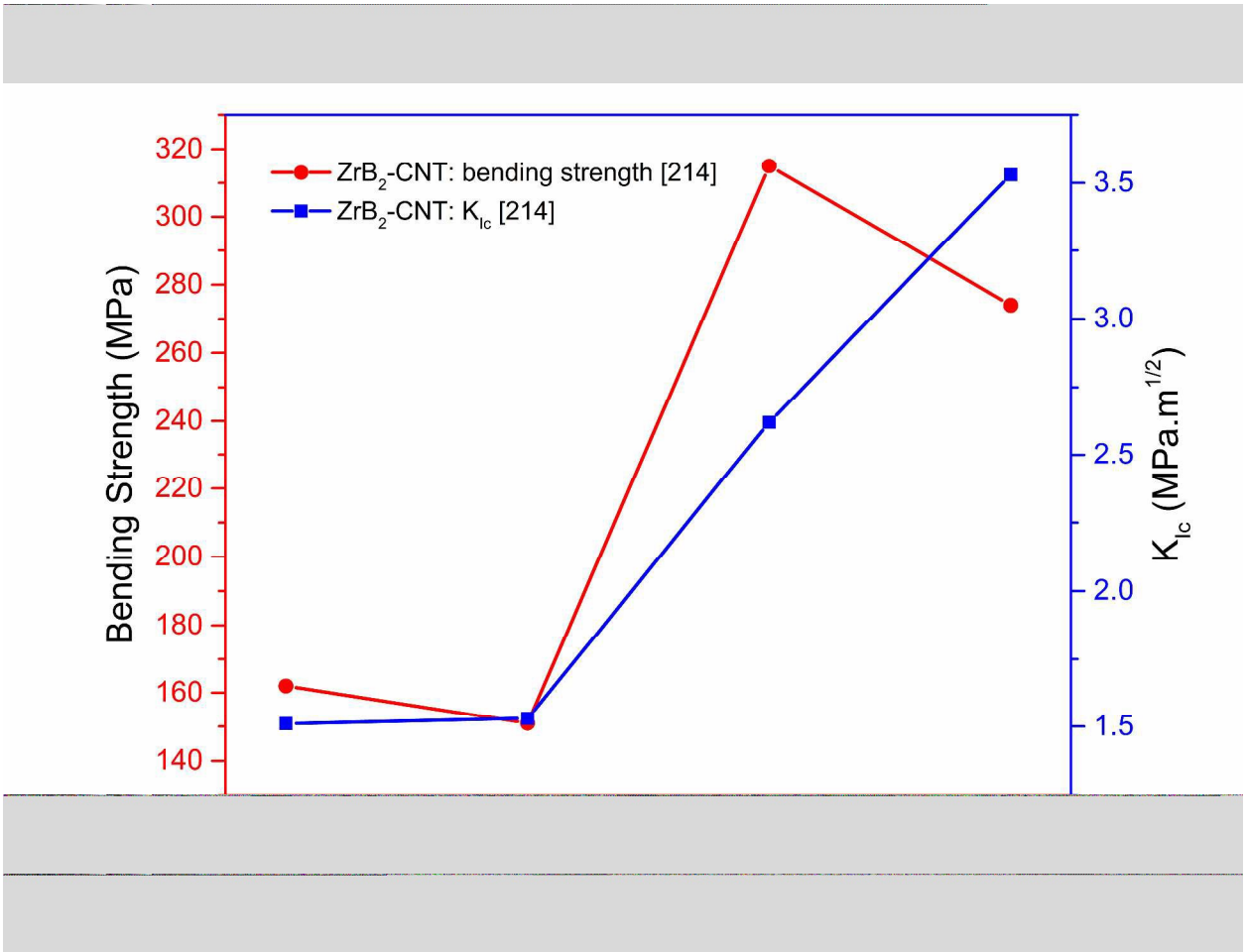

Fig. 38. The variation of bending strength and fracture toughness of SPSed CNT-boride ceramics as a function of CNT content.

Table 5. Fracture toughness of SPSed CNT-containing boride ceramic matrix nanocomposites

Composite system	CNT volume (vol%)	Dispersion method	Fabrication conditions	K_{Ic} (MPa $m^{1/2}$)	Reference
B_4C-CNT	0-2	Ultrasonic mixing in ethanol	SPS (1800 °C, 5 min, 30 MPa, 200°C/min)	22±3.5	[210]
	0.5-10%	Ultrasonic mixing in ethanol	SPS (1850 °C, 10 min, 10 MPa)	2.37-3.10	[211]

View Article Online
DOI: 10.1039/C7NR01878A

	0.5-2	Ultrasonic mixing in ethanol	SPS (1750 °C, 8 min, 16 MPa, 200°C/min)	-	[212]
	0-2	Ultrasonic mixing in ethanol	SPS (1725 °C, 5 min, 40 MPa, 150°C/min)	35±2	[213]
	0.5-3	Ultrasonic mixing in ethanol	SPS (1590-1700°C, 5 min, 40 MPa, 150°C/min	9	[174]
ZrB_2-CNT	2-6	Ball milling	SPS (1900°C, 15 min, 70 MPa, 100°C/min	2.3 3.5	[218]
	15	Ball milling	SPS (1800°C, 10 min, 25 MPa, 100°C/min	8	[144]

2.4. Concluding remarks for material selection

In previous sections, a broad overview of ceramic systems in which CNTs and CNFs are used as reinforcing agents and SPS is employed as the processing method was given. As comprehensively addressed, the physicomechanical properties of CNT-filled ceramic matrix nanocomposites strongly depend on the microstructural features pertinent to CNTs and CNFs. In conformity with the previous discussions, a wide range of properties can be obtained by utilizing a broad spectrum of ceramics as matrix materials and different CNT content as additive. In sophisticated industrial applications, it is significant to easily select the materials suitable from properties points of view. In this section, the authors try to summarize the experimental results reported for different SPSed CNT-containing ceramic systems, so that it is possible to highlight structure-properties relationship in these material systems. Such analyses are useful for designers and engineers involved in materials selection.

For applications in which hardness is a crucial factor, Fig. 39 can help for choosing a proper CNT-ceramic system. This bubble map shows the range in which the hardness of different SPSed CNT-filled ceramic nanocomposites varies. As seen, the highest hardness is for SPSed CNT-B_4C systems with low density. The high hardness and low density make SPSed CNT-B_4C

View Article Online
DOI: 10.1039/C7NR01878A

nanocomposites good candidate for light and hard applications. On the other hand, SPSed CNT-TaC and ZrC are heavy systems with moderate hardness and can be used for applications in which a medium range of hardness is required. However, other CNT-ceramic nanocomposites with moderate hardness such as CNT-Al_2O_3, CNT-Si_3N_4, and CNT-SiC have a density much lower than TaC and can be replaced with SPSed CNT-TaC systems for applications in which hardness and density are crucial factors. The lowest hardness with lowest density belongs to CNT-filled Al_2O_3, HA, SiO_2, and MgO composite systems. Unlike other ceramic systems, SPSed CNT-Al_2O_3 benefits from a wide range of hardness and density and can respond to a wide range of industrial applications.

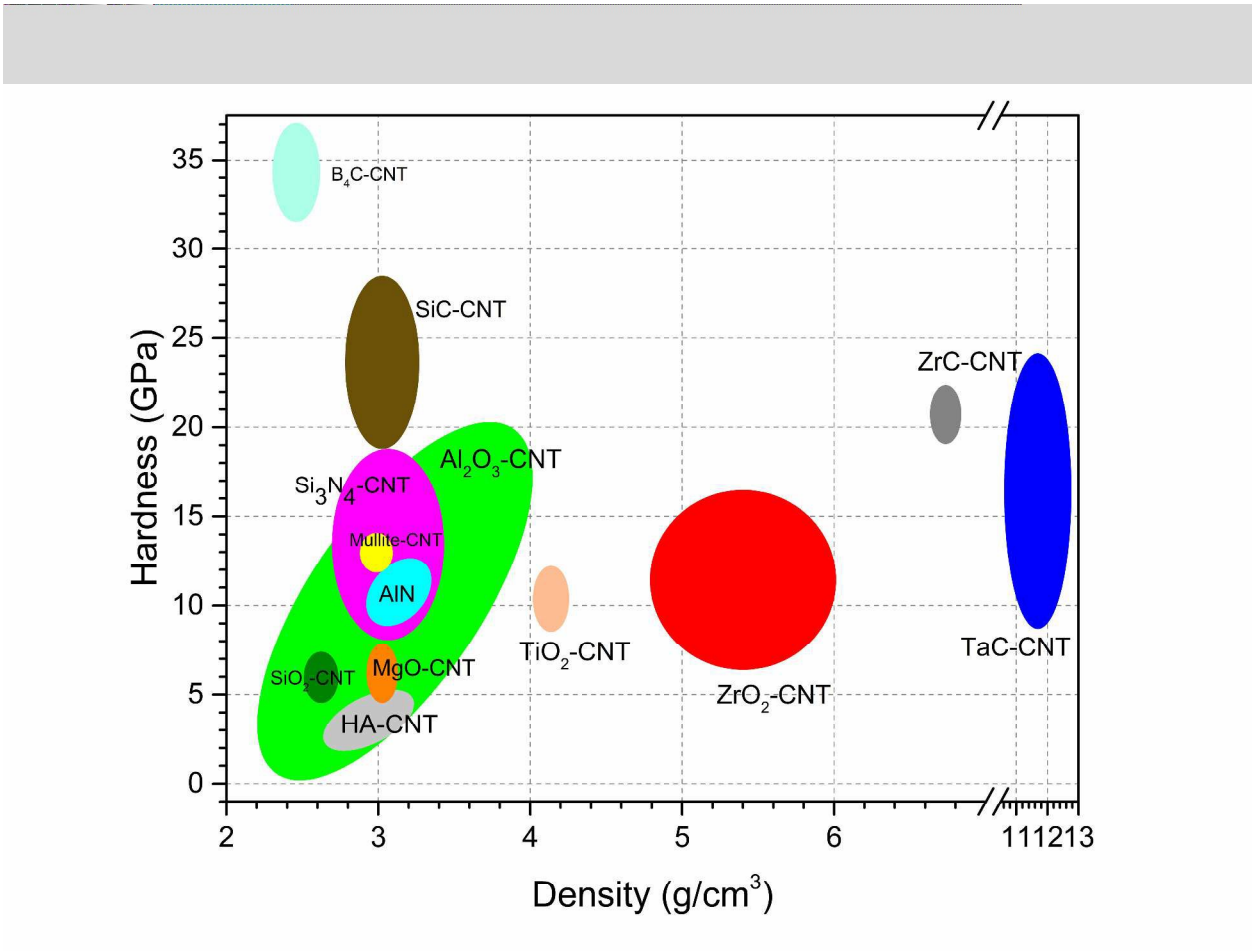

Fig. 39. The hardness variation of SPSed CNT-ceramics as a function of apparent density.

Bending strength is another mechanical property which is of great interest in material selection for industrial applications. Fig. 40 shows the bending strength of different SPSed CNT-containing ceramic nanocomposites with various densities. As seen, the numerical values of

View Article Online
DOI: 10.1039/C7NR01878A

bending strength for these material systems are between 160 and 720 MPa. The highest bending strength in this category belongs to SPSed CNT-SiC, CNT-ZrB_2, and CNT-ZrO_2 systems among which CNT-SiC nanocomposites have the lowest density. This superiority makes these composites suitable for applications in which low weight and high bending strength are required. Among the low-density ceramic materials, CNT-mullite and CNT-AlN nanocomposites have almost the same density as CNT-SiC binary systems with lower bending strength. Additionally, SPSed CNT-ZrO_2 composites benefit from largest range of bending strength values among other ceramics. This feature proves the high ability of these nanocomposites in tuning the bending strength by changing their CNT content and SPS conditions.

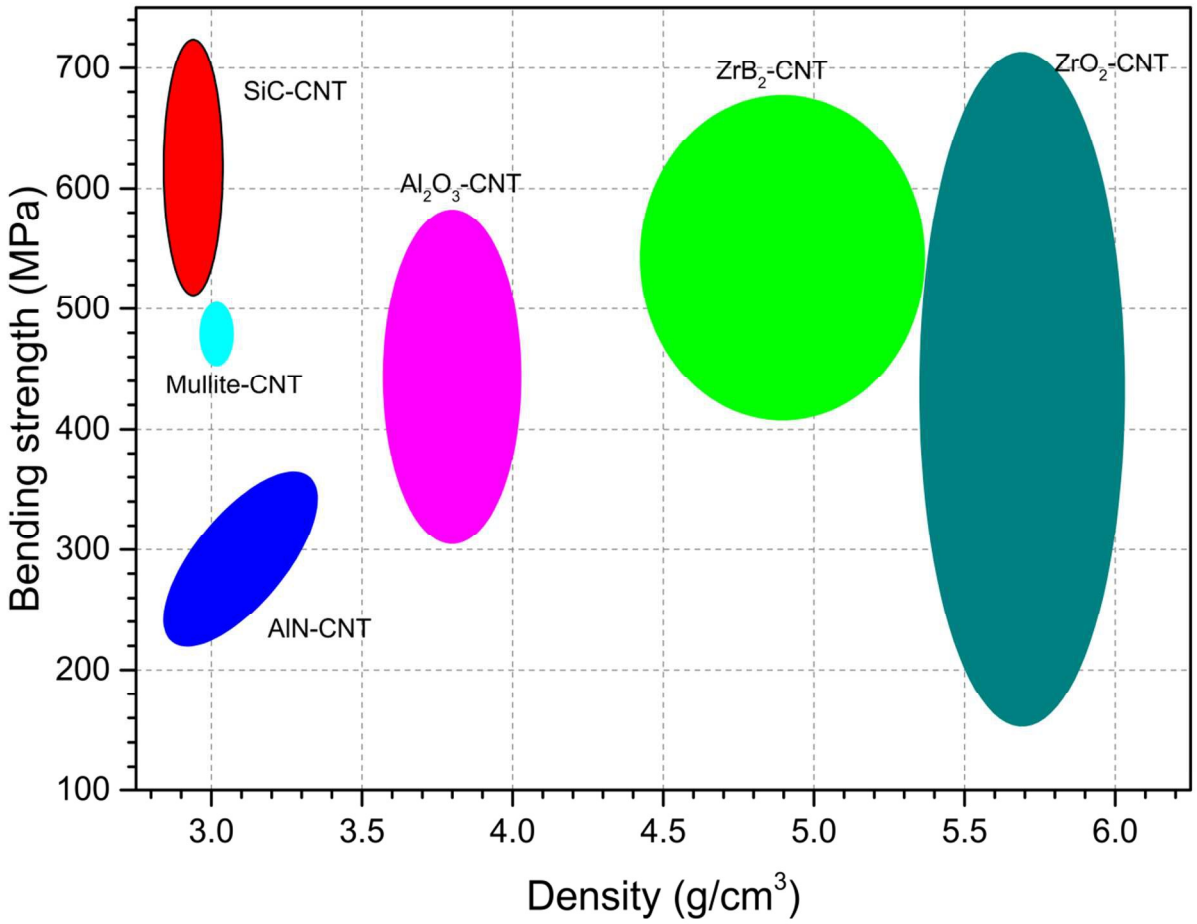

Fig. 40. The bending strength of SPSed CNT-ceramics as a function of apparent density.

Elastic modulus as one of the main properties of structural materials is also an effective factor in material selection for structural applications. Fig. 41 shows the bubble map of elastic modulus

View Article Online
DOI: 10.1039/C7NR01878A

for different SPSed CNT-containing ceramic nanocomposites with various densities. Elastic modulus of these materials ranges between 30-480 MPa. The highest Young's modulus belongs to CNT-filled B_4C, SiC, and TaC nanocomposites among which B_4C and SiC-based systems have lower density and can be good candidates for structural applications in which low weight is preferred.

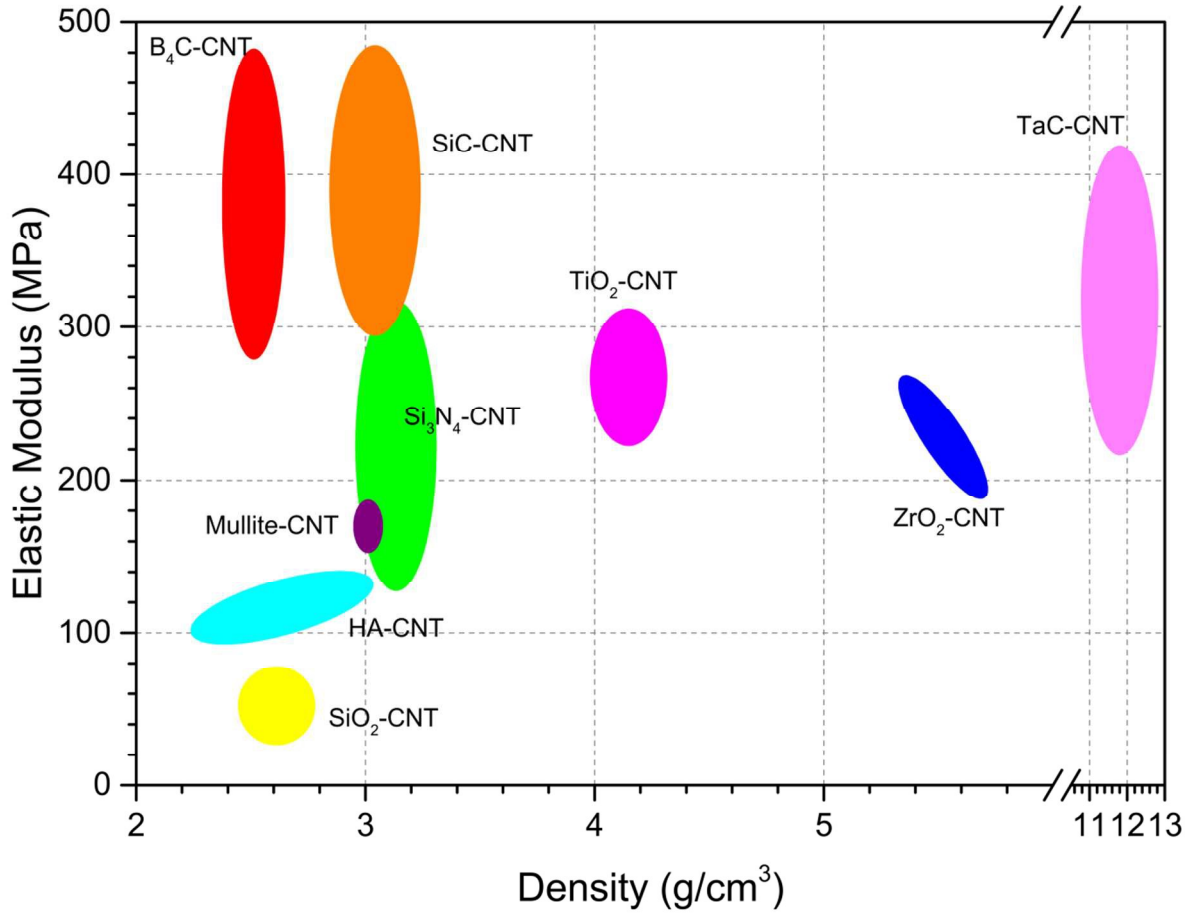

Fig. 41. The elastic modulus of SPSed CNT-ceramics as a function of density.

Fig. 42 displays the bubble map of fracture toughness for different SPSed CNT-containing ceramic nanocomposites with various densities. As seen, the numerical values of K_{Ic} for these binary systems range between 0.6 and 11.2 MPa.m$^{1/2}$. The highest fracture toughness in this category is obtained for CNT-ZrO_2 composites. Other ceramic systems of high K_{Ic} after CNT-ZrO_2 systems include Si_3N_4, ZrB_2, and Al_2O_3-based nanocomposites among which Si_3N_4 ones benefit from the lowest density and can act as proper choices for applications in which low weight and excellent toughness are needed.

View Article Online
DOI: 10.1039/C7NR01878A

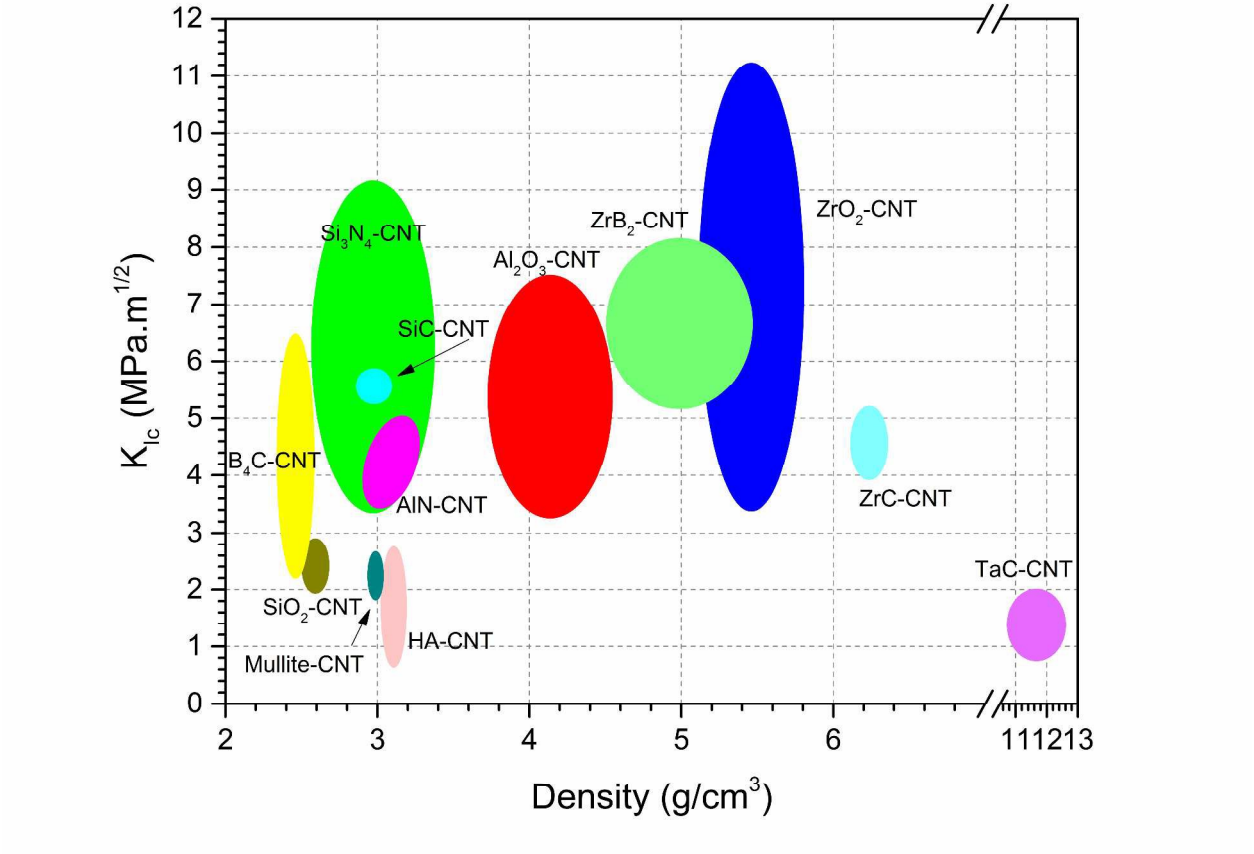

Fig. 42. The bubble map of fracture toughness for SPSed CNT-containing ceramics as a function of density.

Alongside the mechanical characteristics, functional properties such as electrical and thermal conductivities are also of prime significance in materials selection. Fig. 43 shows the electrical conductivity variations of different SPSed CNT-ceramic nanocomposites with various densities. As obviously seen, the addition of CNTs can reinforce the electrical conductivity of insulator ceramics and even make them conductive. The highest electrical conductivity is achieved for SPSed CNT-Si_3N_4 nanocomposites. They also benefit from low density which render them appropriate choices for producing light and electrically conductive ceramic-based devices. Fig. 44 also shows the bubble curve of thermal conductivity for different SPSed ceramic and CNT-filled ceramic nanocomposites as a function of apparent density. As seen, the highest thermal conductivity as well as low density belong to SPSed CNT-Al_2O_3 systems. They also bear the widest range of thermal conductivity (~34-92 W/m.k). As seen in Fig. 44, from thermal application point of view, CNTs have two main effects on SPSed ceramics: (i) CNT addition results in lower density of SPSed ceramics and contributes to a decrement in total weight of

View Article Online
DOI: 10.1039/C7NR01878A

ceramic-based thermal conductors, and (ii) it may increase or decrease the thermal conductivity of SPSed ceramics; adding CNTs to TiN, Al_2O_3, SiO_2 and B_4C ceramics enhances the thermal conductivity.

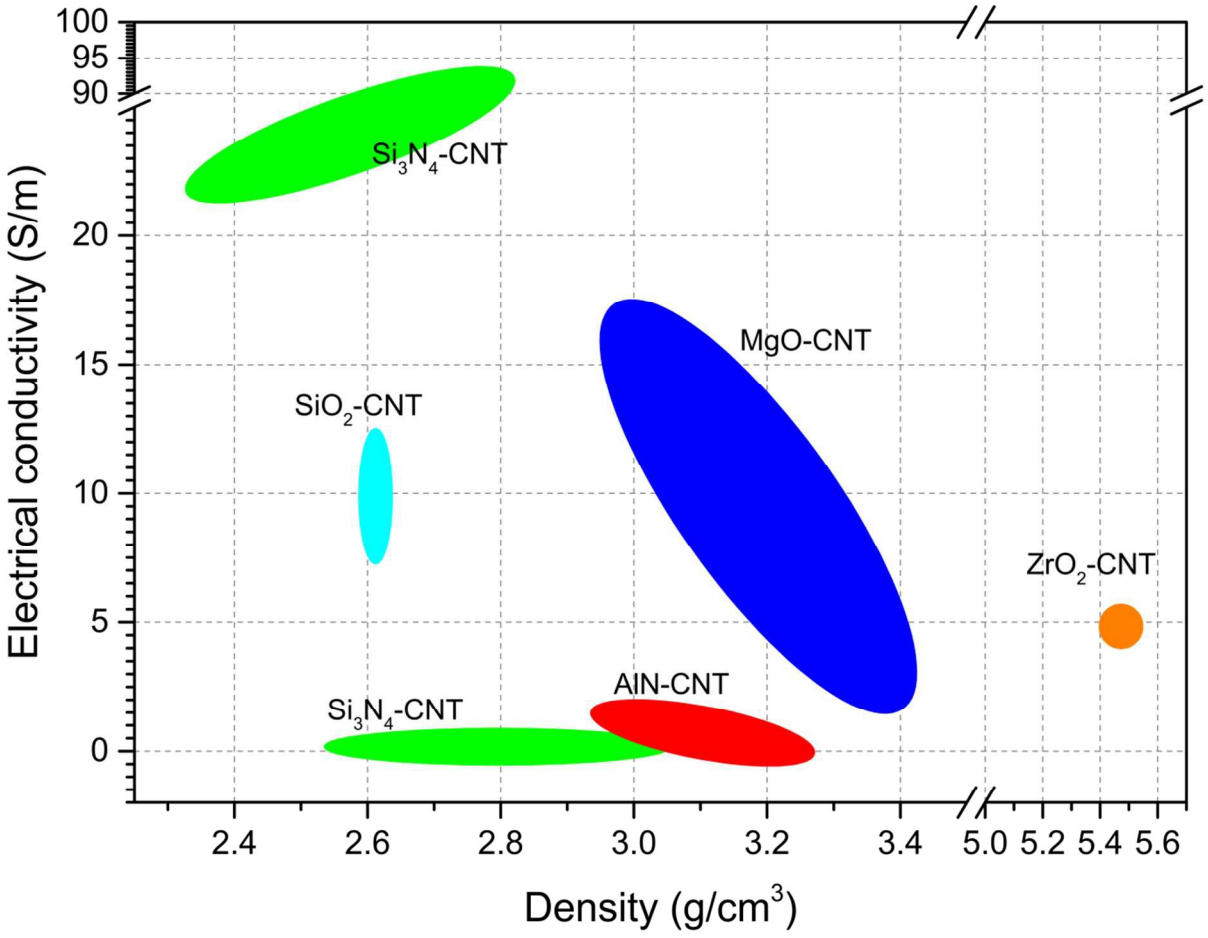

Fig. 43. The electrical conductivity of SPSed CNT-containing ceramics as a function of density.

View Article Online
DOI: 10.1039/C7NR01878A

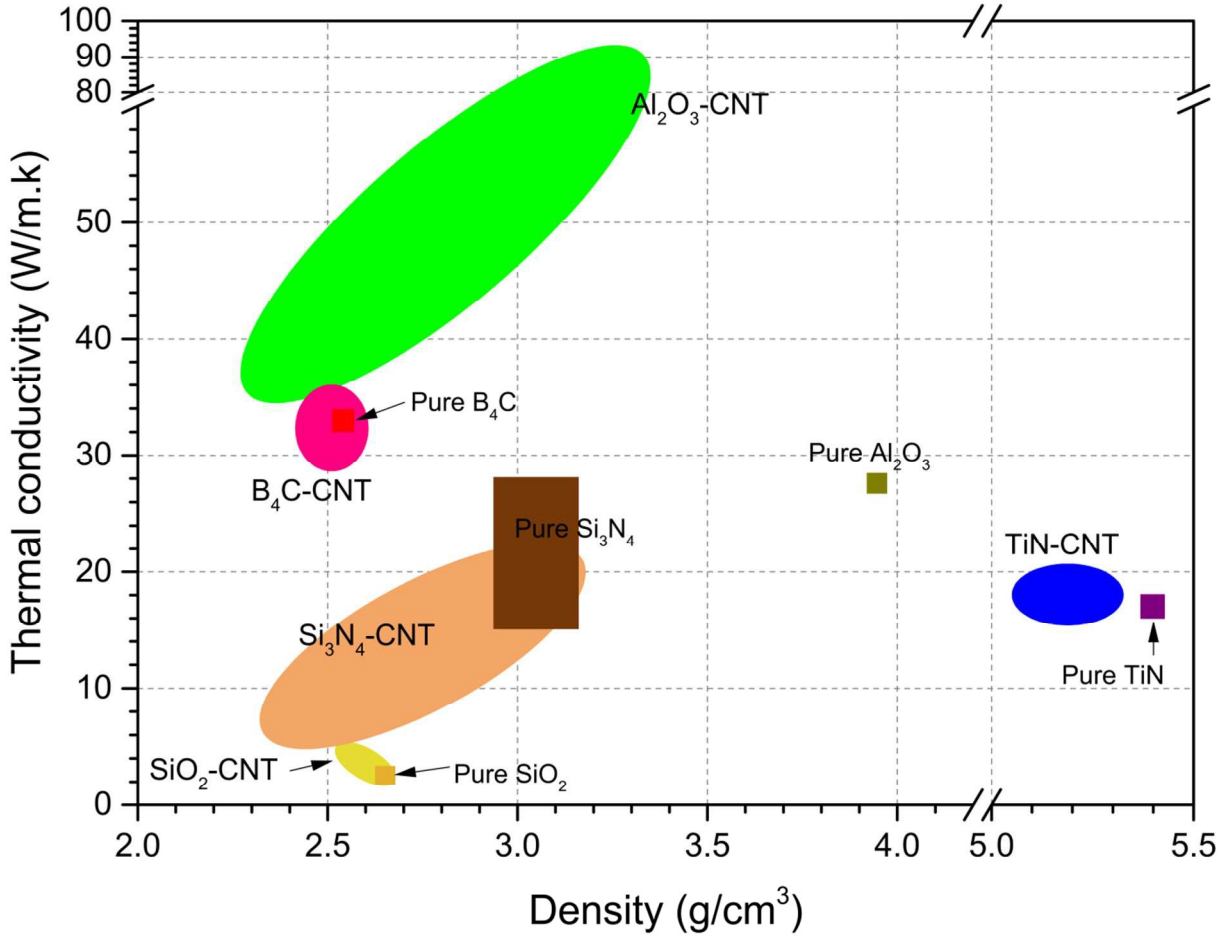

Fig. 44. The thermal conductivity of SPSed CNT-containing ceramics as a function of density.

To analyze the properties of SPSed CNT-ceramic matrix nanocomposites independent of their apparent density, the normalized specific properties can be informative. Therefore, it seems useful to depict some graphs based on different specific structural and functional properties. Such bubble maps can prepare the designers and engineers with some applicable hints to the selection of SPSed CNT-filled ceramic systems for various applications.

Specific hardness as a function of specific fracture toughness is shown in Fig. 45 for different SPSed CNT-containing ceramic-based nanocomposites. As seen, CNT-B_4C systems have the highest specific hardness and K_{Ic}. Such systems can be the best choices for ceramic-based applications in which both high hardness and toughness are a crucial need. In contrast, SPSed CNT-Si_3N_4 systems may have fracture toughness higher than that of SPSed CNT-B_4C ceramics, but their hardness is comparatively lower.

View Article Online
DOI: 10.1039/C7NR01878A

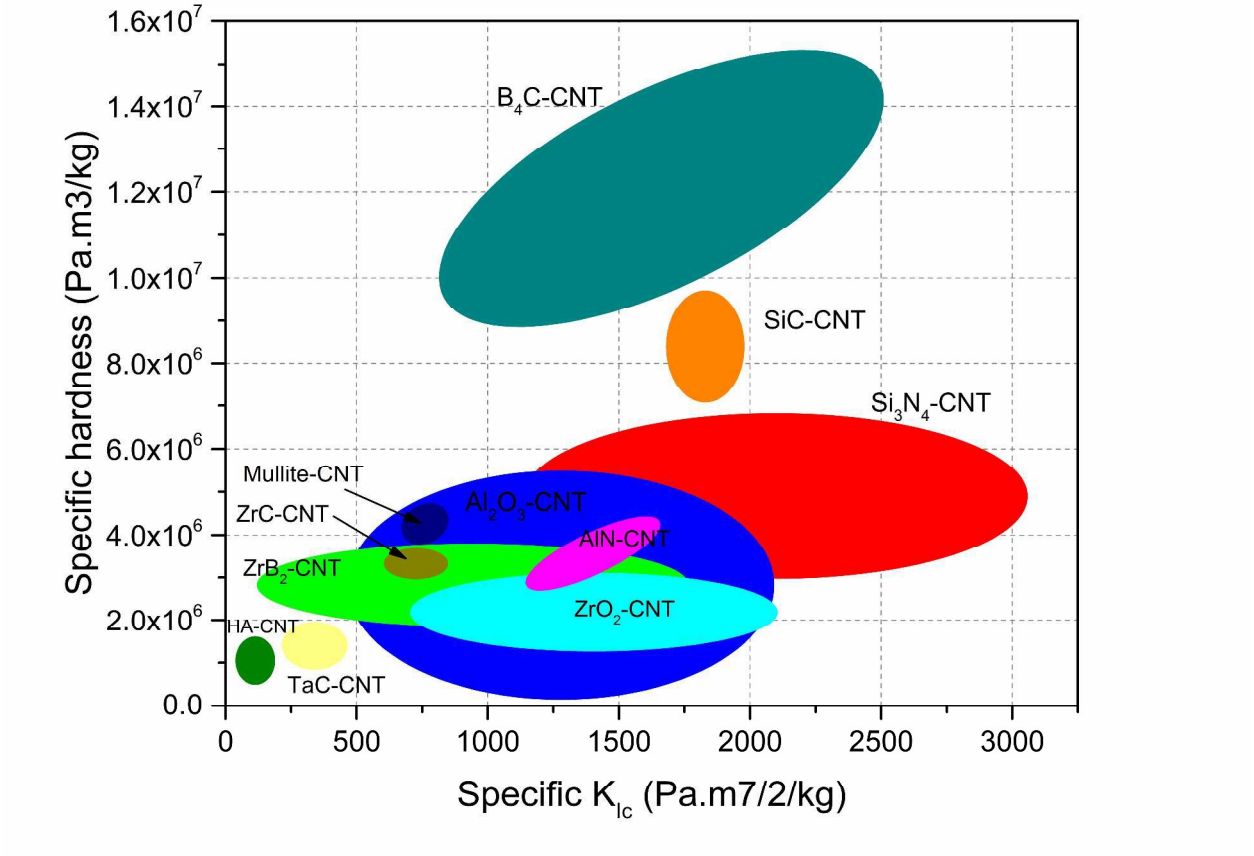

Fig. 45. The specific hardness of SPSed CNT-ceramics versus specific fracture toughness.

The specific bending strength as a function of specific hardness is shown in Fig. 46 for different SPSed CNT-containing ceramic-based nanocomposites. As clearly seen, SiC-based systems have the highest specific bending strength as well as highest specific hardness. This superiority can make these materials good candidates for industrial applications in which both high hardness and bending strength are required.

View Article Online
DOI: 10.1039/C7NR01878A

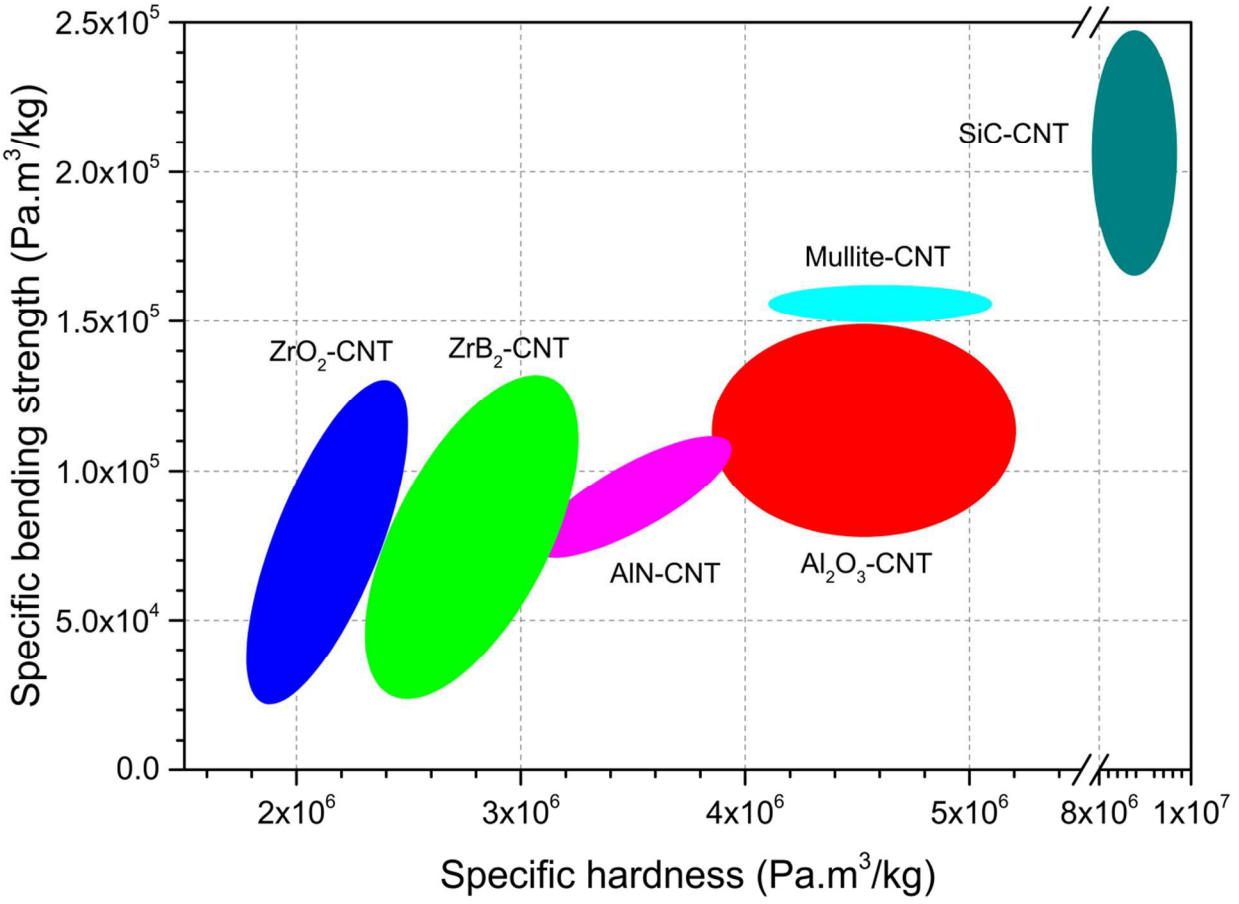

Fig. 46. The specific bending strength of SPSed CNT-ceramics versus specific hardness.

Fig. 47 presents the variations of specific bending strength as a function of specific fracture toughness for different SPSed CNT-filled ceramic-based nanocomposites. As seen, SPSed SiC-based composites benefit from highest specific bending strength alongside highest specific K_{Ic}. On the other hand, SPSed CNT-ZrB_2 systems have the widest range of specific hardness and K_{Ic}. It shows how CNTs can tolerate such great mechanical loads in these systems.

View Article Online
DOI: 10.1039/C7NR01878A

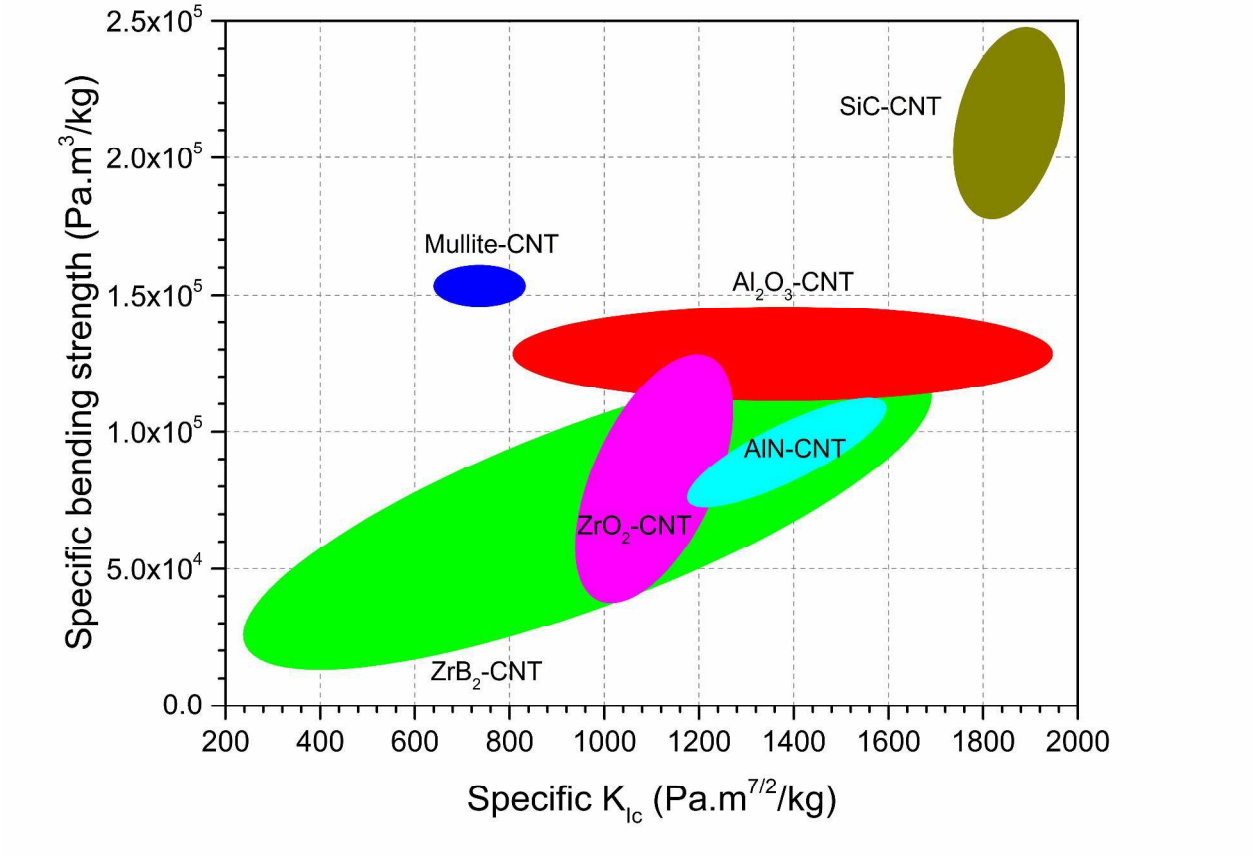

Fig. 47. The specific bending strength of SPSed CNT-containing ceramics versus specific fracture toughness.

The specific elastic modulus as a function of specific hardness is shown in Fig. 48 for different SPSed CNT-containing ceramic-based nanocomposites. In conformity with the bubble map, CNT-B_4C systems have the highest specific elastic modulus as well as highest specific hardness. From this perspective, TaC, HA, and ZrO_2-based systems are of inferior functionality.

View Article Online
DOI: 10.1039/C7NR01878A

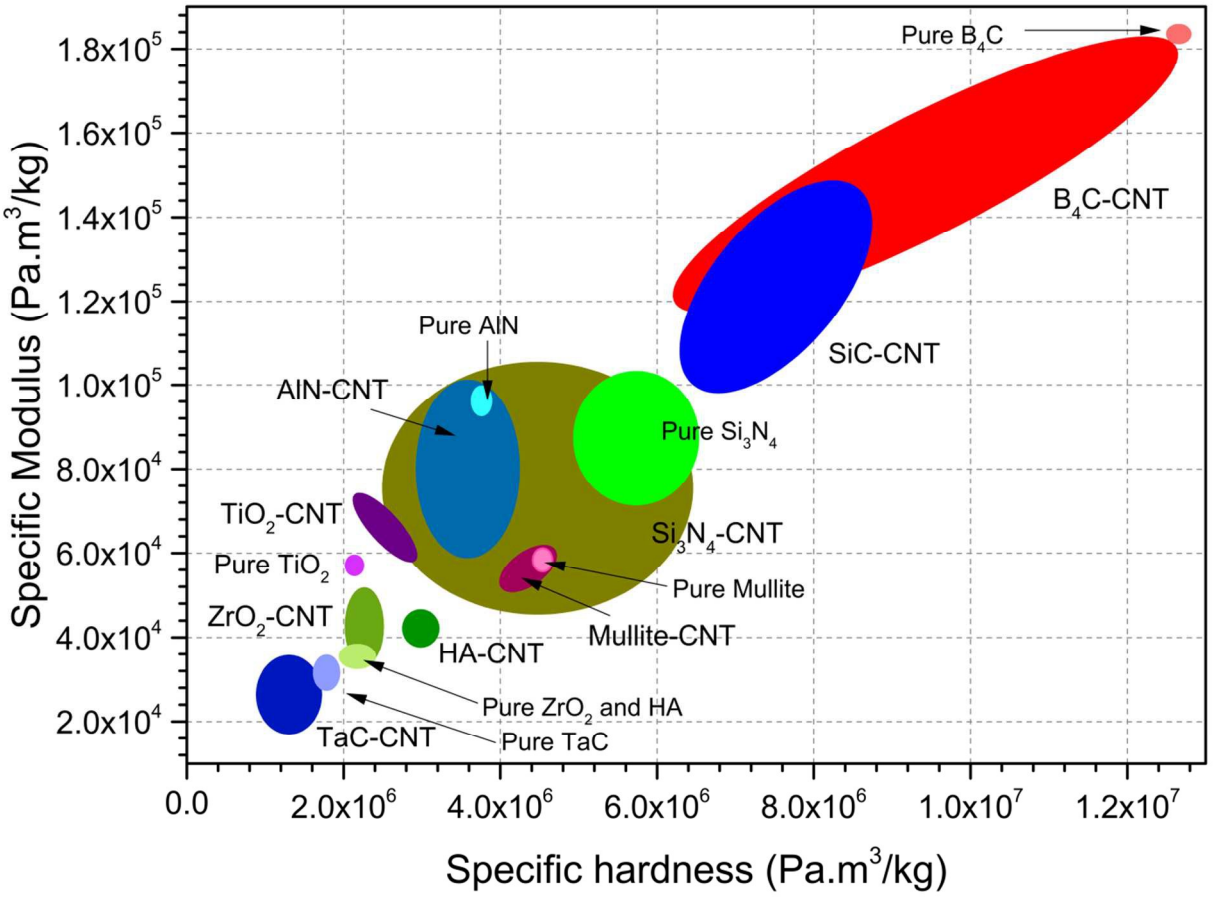

Fig. 48. The specific elastic modulus of SPSed CNT-containing ceramics versus specific hardness.

Fig. 49 displays the specific elastic modulus as a function of specific fracture toughness for different SPSed ceramics and CNT-containing ceramic matrix nanocomposites. As seen, SPSed pure Si_3N_4, CNT-Si_3N_4, and CNT-ZrO_2 systems have the highest specific K_{Ic}, but their specific elastic modulus is lower than that of SPSed pure B_4C and CNT-B_4C systems.

View Article Online
DOI: 10.1039/C7NR01878A

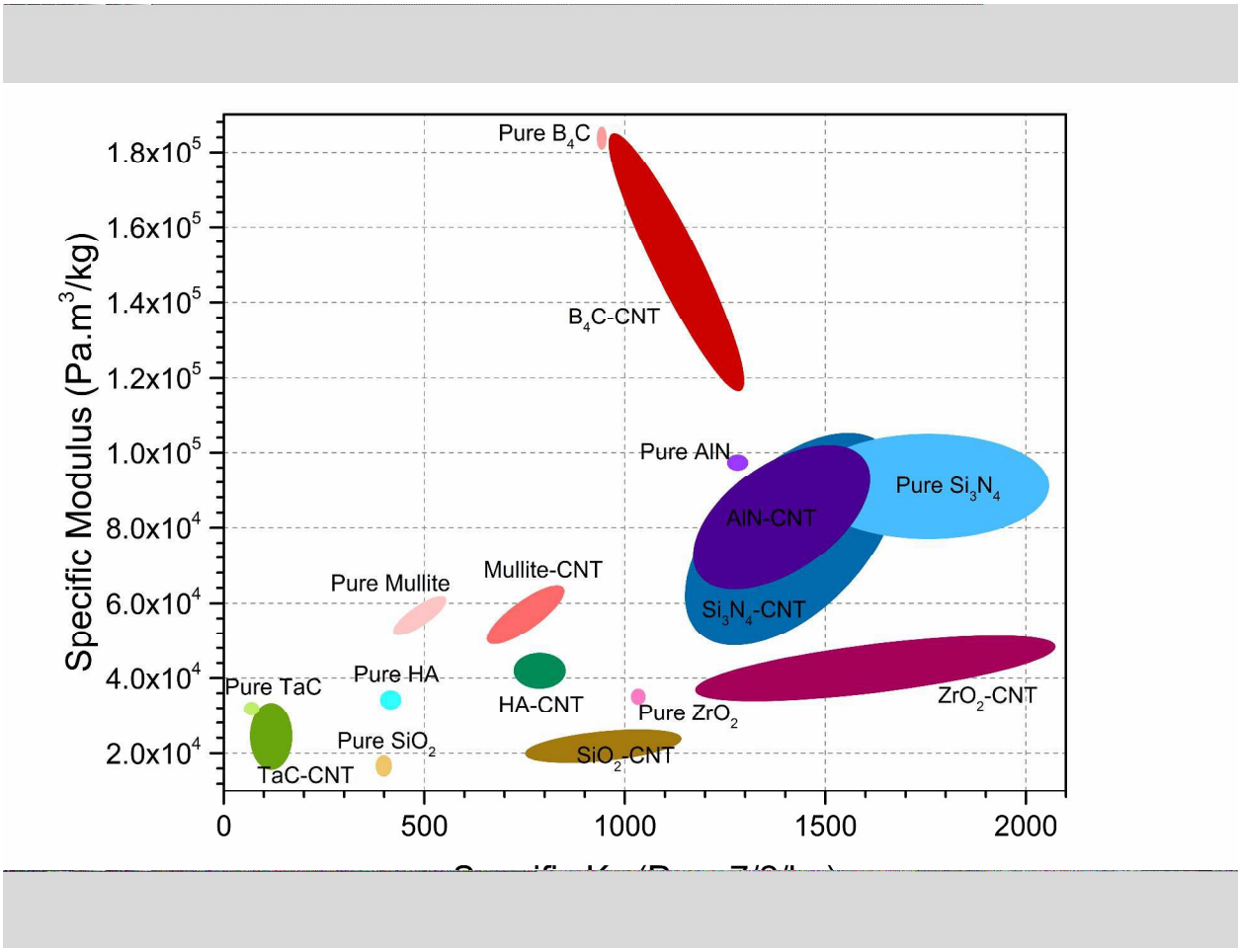

Fig. 49. The specific elastic modulus of SPSed CNT-containing ceramics versus specific fracture toughness.

3. Current challenges in SPSed CNT-ceramic matrix nanocomposites

The present review paper addressed the potential influences of CNTs on the physical and mechanical properties of SPSed ceramic matrix nanocomposites. As widely discussed, the vast majority of these effects is favorable and may be exploited for many functional and structural applications. However, the CNT addition to some ceramic systems may degrade their physicomechanical characteristics due to some special microstructural manipulation, high-temperature phase transformations and change of some physical parameters such as relative density and sinterability. The beneficial effects of CNT addition will emerge whenever a uniform distribution of intact nanotubes is obtained as well as good CNT/ceramic interfacial adhesion. In practice, the full exploitation of CNTs extraordinary features in ceramic matrix nanocomposites is hindered due to some technical constraints and processing issues. These drawbacks include: (i)

View Article Online
DOI: 10.1039/C7NR01878A

thermal degradation of CNTs; (ii) uniform dispersion of CNTs in ceramic matrix; and (iii) weak interfacial adhesion.

3.1. Dispersion of CNTs and interfacial interactions

Even after a decade of research, it has not been possible to exploit the full capacity of CNTs as reinforcement, toughening agent, or modification component in ceramic-based nanocomposites due to some microstructural constraints involving the non-uniform dispersion of entangled CNT bundles as well as weak interaction between CNTs and ceramic. These disadvantages originate from the high aspect ratio of CNTs and their inherent tendency to get entangled. A large number of research works are dedicated to homogenously disperse CNTs in ceramic systems and create a strongly bonded interface between CNT and matrix. To date, some dispersion methods are suggested among which mechanical mixing [8], colloidal mixing [101], sol gel [14], electrophoretic deposition (EPD) [220], and catalytic chemical vapor deposition (CCVD) [7] are widely used. These techniques strive to modify the surface of nanotubes or open entangled bundles of CNTs thereby homogenously distributing them in ceramic matrices. However, there exist some other approaches such as functionalization to improve both wettability in CNT/matrix interfaces and water solubility of nanotubes for the aqueous dispersion techniques [220-222]. Fig. 50 shows SEM micrographs of pure CNTs before and after functionalization and types of surface treatments by which CNTs are superficially modified. As observed, the functionalization can alleviate the agglomeration of entangled CNTs and contribute to their uniform distribution.

View Article Online
DOI: 10.1039/C7NR01878A

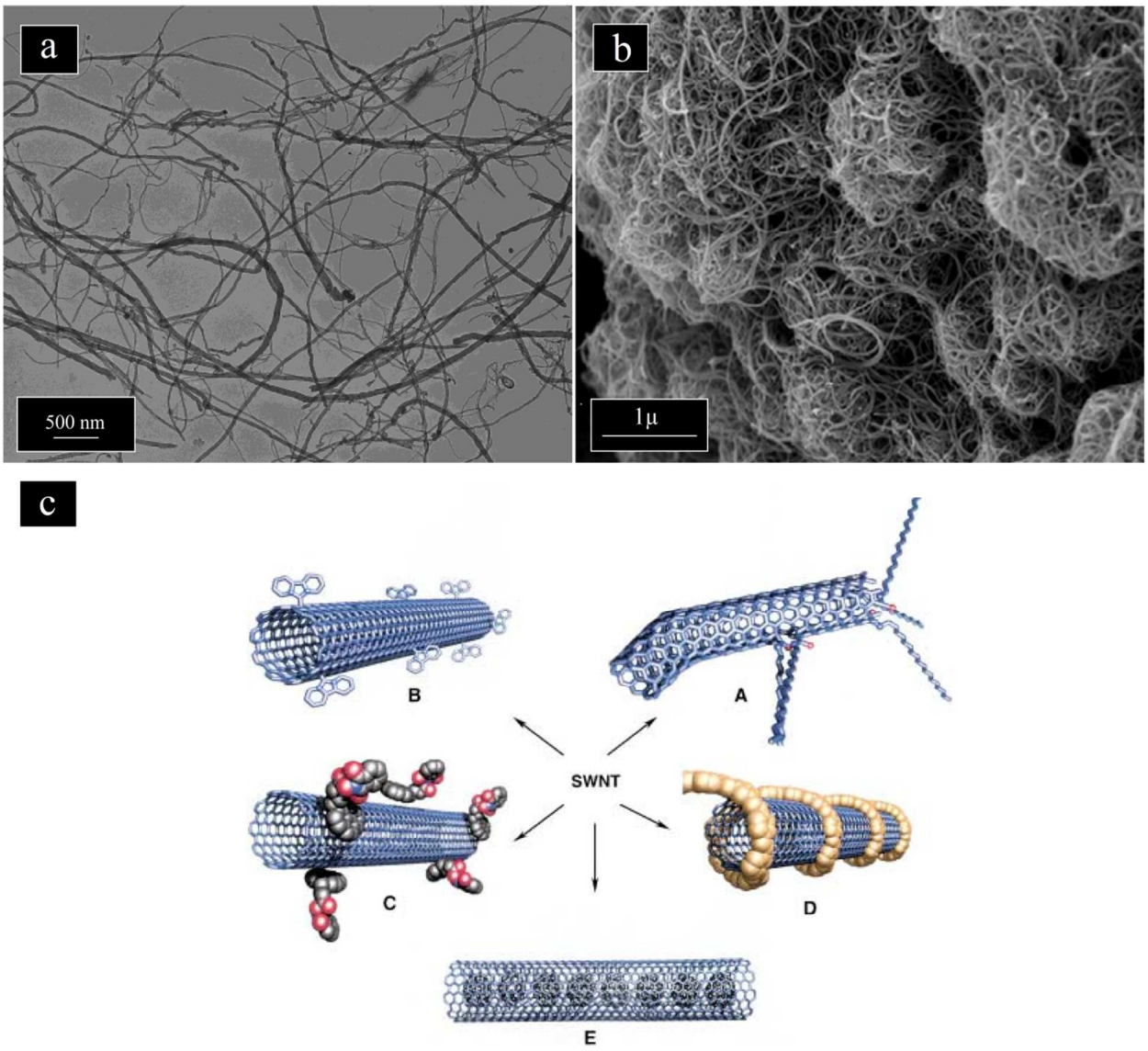

Fig. 50. (a) SEM micrograph of pure CNTs with no surface modification (Reproduced from ref. 223 with permission from Elsevier [223]); (b); TEM image of functionalized CNTs (Reproduced from ref. 224 with permission from American Chemical Society [224]); and (c) a representative schematic of functionalization and its types: (A) defect-group functionalization; (B) covalent sidewall functionalization; (C) non-covalent exohedral functionalization with surfactants; (D) non-covalent exohedral functionalization with polymers; and (E) endohedral functionalization with C_{60} (Reproduced from ref. 222 with permission from Wiley [222]).

View Article Online
DOI: 10.1039/C7NR01878A

3.2. Thermal degradation of CNTs

Usually in SPS process, high sintering temperatures, long processing times, and high applied pressures may destroy the crystallographic nature of CNTs and gives rise to an allotropic phase transformation [169, 225]. The literature has reported some contradictory results about the formation of different allotropes through the thermal degradation of pure CNTs under severe SPS conditions. In conformity with the broad spectrum of the empirical results, the common allotropes include mono/multi-layer graphene [167], cubic diamond [168], n-diamond [169], and graphite sheets [15]. However, other research works have not reported any allotropic phase transformations at similar conditions. For example, Zhang et al. [65] did not observe any new allotropes after sintering of pure CNTs by SPS at 2000 °C under 50 MPa. In contrast, Li et al. [167] reported the in situ formation of graphene layers in pure CNTs after SPS at 1600 °C under 60 MPa. What is of important is that the formation of imperfections in the crystallographic structure of CNTs, their incomplete decomposition, and more importantly complete degradation of nanotubes avoid exploiting the full potential of CNTs as reinforcement or modifying agent and lead to a failure in obtaining the superior properties. Therefore, it is compulsory to use SPS approach at a safe experimental area, i.e. sufficiently low pressures, temperatures, and sintering times. A great deal of efforts is required to determine the safe limits of SPS process for CNT-dispersed ceramic matrix nanocomposites.

4. Conclusion and future perspective

The present paper has reviewed the vast majority of research works reported yet about the spark plasma sintering (SPS) of CNT-dispersed ceramic matrix nanocomposites and provided a broad overview of the potential effects of CNTs on the engineering ceramics. These material systems are categorized into five groups: (i) CNT-oxide ceramic nanocomposites including CNT-Al_2O_3, CNT-ZrO_2, CNT-SiO_2, CNT-HA, CNT-MgO, CNT-mullite, and CNT-TiO_2 nanocomposites; (ii) CNT-carbide ceramic matrix nanocomposites including CNT-SiC, CNT-TaC, and CNT-ZrC nanocomposites; (iii) CNT-nitride ceramic matrix nanocomposites including CNT-AlN, CNT-Si_3N_4, and CNT-TiN nanocomposites; (iv) CNT-boride ceramic matrix nanocomposites including CNT-B_4C and CNT-ZrB_2 nanocomposites; and (v) CNT-dispersed complex ceramic matrix nanocomposites such as ternary CNT-Mg_2Si-MgO systems, CNT- NiTi nanocomposites, and binary CNT-Ti_3SiC_2 bulk materials. The authors addressed these binary or ternary systems as property-oriented. They have strived to obviously discuss the potential influences of CNT addition on the mechanical and physical properties of engineering systems and the stimulated active mechanisms. A concise summary of experimental works, microstructure development and the obtained properties in SPSed CNT-dispersed ceramic systems are provided to enable the readers to deeply understand what happens during SPS of these materials and why the superior properties can be achieved. Finally, the unsolved challenges and the appropriate solutions for them were addressed. These challenges included uniform distribution of CNTs within the ceramic matrices, weakly bonded interfacial adhesion, and unfavorable thermal degradation of

View Article Online
DOI: 10.1039/C7NR01878A

nanotubes to limit their full potential for sophisticated applications. The authors believe that a profound insight and deep understanding are required in recent experimental researches to shed light on the microstructural phenomena and their implicit effects on the inherent characteristics of SPSed CNT-added ceramics. Indeed, we need to switch from mere experimental reports to deeply scientific application-directed studies.

References

1. S. Iijima, Nature, 1991, 354, 56-58.

2. S. Fatemi and M. Foroutan, Int. J. Environ. Sci. Technol., 2016, 13, 457-470.

3. U. Kumar, S. Sikarwar, R. K. Sonker and B. Yadav, J. Inorg. Organomet. Polym. Mater., 2016, 26(6), 1231-1242.

4. P. R. Bandaru, J. Nanosci. Nanotechnol., 2007, 7, 1239-1267.

5. C. Qin, X. Shi, S. Bai, L. Chen and L. Wang, Mater. Sci. Eng. A, 2006, 420, 208-211.

6. O. Lourie, D. Cox and H. Wagner, Phys. Rev. Lett., 1998, 81, 1638.

7. J. Cho, A. R. Boccaccini and M. S. Shaffer, J. Mater. Sci., 2009, 44, 1934-1951.

8. S. C. Tjong, Carbon nanotube reinforced composites: metal and ceramic matrices, John Wiley & Sons, US, 2009.

9. S. P. Yadav and S. Singh, Prog. Mater Sci., 2016, 80, 38-76.

10. C. Laurent, A. Peigney, O. Dumortier and A. Rousset, J. Eur. Ceram. Soc., 1998, 18, 2005-2013.

11. R. Poyato, A. L. Vasiliev, N. P. Padture, H. Tanaka and T. Nishimura, Nanotechnology, 2006, 17, 1770.

12. A. R. Boccaccini, J. Cho, J. A. Roether, B. J. Thomas, E. J. Minay and M. S. Shaffer, Carbon, 2006, 44, 3149-3160.

13. C.-W. Nan, G. Liu, Y. Lin and M. Li, Appl. Phys. Lett., 2004, 85, 3549-3551.

14. K. Chu, Q. Wu, C. Jia, X. Liang, J. Nie, W. Tian, G. Gai and H. Guo, Compos. Sci. Technol., 2010, 70, 298-304.

15. F. Zhang, J. Shen, J. Sun and D. McCartney, Carbon, 2006, 44, 3136-3138.

View Article Online
DOI: 10.1039/C7NR01878A

16. K. Yang, J. He, Z. Su, J. B. Reppert, M. J. Skove, T. M. Tritt and A. M. Rao, Carbon, 2010, 48, 756-762.

17. K. Hirota, H. Hara and M. Kato, Mater. Sci. Eng. A, 2007, 458, 216-225.

18. K. Shimoda, T. Hinoki and A. Kohyama, Compos. Sci. Technol., 2010, 70, 387-392.

19. V. G. Rocha, A. Borrell, R. Torrecillas and A. Fernández, Mater. Sci. Eng. A, 2012, 556, 414-419.

20. P. Dong, Z. Wang, W. Wang, S. Chen and J. Zhou, Scripta Mater., 2016, 123, 118-121.

21. Y. Kobayashi, T. Takeuchi, M. Tabuchi, K. Ado and H. Kageyama, J. Power Sources, 1999, 81, 853-858.

22. M. Botros, R. Djenadic, O. Clemens, M. Möller and H. Hahn, J. Power Sources, 2016, 309, 108-115.

23. H. Yamada, T. Ito and R. H. Basappa, Electrochim. Acta, 2016, 222, 648-656.

24. P. Nithyadharseni, M. Reddy, B. Nalini, P. Saravanan, V. Vinod, M. Černík and B. Chowdari, J. Solid State Electrochem., 2016, 20, 1743-1751.

25. H. Borodianska, P. Badica, T. Uchikoshi, Y. Sakka and O. Vasylkiv, J. Alloys Compd., 2011, 509, 2535-2539.

26. O. Bezdorozhev, H. Borodianska, Y. Sakka and O. Vasylkiv, J. Nanosci. Nanotechnol., 2014, 14, 4218-4223.

27. K. Khor, X. Chen, S. Chan and L. Yu, Mater. Sci. Eng. A, 2004, 366, 120-126.

28. R. Dobedoe, G. West and M. Lewis, Adv. App. Cerm., 2005, 104, 110-116.

29. C. Balázsi, Z. Shen, Z. Kónya, Z. Kasztovszky, F. Weber, Z. Vertesy, L. Biro, I. Kiricsi and P. Arato, Compos. Sci. Technol., 2005, 65, 727-733.

30. O. Tapaszto, P. Kun, F. Weber, G. Gergely, K. Balazsi, J. Pfeifer, P. Arató, A. Kidari, S. Hampshire and C. Balázsi, Ceram. Int., 2011, 37, 3457-3461.

31. R. H. Hannink, P. M. Kelly and B. C. Muddle, J. Am. Ceram. Soc., 2000, 83, 461-487.

32. J. Chevalier, L. Gremillard, A. V. Virkar and D. R. Clarke, J. Am. Ceram. Soc., 2009, 92, 1901-1920.

33. J. R. Kelly and I. Denry, Dent. Mater. J., 2008, 24, 289-298.

View Article Online
DOI: 10.1039/C7NR01878A

34. J. Chevalier, Biomaterials, 2006, 27, 535-543.

35. P. F. Manicone, P. R. Iommetti and L. Raffaelli, J. Dent., 2007, 35, 819-826.

36. P. Palmero, M. Fornabaio, L. Montanaro, H. Reveron, C. Esnouf and J. Chevalier, Biomaterials, 2015, 50, 38-46.

37. R. Chintapalli, A. Mestra, F. García Marro, H. Yan, M. Reece and M. Anglada, Materials, 2010, 3, 800-814.

38. L. Melk, M. Turon-Vinas, J. J. Roa, M.-L. Antti and M. Anglada, J. Eur. Ceram. Soc., 2016, 36, 147-153.

39. S. Mallakpour and E. Khadem, Chem. Eng. J., 2016, 302, 344-367.

40. G. Anstis, P. Chantikul, B. R. Lawn and D. Marshall, J. Am. Ceram. Soc., 1981, 64, 533-538.

41. K. Niihara, R. Morena and D. Hasselman, J. Mater. Sci. Lett., 1982, 1, 13-16.

42. L. Melk, J. J. R. Rovira, F. García-Marro, M.-L. Antti, B. Milsom, M. J. Reece and M. Anglada, Ceram. Int., 2015, 41, 2453-2461.

43. D. Munz and T. Fett, Ceramics: mechanical properties, failure behaviour, materials selection, Springer Science & Business Media, Germany, 2013.

44. L. Melk, J. J. R. Rovira, M.-L. Antti and M. Anglada, Ceram. Int., 2015, 41, 459-468.

45. J. Sun, L. Gao, M. Iwasa, T. Nakayama and K. Niihara, Ceram. Int., 2005, 31, 1131-1134.

46. A. Datye, K.-H. Wu, G. Gomes, V. Monroy, H.-T. Lin, J. Vleugels and K. Vanmeensel, Compos. Sci. Technol., 2010, 70, 2086-2092.

47. M. Mazaheri, D. Mari, R. Schaller, G. Bonnefont and G. Fantozzi, J. Eur. Ceram. Soc., 2011, 31, 2691-2698.

48. M. Mazaheri, D. Mari, Z. R. Hesabi, R. Schaller and G. Fantozzi, Compos. Sci. Technol., 2011, 71, 939-945.

49. M. Mazaheri, D. Mari and R. Schaller, Phys. Status Solidi (a), 2010, 207, 2456-2460.

50. M. Castillo-Rodríguez, A. Muñoz and A. Domínguez-Rodríguez, J. Am. Ceram. Soc., 2016, 99, 286-292.

View Article Online
DOI: 10.1039/C7NR01878A

51. M. Castillo-Rodríguez, A. Muñoz, A. Morales-Rodríguez, R. Poyato, Á. Gallardo-López and A. Domínguez-Rodríguez, J. Am. Ceram. Soc., 2015, 98, 645-653.

52. M. Castillo-Rodríguez, A. Muñoz and A. Domínguez-Rodríguez, J. Eur. Ceram. Soc., 2016, 36, 2573-2578.

53. R. Poyato, J. Macías-Delgado, A. Gallardo-López, A. Muñoz and A. Domínguez-Rodríguez, Ceram. Int., 2015, 41, 12861-12868.

54. V. Almeida, N. Balzaretti, T. Costa, G. Machado and M. Gallas, J. Sol-Gel Sci. Technol., 2013, 65, 143-149.

55. R. Poyato, J. Macías-Delgado, A. García-Valenzuela, Á. Gallardo-López, A. Morales-Rodríguez, A. Muñoz and A. Domínguez-Rodríguez, J. Eur. Ceram. Soc., 2015, 35, 2351-2359.

56. M. Poorteman, M. Traianidis, G. Bister and F. Cambier, J. Eur. Ceram. Soc., 2009, 29, 669-675.

57. J. González-Julián, Y. Iglesias, A. Caballero, M. Belmonte, L. Garzón, C. Ocal, P. Miranzo and M. Osendi, Compos. Sci. Technol., 2011, 71, 60-66.

58. K. Ahmad and W. Pan, Compos. Sci. Technol., 2009, 69, 1016-1021.

59. F. Fonseca, R. Muccillo, D. De Florio, L. Ladeira and A. Ferlauto, Appl. Phys. Lett., 2007, 91, 243107.

60. O. Malek, J. Vleugels, Y. Perez, P. De Baets, J. Liu, S. Van den Berghe and B. Lauwers, Mater. Chem. Phys., 2010, 123, 114-120.

61. L. Gu, L. Li, W. Zhao and K. P. Rajurkar, Int. J. Mach. Tool. Manu., 2012, 53, 100-106.

62. T. Ukai, T. Sekino, A. T. Hirvonen, N. Tanaka, T. Kusunose, T. Nakayama and K. Niihara, Key Eng. Mater., 2006, 317, 661-664.

63. L. Melk, M.-L. Antti and M. Anglada, Ceram. Int., 2016, 42, 5792-5801.

64. S. R. Brown, S. M. Kauzlarich, F. Gascoin and G. J. Snyder, Chem. Mater., 2006, 18, 1873-1877.

65. H. Zhang, J.-F. Li, K. Yao and L. Chen, J. Appl. Phys., 2005, 97, 114310.

66. K. T. Kim, S. Y. Choi, E. H. Shin, K. S. Moon, H. Y. Koo, G.-G. Lee and G. H. Ha, Carbon, 2013, 52, 541-549.

67. G.-D. Zhan, J. D. Kuntz, H. Wang, C.-M. Wang and A. K. Mukherjee‖, Philos. Mag. Lett., 2004, 84, 419-423.

View Article Online
DOI: 10.1039/C7NR01878A

68. G. D. Zhan and A. K. Mukherjee, Int. J. Appl. Ceram. Technol., 2004, 1, 161-171.

69. G.-D. Zhan, J. D. Kuntz, A. K. Mukherjee, P. Zhu and K. Koumoto, Scripta Mater., 2006, 54, 77-82.

70. A. Duszová, J. Dusza, K. Tomášek, G. Blugan and J. Kuebler, J. Eur. Ceram. Soc., 2008, 28, 1023-1027.

71. B. Milsom, G. Viola, Z. Gao, F. Inam, T. Peijs and M. J. Reece, J. Eur. Ceram. Soc., 2012, 32, 4149-4156.

72. A. Karanam, L. Bichler and R. Fong, Metall. Mater. Trans. B, 2015, 46, 1666-1673.

73. L. Shen, Y.-H. Han, C. Xiang, H. Tang, A. Mukherjee, S. Kim, S. I. Bae and Q. Huang, Scripta Mater., 2013, 69, 736-739.

74. A. Zahedi, J. Gonzalez-Julian, M. Mazaheri, J. Javadpour, H. Rezaie and O. Guillon, J. Eur. Ceram. Soc., 2015, 35, 4241-4249.

75. S. Smart, A. Cassady, G. Lu and D. Martin, Carbon, 2006, 44, 1034-1047.

76. K. Pulskamp, S. Diabaté and H. F. Krug, Toxicol. Lett., 2007, 168, 58-74.

77. C.-w. Lam, J. T. James, R. McCluskey, S. Arepalli and R. L. Hunter, Crit. Rev. Toxicol., 2006, 36, 189-217.

78. Y. Liu, Y. Zhao, B. Sun and C. Chen, Acc. Chem. Res., 2012, 46, 702-713.

79. E. Mohamed, M. Taheri, M. Mehrjoo, M. Mazaheri, A. Zahedi, M. Shokrgozar and F. Golestani-Fard, Ceram. Int., 2015, 41, 12773-12781.

80. W. Kou, T. Akasaka, F. Watari and G. Sjögren, ISRN Dent., 2013, 2013, 1-6.

81. M. Das, C. Dhand, G. Sumana, A. Srivastava, N. Vijayan, R. Nagarajan and B. Malhotra, Appl. Phys. Lett., 2011, 99, 143702.

82. O. Hanzel, J. Sedláček and P. Šajgalík, J. Eur. Ceram. Soc., 2014, 34, 1845-1851.

83. A. K. Keshri, J. Huang, V. Singh, W. Choi, S. Seal and A. Agarwal, Carbon, 2010, 48, 431-442.

84. S. C. Zhang, W. G. Fahrenholtz, G. E. Hilmas and E. J. Yadlowsky, J. Eur. Ceram. Soc., 2010, 30, 1373-1380.

85. D. Chakravarty, S. Bysakh, K. Muraleedharan, T. N. Rao and R. Sundaresan, J. Am. Ceram. Soc., 2008, 91, 203-208.

View Article Online
DOI: 10.1039/C7NR01878A

86. S. Maensiri, P. Laokul, J. Klinkaewnarong and V. Amornkitbamrung, Mater. Sci. Eng. A, 2007, 447, 44-50.

87. I. Ahmad, H. Cao, H. Chen, H. Zhao, A. Kennedy and Y. Q. Zhu, J. Eur. Ceram. Soc., 2010, 30, 865-873.

88. A. Kasperski, A. Weibel, C. Estournès, C. Laurent and A. Peigney, Scripta Mater., 2014, 75, 46-49.

89. D. Jiang, K. Thomson, J. D. Kuntz, J. W. Ager and A. K. Mukherjee, Scripta Mater., 2007, 56, 959-962.

90. T. Zhang, L. Kumari, G. Du, W. Li, Q. Wang, K. Balani and A. Agarwal, Compos. Part A Appl. Sci. Manuf., 2009, 40, 86-93.

91. V. Puchy, P. Hvizdos, J. Dusza, F. Kovac, F. Inam and M. Reece, Ceram. Int., 2013, 39, 5821-5826.

92. F. Inam, H. Yan, D. D. Jayaseelan, T. Peijs and M. J. Reece, J. Eur. Ceram. Soc., 2010, 30, 153-157.

93. L. Kumari, T. Zhang, G. Du, W. Li, Q. Wang, A. Datye and K. Wu, Ceram. Int., 2009, 35, 1775-1781.

94. P. Sikder, S. Sarkar, K. G. Biswas, S. Das, S. Basu and P. K. Das, Mater. Chem. Phys., 2016, 170, 99-107.

95. M. V. Bazylenko, M. Gross, E. Gauja and P. L. Chu, US Pat., 6154582 A, 2000.

96. R. Brückner, J. Non-Cryst. Solids, 1970, 5, 123-175.

97. M. Chen, Y. Zhu, Y. Pan, H. Kou, H. Xu and J. Guo, Mater. Des., 2011, 32, 3013-3016.

98. S. Loo, S. Idapalapati, S. Wang, L. Shen and S. G. Mhaisalkar, Scripta Mater., 2007, 57, 1157-1160.

99. J. DiMaio, S. Rhyne, Z. Yang, K. Fu, R. Czerw, J. Xu, S. Webster, Y.-P. Sun, D. Carroll and J. Ballato, Inf. Sci., 2003, 149, 69-73.

100. C. Xiang, Y. Pan, X. Liu, X. Sun, X. Shi and J. Guo, Appl. Phys. Lett., 2005, 87, 123103.

101. M. J. de Andrade, A. Weibel, C. Laurent, S. Roth, C. P. Bergmann, C. Estournes and A. Peigney, Scripta Mater., 2009, 61, 988-991.

102. S. Guo, R. Sivakumar, H. Kitazawa and Y. Kagawa, J. Am. Ceram. Soc., 2007, 90, 1667-1670.

View Article Online
DOI: 10.1039/C7NR01878A

103. C. S. Xiang, X. M. Shi, Y. B. Pan and J. K. Guo, Key Eng. Mater., 2005, 280, 123-126.

104. M. Jung de Andrade, M. D. Lima, L. Stein, C. Perez and S. Roth, phys. status solidi (b), 2007, 244, 4218-4222.

105. J. Ning, J. Zhang, Y. Pan and J. Guo, Ceram. Int., 2004, 30, 63-67.

106. F. Dillon, J. Moghal, A. Koós, J. Lozano, L. Miranda, H. Porwal, M. Reece and N. Grobert, Microporous Mesoporous Mater., 2015, 217, 159-166.

107. S. Guo, R. Sivakumar and Y. Kagawa, Adv. Eng. Mater., 2007, 9, 84-87.

108. R. Sivakumar, S. Guo, T. Nishimura and Y. Kagawa, Scripta Mater., 2007, 56, 265-268.

109. C.-W. Nan, Z. Shi and Y. Lin, Chem. Phys. Lett., 2003, 375, 666-669.

110. A. A. White, S. M. Best and I. A. Kinloch, Int. J. Appl. Ceram. Technol., 2007, 4, 1-13.

111. J. Zhu, S. C. Tjong and X. Q. Li, Adv. Eng. Mater., 2010, 12, 1161-1165.

112. D. Lahiri, S. Ghosh and A. Agarwal, Mater. Sci. Eng. C, 2012, 32, 1727-1758.

113. D.-Y. Kim, Y.-H. Han, J. H. Lee, I.-K. Kang, B.-K. Jang and S. Kim, BioMed Res. Int., 2014, 2014, 1-10.

114. W. Wang, Y. Zhu, F. Watari, S. Liao, A. Yokoyama, M. Omori, H. Ai and F. Cui, Appl. Surf. Sci., 2012, 262, 194-199.

115. D. Lahiri, V. Singh, A. K. Keshri, S. Seal and A. Agarwal, Carbon, 2010, 48, 3103-3120.

116. K. Herkendell, V. R. Shukla, A. K. Patel and K. Balani, Mater. Sci. Eng. C, 2014, 34, 455-467.

117. J. Zhu, H. M. Wong, K. W. K. Yeung and S. C. Tjong, Adv. Eng. Mater., 2011, 13, 336-341.

118. M. Omori, A. Okubo, M. Otsubo, T. Hashida and K. Tohji, Key Eng. Mater., 2004, 254, 395-398.

119. S. K. Sarkar, M. H. Youn, I. H. Oh and B. T. Lee, Mater. Sci. Forum, 2007, 534, 893-896.

120. J. Xu, K. A. Khor, J. Sui and W. Chen, Mater. Sci. Eng. C, 2009, 29, 44-49.

121. J. Xu, K. A. Khor, J. Sui and W. Chen, Key Eng. Mater., 2008, 361, 1047-105.

View Article Online
DOI: 10.1039/C7NR01878A

122. K. Karthikeyan, S. Amaresh, V. Aravindan and Y. Lee, J. Mater. Chem. A, 2013, 1, 4105-4111.

123. F. Taleshi and A. A. Hosseini, J. Nanostruct. Chem., 2012, 3, 1-5.

124. E. Flahaut, A. Peigney, C. Laurent, C. Marliere, F. Chastel and A. Rousset, Acta Mater., 2000, 48, 3803-3812.

125. A. Peigney, F. L. Garcia, C. Estournès, A. Weibel and C. Laurent, Carbon, 2010, 48, 1952-1960.

126. F. L. Garcia, C. Estournès, A. Peigney, A. Weibel, E. Flahaut and C. Laurent, Scripta Mater., 2009, 60, 741-744.

127. D. Rodríguez, I. Cano, J. Fernández, J. Farinas and R. Moreno, J. Eur. Ceram. Soc., 2014, 34, 475-483.

128. D. Ghahremani, T. Ebadzadeh and A. Maghsodipour, Ceram. Int., 2015, 41, 6409-6416.

129. A. Cascales, N. Tabares, J. F. Bartolomé, A. Cerpa, A. Smirnov, R. Moreno and M. I. Nieto, J. Eur. Ceram. Soc., 2015, 35, 3613-3621.

130. A. Weibel, A. Peigney, G. Chevallier, C. Estournès and C. Laurent, Ceram. Int., 2013, 39, 5513-5519.

131. J. Wang, H. Kou, X. Liu, Y. Pan and J. Guo, Ceram. Int., 2007, 33, 719-722.

132. M.F. Zawrah and M. Aly, Ceram. Int., 2006, 32, 21-28 .

133. J. Wang, H. Kou, Y. Pan and J. Guo, Solide State phenom., 2007, 121, 135-138.

134. K. Woan, G. Pyrgiotakis and W. Sigmund, Adv. Mater., 2009, 21, 2233-2239.

135. Y. Yao, G. Li, S. Ciston, R. M. Lueptow and K. A. Gray, Environ. Sci. Technol., 2008, 42, 4952-4957.

136. K. Kondoh, T. Threrujirapapong, H. Imai, J. Umeda and B. Fugetsu, Compos. Sci. Technol., 2009, 69, 1077-1081.

137. P. Angerer, L. Yu, K. A. Khor and G. Krumpel, Mater. Sci. Eng. A, 2004, 381, 16-19.

138. S. G. Seo, W. H. Nam, Y. S. Lim, W.-S. Seo, Y. S. Cho and J. Y. Lee, Carbon, 2014, 67, 688-693.

139. B. Debalina, N. Vaishakh, M. Jagannatham, K. Vasanthakumar, N. Karthiselva, R. Vinu, P. Haridoss and S. Bakshi, Ceram. Int., 2016, 42, 14266-14277.

View Article Online
DOI: 10.1039/C7NR01878A

140. R. Leary and A. Westwood, Carbon, 2011, 49, 741-772.

141. N. Bouazza, M. Ouzzine, M. Lillo-Ródenas, D. Eder and A. Linares-Solano, Appl. Catal. B., 2009, 92, 377-383.

142. P. Daram, C. Banjongprasert, W. Thongsuwan and S. Jiansirisomboon, Surf. Coat. Technol., 2016, 306, 290-294.

143. M. Zhang, J. Xu, R. Zong and Y. Zhu, Appl. Catal. B., 2014, 147, 229-235.

144. B. Debalina, N. Vaishakh, M. Jagannatham, K. Vasanthakumar, N. Karthiselva, R. Vinu, P. Haridoss and S. R. Bakshi, Ceram. Int., 2016, 42, 14266-14277.

145. S.-H. Huang, S.-Y. Liao, C.-C. Wang, C.-C. Kei, J.-Y. Gan and T.-P. Perng, Nanotechnology, 2016, 27, 405702.

146. M. Wongaree, S. Chiarakorn, S. Chuangchote and T. Sagawa, Environ. Sci. Pollut. Res., 2016, 23, 21395-21406.

147. K. Zhang, F. J. Zhang, M. L. Chen and W. C. Oh, Ultrason. Sonochem., 2011, 18, 765-772.

148. K. Ahmad and W. Pan, Compos. Sci. Technol., 2008, 68, 1321-1327.

149. F. Inam, H. Yan, T. Peijs and M. J. Reece, Compos. Sci. Technol., 2010, 70, 947-952.

150. Q. Xie and S. N. Wosu, J. Compos. Mater., 2016, 50, 739-749.

151. K. Sarkar, S. Sarkar and P. K. Das, J. Mater. Sci., 2016, 51, 6697-6710.

152. I. Ahmad, M. Fay, A. Kennedy and Y. Zhu, Com. Sci. Tech., 2010, 70, 1199-1206.

153. J.-H. Shin and S.-H. Hong, Mater. Sci. Eng. A, 2012, 556, 382-387.

154. A. Kasperski, A. Weibel, D. Alkattan, C. Estournès, C. Laurent and A. Peigney, Ceram. Int., 2015, 41, 13731-13738.

155. A. Gallardo-López, A. Morales-Rodríguez, J. Vega-Padillo, R. Poyato, A. Muñoz and A. Domínguez-Rodríguez, J. Alloys Compd., 2016, 682, 70-79.

156. Q. Xie and S. N. Wosu, Adv. Mater. Sci. Eng., 2015, 2015, 1-8.

157. Q. Xie and S. N. Wosu, J. Mater. Eng. Perform., 2016, 25, 874-883.

158. Y. Morisada, Y. Miyamoto, Y. Takaura, K. Hirota and N. Tamari, Int. J. Refract. Met. Hard Mater., 2007, 25, 322-327.

View Article Online
DOI: 10.1039/C7NR01878A

159. V. M. Candelario, R. Moreno, F. Guiberteau and A. L. Ortiz, J. Eur. Ceram. Soc., 2016, 36, 3083-3089.

160. A. Borrell, R. Torrecillas, V. G. Rocha, A. Fernández, V. Bonache and M. Salvador, Wear, 2012, 274, 94-99.

161. A. Nieto, D. Lahiri and A. Agarwal, Mater. Sci. Eng. A, 2013, 582, 338-346.

162. J. Sha, J. Li, S. Wang, Z. Zhang, Y. Wang and J. Dai, Mater. Des., 2016, 107, 520-528.

163. H. Liu, L. Liu, F. Ye, Z. Zhang and Y. Zhou, J. Eur. Ceram. Soc., 2012, 32, 3617-3625.

164. S. R. Bakshi, V. Musaramthota, D. Lahiri, V. Singh, S. Seal and A. Agarwal, Mater. Sci. Eng. A, 2011, 528, 1287-1295.

165. S. R. Bakshi, V. Musaramthota, D. A. Virzi, A. K. Keshri, D. Lahiri, V. Singh, S. Seal and A. Agarwal, Mater. Sci. Eng. A, 2011, 528, 2538-2547.

166. D. Lahiri, E. Khaleghi, S. R. Bakshi, W. Li, E. A. Olevsky and A. Agarwal, Scripta Mater., 2013, 68, 285-288.

167. J. Li, L. Wang, T. He and W. Jiang, Carbon, 2007, 45, 2636-2642.

168. F. Zhang, J. Shen, J. Sun, Y. Q. Zhu, G. Wang and G. McCartney, Carbon, 2005, 43, 1254-1258.

169. M. Yao, Z. Zhangjian, T. Jun and L. Ming, Rare Metal Mat. Eng., 2011, 40, 4-8.

170. E. Khaleghi, Y.-S. Lin, M. A. Meyers and E. A. Olevsky, Scripta Mater., 2010, 63, 577-580.

171. A. Nisar, S. Ariharan and K. Balani, J. Mater. Res., 2016, 31, 682-692.

172. R. B. Acicbe and G. Goller, J. Mater. Sci., 2013, 48, 2388-2393.

173. A. Nisar, S. Ariharan, T. Venkateswaran, N. Sreenivas and K. Balani, Corros. Sci., 2016, 109, 50-61.

174. B. Yavas, F. Sahin, O. Yucel and G. Goller, Ceram. Int., 41, 8936-8944.

175. S. Pasupuleti, R. Peddetti, S. Santhanam, K.-P. Jen, Z. N. Wing, M. Hecht and J. P. Halloran, Mater. Sci. Eng. A, 2008, 491, 224-229.

176. J. Tatami, T. Katashima, K. Komeya, T. Meguro and T. Wakihara, J. Am. Ceram. Soc., 2005, 88, 2889-2893.

View Article Online
DOI: 10.1039/C7NR01878A

177. C. Balázsi, F. Wéber, Z. Kövér, Z. Shen, Z. Konya, Z. Kasztovszky, Z. Vértesy, L. Biró, I. Kiricsi and P. Arato, Curr. Appl Phys., 2006, 6, 124-130.

178. P. Miranzo, J. González-Julián, M. I. Osendi and M. Belmonte, Ceram. Int., 2011, 37, 159-166.

179. M. Belmonte, J. González-Julián, P. Miranzo and M. Osendi, J. Eur. Ceram. Soc., 2010, 30, 2937-2946.

180. E. L. Corral, J. Cesarano, A. Shyam, E. Lara-Curzio, N. Bell, J. Stuecker, N. Perry, M. Di Prima, Z. Munir and J. Garay, J. Am. Ceram. Soc., 2008, 91, 3129-3137.

181. M. Osendi, F. Gautheron, P. Miranzo and M. Belmonte, J. Nanosci. Nanotechnol., 2009, 9, 6188-6194.

182. J. Gonzalez-Julian, J. Schneider, P. Miranzo, M. I. Osendi and M. Belmonte, J. Am. Ceram. Soc., 2011, 94, 2542-2548.

183. J. Gonzalez-Julian, A. Datye, K.-H. Wu, J. Schneider and M. Belmonte, Carbon, 2014, 72, 338-347.

184. E. L. Corral, H. Wang, J. Garay, Z. Munir and E. V. Barrera, J. Eur. Ceram. Soc., 2011, 31, 391-400.

185. M. Chen, X. Yin, M. Li, L. Chen, L. Cheng and L. Zhang, Ceram. Int., 2015, 41, 2467-2475.

186. M. J. Gasch, D. T. Ellerby and S. M. Johnson, in Handbook of ceramic composites, ed. N. P. Bansal, Springer, US, 2005, Chapter 9, 197-224.

187. J. N. Musher and R. G. Gordon, J. Mater. Res., 1996, 11, 989-1001.

188. J. Xue, M. Dong, J. Li, G. Zhou and S. Wang, J. Am. Ceram. Soc., 2010, 93, 928-930.

189. R. Kalyanaraman, S. Yoo, M. Krupashankara, T. Sudarshan and R. Dowding, Powder Metall., 2000, 43, 380-385.

190. L. M. Sheppard, Am. Ceram. Soc. Bull., 1990, 69, 1801-1812.

191. Z. Shi, S. Chen, J. Wang, G. Qiao and Z. Jin, J. Eur. Ceram. Soc., 2011, 31, 2137-2143.

192. L. Jiang and L. Gao, Ceram. Int., 2008, 34, 231-235.

193. S. Yoshio, J. Tatami, T. Wakihara, T. Yamakawa, H. Nakano, K. Komeya and T. Meguro, J. Ceram. Soc. Jpn., 2011, 119, 70-75.

View Article Online
DOI: 10.1039/C7NR01878A

194. K. Sairam, J. K. Sonber, T. S. R. C. Murthy, C. Subramanian, R. K. Fotedar, P. Nanekar and R. C. Hubli, Int. J. Refract. Met. Hard Mater., 42, 185-192.

195. M. A. Kuzenkova, P. S. Kislyi, B. L. Grabchuk and N. I. Bodnaruk, J. Less Common Met., 1979, 67, 217-223.

196. S. L. Dole, S. Prochazka and R. H. Doremus, J. Am. Ceram. Soc., 1989, 72, 958-966.

197. F. Thevenot, J. Eur. Ceram. Soc., 1990, 6, 205-225.

198. A. K. Suri, C. Subramanian, J. K. Sonber and T. S. R. C. Murthy, Int. Mater. Rev., 55, 4-40.

199. R. Angers and M. Beauvy, Ceram. Int., 1984, 10, 49-55.

200. B. M. Moshtaghioun, F. L. Cumbrera-Hernandez, D. Gomez-Garcia, S. de Bernardi-Martin, A. Dominguez-Rodriguez, A. Monshi and M. H. Abbasi, J. Eur. Ceram. Soc., 2013, 33, 361-369.

201. I. T. Ostapenko, V. V. Slezov, R. V. Tarasov, N. F. Kartsev and V. P. Podtykan, Powder Metall. Met. Ceram., 1979, 18, 312-316.

202. N. Cho, Z. Bao and R. F. Speyer, J. Mater. Res., 2005, 20, 2110-2116.

203. P. Larsson, N. Axen and S. Hogmark, J. Mater. Sci., 2000, 35, 3433-3440.

204. K. Hirao, S. Sakaguchi, Y. Yamauchi, S. Kanzaki and S. Yamada, US Pat., 7417002 B2, 2008.

205. H. Wang, H. Yuan, S. S. Hong, Y. Li and Y. Cui, Chem. Soc. Rev., 2015, 44, 2664-2680.

206. A. Krishnan, E. Dujardin, T. W. Ebbesen, P. N. Yianilos and M. M. J. Treacy, Phys. Rev. B, 1998, 58, 14013-14019.

207. C. L. Xu, B. Q. Wei, R. Z. Ma, J. Liang, X. K. Ma and D. H. Wu, Carbon, 1999, 37, 855-858.

208. A. Peigney, C. Laurent, E. Flahaut and A. Rousset, Ceram. Int, 2000, 26, 677-683.

209. Z. A. Munir, U. Anselmi-Tamburini and M. Ohyanagi, J. Mater. Sci., 2006, 41, 763-777.

210. F. Zhang, Z. Y. Fu, J. Y. Zhang, H. Wang, W. M. Wang and Y. C. Wang, J. Alloys Compd., 2009, 485, L31-L34.

211. T. Kobayashi, K. Yoshida and T. Yano, J. Nucl. Mater., 2013, 440, 524-529.

View Article Online
DOI: 10.1039/C7NR01878A

212. B. Milsom, PhD thesis, The Effect of CNTs on the Sintering Behaviour and Properties of Structural Ceramic Composites, Queen Mary University of London, 2013.

213. B. Apak and F. Sahin, Acta. Phys. Pol. A, 2015, 127, 1029-1031.

214. J. Han, P. Hu, X. Zhang and S. Meng, Scripta Mater., 2007, 57, 825-828.

215. P. Sarin, P. E. Driemeyer, R. P. Haggerty, D. K. Kim, J. L. Bell, Z. D. Apostolov and W. M. Kriven, J. Eur. Ceram. Soc., 2010, 30, 2375-2386.

216. S.-Q. Guo, J. Eur. Ceram. Soc., 2009, 29, 995-1011.

217. W.-B. Tian, Y.-M. Kan, G.-J. Zhang and P.-L. Wang, Mater. Sci. Eng. A, 2008, 487, 568-573.

218. G. B. Yadhukulakrishnan, A. Rahman, S. Karumuri, M. M. Stackpoole, A. K. Kalkan, R. P. Singh and S. P. Harimkar, Mater. Sci. Eng. A, 2012, 552, 125-133.

219. J. Lin, Y. Huang, H. Zhang, Y. Yang and Y. Hong, Adv. App. Cerm., 2016, 115, 308-312.

220. A. Boccaccini, J. Cho, T. Subhani, C. Kaya and F. Kaya, J. Eur. Ceram. Soc., 2010, 30, 1115-1129.

221. D. Tasis, N. Tagmatarchis, A. Bianco and M. Prato, Chem. Rev., 2006, 106, 1105-1136.

222. A. Hirsch, Angew. Chem. Int. Ed., 2002, 41, 1853-1859.

223. P.-C. Ma, N. A. Siddiqui, G. Marom and J.-K. Kim, Compos. Part A Appl. Sci. Manuf., 2010, 41, 1345-1367.

224. Y.-P. Sun, K. Fu, Y. Lin and W. Huang, Acc. Chem. Res., 2002, 35, 1096-1104.

225. P. Hojati-Talemi, A. G. Kannan and G. P. Simon, Carbon, 2012, 50, 356-361.

View Article Online
DOI: 10.1039/C7NR01878A

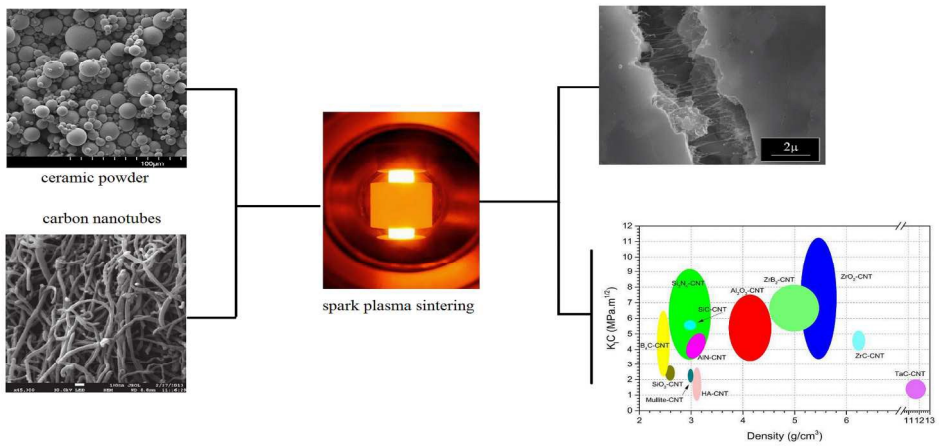

2116x1058mm (96 x 96 DPI)